Scuola di Dottorato di Ricerca
High Mechanics and Automotive Design And Technology
(Meccanica Avanzata e Tecnica del Veicolo)
XXVI Ciclo

# Modeling and optimization of advanced systems for electrical energy production from wood biomass


**Tutore scientifico**
Chiar.mo Prof. Ing. Paolo Tartarini
**Coordinatore della scuola di dottorato**
Chiar.mo Prof. Ing. Paolo Tartarini

**Candidato**
Dott. Ing. Simone Pedrazzi



Università degli Studi di Modena e Reggio Emilia
Anno Accademico 2012-2013

*Alla mia famiglia*

# Sommario in lingua italiana

Lo sfruttamento a fini energetici della biomassa é un tema di grande interesse nel panorama energetico italiano. I motivi preponderanti di questo interesse sono l'abbondante disponibilitá ben distribuita sul territorio, il buon grado di efficienza ed affidabilitá delle tecnologie di conversione e la generosa incentivazione economica dell'energia elettrica prodotta dettata dai recenti decreti ministeriali.

In questo contesto, una tecnologia di grande interessante risulta essere la gassificazione di biomassa ligno-cellulosica. La tecnologia in questione é in grado di convertire la biomassa solida in un vettore gassoso che puó essere a sua volta convertito in energia elettrica attraverso sistemi quali macchine a fluido o dispositivi elettrochimici. La gassificazione é ad oggi la tecnologia piú efficiente per convertire biomassa ligno-cellulosica in energia elettrica, inoltre risulta sostenibile per quanto riguarda il bilancio ambientale della $CO_2$.

Questo lavoro di tesi risulta quindi incentrato su sistemi tecnologicamente avanzati che gassificano biomassa ligno-cellulosica al fine di alimentare generatori stazionari di energia elettrica. La prima parte dell'elaborato é focalizzato sulla caratterizzazione chimico-fisica delle biomasse impiegate. Successivamente viene trattata la gassificazione sia da un punto di vista chimico-analitico sia tecnologico, sono presentate e discusse le tipologie di gassificatori piú diffuse nel panorama scientifico con particolare dettaglio in merito alle piú idonee a processare biomassa ligno-cellulosica. Si é poi trattata la modellazione dei reattori di gassificazione a letto fisso in cui sono illustrati tre diversi approcci modellistici di completezza e complessitá crescente. Per ogni modello, sviluppato partendo dalla letteratura di riferimento, é illustrata la validazione sperimentale ed il campo di applicabilitá.

Nel seguito sono descritti e simulati al calcolatore alcuni sistemi di generazione comprensivi dello stadio di filtraggio/purificazione del gas, eventuale stoccaggio del gas e sua conversione in energia elettrica.

Sono presi in considerazione alcune applicazioni d'avanguardia: sistemi di stoccaggio ad assorbimento attivo della $CO_2$ tramite zeoliti, sistemi di riduzione dell'azoto nell'aria intesa come agente gassificante e sistemi elettrochimici con celle a combustibile ad ossidi solidi per la generazione elettrica. A conclusione dell'indagine analitica sulla tecnologia si é effettuata un'analisi economica costi-benefici di alcuni impianti commerciali a gassificazione ligno-cellulosica di piccola taglia.

Sono descritti i guadagni derivanti dalla vendita dell'energia elettrica prodotta secondo il programma d'incentivazione nazionale vigente ma anche i costi legati alla manutenzione degli impianti e allo smaltimento dei sottoprodotti quali carbonella, catrami e condensati.

Per completezza viene illustrata un interessante applicazione della gassificazione: un impianto per la generazione distribuita di biodiesel ed energia elettrica partendo da coltivazioni energetiche in cui la gassificazione svolge un ruolo fondamentale nel processo di produzione del biodiesel.

# Contents

# Chapter 1

# Introduction

## 1.1 Abstract

The biomass utilization for energy purposes is a topic of great interest in Italian energy scenario. The predominant reasons of this are: the abundant availability and distribution in the country, the good degree of reliability and efficiency of the conversion technologies and the high founds for the yield electricity applied by the recent government rules.

In this context, a technology of great validity is the gasification of wood biomass. This technology is able to turn solid biomass into a gaseous carrier called syngas which can be converted into electrical energy through systems such as fluid machines or electrochemical devices. The gasification is today the most efficient technology to convert wood into electricity and it is also sustainable in terms of the environmental balance of $CO_2$.

Therefore, the thesis is focused on technological advanced systems which gasify wood biomass in order to feed stationary generators of electricity. Chapter 2 is focused on the physical-chemical characterization of wood biomass. Subsequently, in Chapter 3 gasification is described from the chemical and analytical point of view and some applications are introduced. The most common types of gasifiers in the scientific field are presented and discussed. More details about the fixed bed gasifiers which are the most suitable reactors able to process wood biomass are reported.

The modeling of fixed bed gasifier is presented in Chapter 4 and three different modeling approaches of increasing complexity and completeness are discusses. For each model the experimental validation and the applicability domain are shown. Chapter 5 describes the modeling and the simulation of some biomass generation systems. The filtration, purification and storage of the syngas and its conversion into electrical energy are taken into account. Some advance applications are also considered: storage systems with absorption of $CO_2$ using zeolite, reduction of the nitrogen in the inlet air considered as gasifier agent and an electrochemical Solid Oxide Fuel Cell system for the electrical generation.

An economical cost - benefit analysis of some commercially available wood gasification plants are made in Chapter 6. The profits from the sale of the generated electricity are calculated taking into account the national founds program, furthermore the costs related to the plant maintenance and disposal of byproducts such as charcoal and tar are reported. Finally, an interesting application of gasification is described in Chapter 7: a plant for the generation of biodiesel and electricity using oleaginose energy crops as source. In this plant, the gasification of the protein cake obtained from the seeds pressing is used within the production process of biodiesel.

## 1.2 Biomass as renewable source: today and tomorrow

Biomass is today the largest source of worldwide renewable energy. About 10% of our primary energy demand is currently met by biomass [1]. Biomass can provide all kinds of energy that humans need: heat, electricity and also fuel for transport. The energy derived from the biomass conversion, called bioenergy, is mainly used in residential areas in developing countries and in the stationary power generation of the UE and US regions as shown in Figure 1.1 [1, 2].

In developing countries, the common use of biomass is cooking appliances or fuel for fires which has a very low efficiency and high pollution. Over the next few decades, the population growth in these areas will increase the biomass utilization. In this scenario, the goal is to increase efficiency and to decrease the pollution of this rural system in order to prevent health problems [1].

In OECD (Organisation for Economic Co-operation and Development) regions, the biomass used in the home through technologies such as pellet or wood stoves is smaller than the emerging countries. The use of the biomass for district heating or for co-firing in coal plants is widespread in some countries such as Sweden, Finland, and Austria [1].

Power generation from biomass is predominant in the OECD countries thanks to the previous national subsidies for renewable energy production, but China and Brazil have quickly increased the bioenergy production in the last number of years [1].

So far, the bioenergy was strictly dependent on the state energy policy[3]. Unfortunetely, in some countries the bioenergy production is now at a standstill due to the decrease of funds and the increase of the cost of biomass [1]. The development of technology and scale-economics are two crucial issues for the sustainability of bioenergy.

A statistical analysis of the growth of bioenergy predicts that by 2050, these will be an increase to 160 EJ (exa-joules) which represents about 24 % of the world demand for primary energy [1]. An amount of 60 EJ will be used for biofuels and 100 EJ for electricity [4]. The upper part of Figure 1.2 shows the predicted bioenergy consumption in the different sector and the lower part of Figure 1.2 shows the predicted electricity generation by region.

In the future, small scale heating systems, including advanced biomass stoves, will replace fires and the old biomass stoves in emerging countries. Biomass will substite coal in old coal-fired plants. Gasification will be used to produce bioenergy and Biomethane will replace methane [1]. Renewable electricity will increase from 19% in 2009 to almost 60% by 2050, with the remaining 40% coming from nuclear, coal, natural gas and other fossil sources.

Bioenergy is generally a more usable source because it is more stable than other renewable sources such as wind or solar photovoltaics [1]. Biogas and biomethane from anaerobic digestion will be stored and used to produce electricity when demands peak. However, the use of biomass for power generation varies between regions, depending on the availability of biomass, conversion costs, and the availability of alternative low-carbon energy sources. The goverment needs to reach policy goals to promote the proper use of biomass.

Reference [2] descibes a method to put in place a rigorous national planning policy strategy starting with the biomass plannig of a small region. Even if a country does not have a national plan, it does not stop the regions from planning their regional biomass use. Regional laws and commitments will strengthen the efforts of national governments to

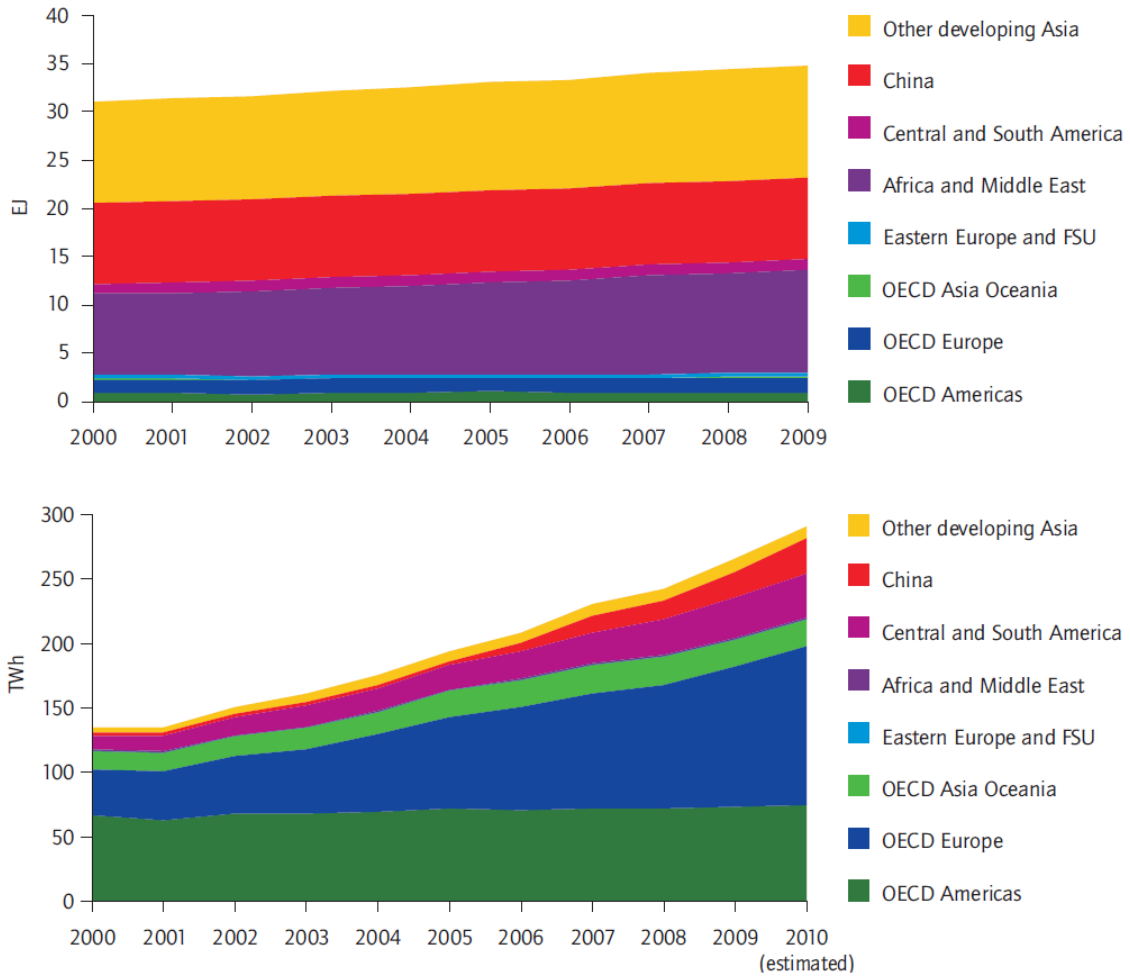


Figure 1.1: Global bioenergy consumption in buildings (up) and Global bioenergy electricity generation (down) (adapted from [1])

apply rules applicable to the whole country. Regional planning will lead to the application of national law which will enhance the expertise of the local economy in this area. General rules for good national biomass planning are:

- To study the connections between national and regional targets to better monitor the progress.
- The evaluation of the impacts of increased biomass use for energy taking into account other uses of biomass.
- A clearer outline of how planning outcomes will be realised.
- The development of improved mechanisms to share best experiences and practices.
- National level recognition of the competencies which will ensure planned changes are carried out more effectively.

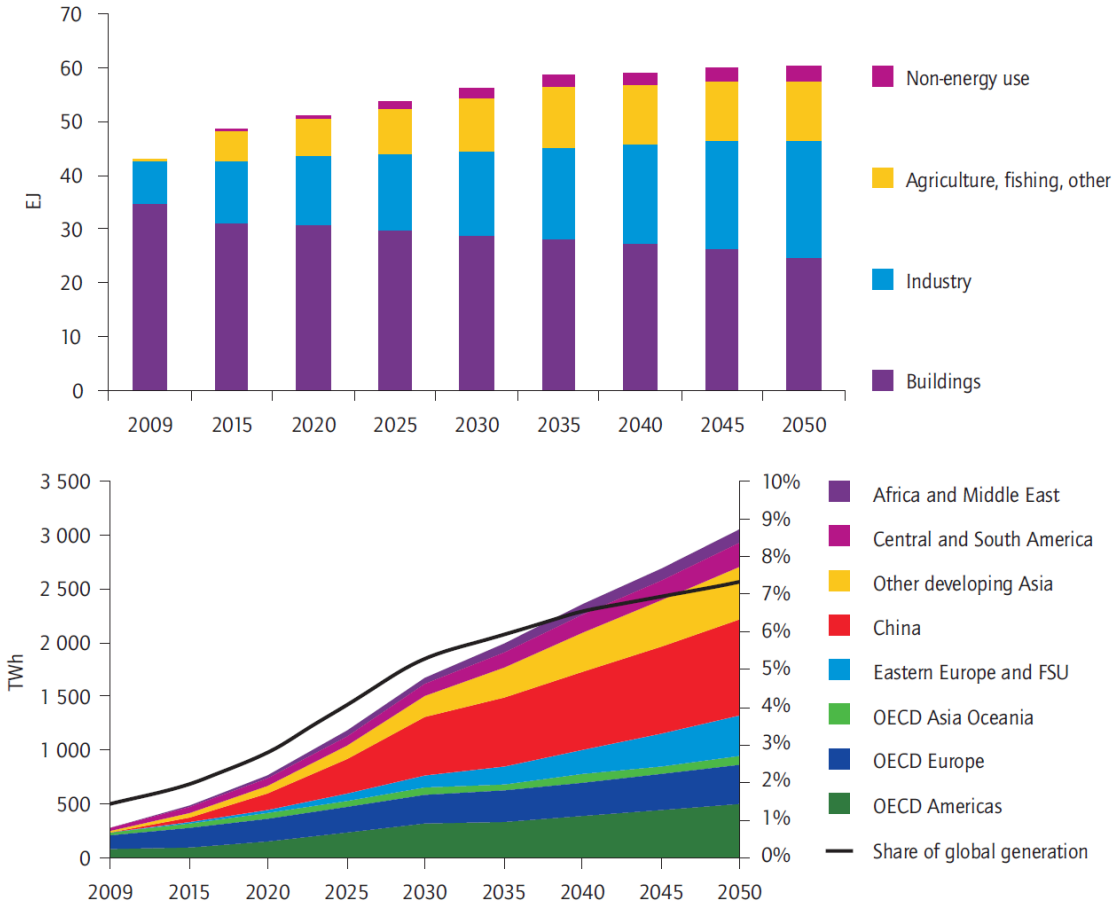


Figure 1.2: Prediction of global bioenergy consumption in different sector (up) and Prediction of global bioenergy electricity generation (down) (adapted from [1])

## 1.3 Biomass to energy

### 1.3.1 Biomass definition and biomass feedstocks

A commonly used definition of biomass is: *any organic, i.e. decomposing, matter derived from plants or animals available on a renewable basis. Biomass includes woods, agricultural crops, herbaceous and woodsy energy crops, municipal organic wastes as well as manure* [1, 5, 6].

Unlike fossil fuel, biomass does not take millions of years to develop. Plants use sunlight through photosynthesis to metabolize atmospheric carbon dioxide and grow. Animals grow by taking in food from biomass. When it burns, the biomass releases carbon dioxide that the plants absorb from the atmosphere. Thus, any burning of biomass does not add to the Earth's carbon dioxide balance. For this reason biomass conversion is considered to be a "carbon neutral" technology.

A byproduct of the thermal conversion of biomass called biochar is considered as a "carbon sequestration" method. Infact, the biochar applied to the soil allows the storage of the carbon in the ground [7, 8, 9, 10]. Pyrolysis and gasification, detailed below, have biochar as a byproduct therefore they are "carbon negative" technologies. Figure 1.3 depicts the carbon cycle during bioenergy production on the left and the carbon cycle during bioenergy and biochar production on the right [7].

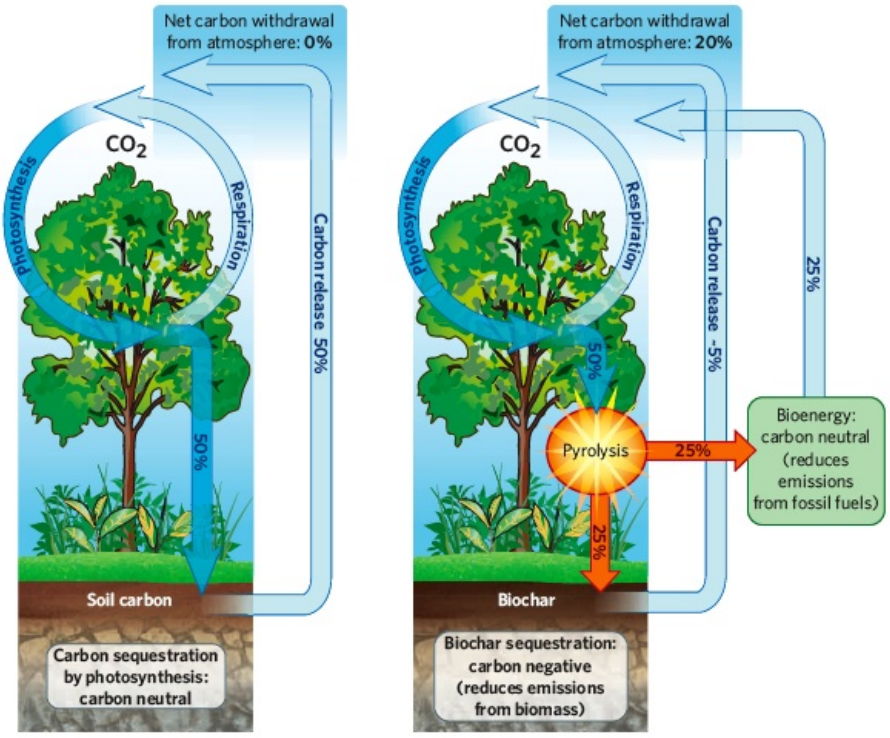


Figure 1.3: Bioenergy carbon cycle (left) and bioenergy plus biochar carbon cycle (right)[7]

A wide range of biomass feedstocks can be used for heat and/or power production. Figure 1.4 summarizes the widely used feedstocks for bioenergy production. Using wastes such as sewage sludge and the organic fraction of municipal solid waste (MSW) as fuel

provides an alternative method of disposal or offers an environmental treatment option that reduces disposal costs. Environmental founds are often necessary to make projects economically viable because the difficult characteristics of the feedstocks require specific technologies with high capital and operating costs [1]. The technologies able to convert waste into energy are combustion, anaerobic digestion and gasification [1, 11].

Many bio-based industrial processes lead to the collection and concentration of large volumes of residues at the point of production. The most suitable residues are sawdust and wood for the timber industry and other by-products biologically degradable. For process residues, the size of the bioenergy plant operation is determined by the availability of raw materials [1].

The locally collected feedstocks, which are produced during harvesting operations in agriculture or forestry, can be collected and brought to a central point for the conversion into energy. These residues can be integrated with energy crops such as Short Rotation Plantation (SRP) or Short Rotation Forestry (SRF) in order to boost the local availability of raw materials and allow for operation on a larger scale [1].

The fourth category is pretreat solid, liquid and gaseous biomass feedstocks with high energy density. This is suitable for international long-distance shipping and for use in centralised heat (mainly industrial use) and power generation. Given the attractive incentives in several European countries and the good degree of reliability and efficiency of conversion technologies, many European companies are funding projects which adopt these feedstocks as resource. Generally, biomass has several advantages over fossil fuels:

- Its abundant availability.
- Its widespread distribution.
- Its ease of collection.
- Its utilization in "Carbon neutral or "carbon negative" processes in several cases.
- Its contains less sulphur than oil or coal.
- It increase the value of the agro-forestal production and therefore it helps the economics growth of the territory.

On the other hand, these are the following technical and economical disadvantages of using biomass energy:

- The bulk density and calorific value are lower than oil, coal and gas, which means that transporting untreated feedstocks can be more difficult and costly.
- Some of the biomasses are only available for part of the year which means that the logistics of these biomasses are complicated and expensive.
- Systems for storing and handling raw biomass are bigger and more costly than their fossil fuels equivalents.
- Untreated biomass often contains high levels of moisture which reduces the net calorific value, the system performance and the density of energy storage.

- Pyrolysis, gasification and combustion systems have to be designed specifically taking into account the chemical and physical characteristics of the biomass to avoid fouling and corrosion problems.

All these issues suggest that systems for using biomass have to be specifically designed to match the feedstock properties, and that pre-treatment of biomass before conversion to energy is often necessary [1].

Common forms of pre-treatment include the most basic, drying, which aims to reduce transport costs by reducing the high initial moisture content of many biomass feedstocks, while also improving combustion efficiency and thus the overall economics of the process. Pelletisation and Briquetting are commercially available, relatively simple technologies used to mechanically compact bulky biomass such as sawdust or agricultural residues [12]. In Torrefaction, a process somewhat similar to traditional charcoal production, biomass is heated up in the absence of oxygen to between 200 $^{o}$C and 300 $^{o}$C and turned into char. The torrefied wood is typically pelletised and has a higher bulk density and 25% to 30% higher energy density than conventional wood pellets, and properties closer to those of coal [13, 14]. Another thermochemical pre-treatment process is pyrolysis, during which biomass is heated to temperatures between 400-600 $^{o}$C in absence of oxygen to produce liquid pyrolysis oil (also referred to bio-oil), solid charcoal, and a product gas[5, 15, 16, 17]. Pyrolysis oil has about twice the energy density of wood pellets, making it viable for long-distance transport [1].

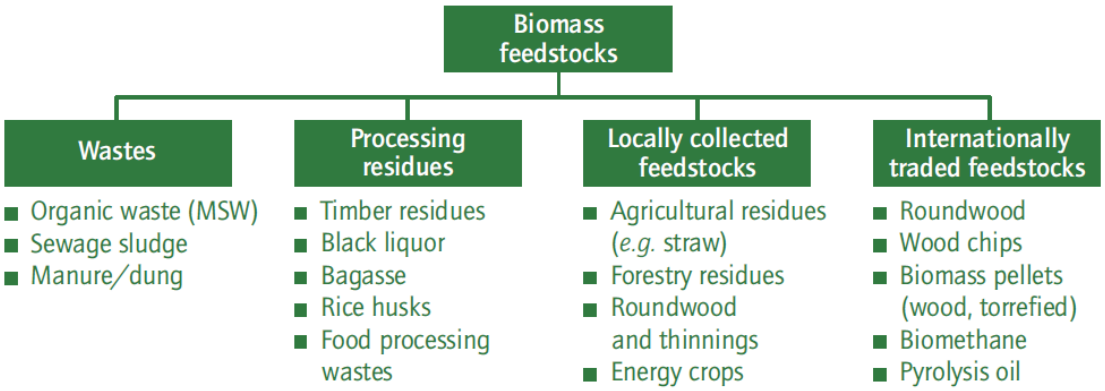


Figure 1.4: Different biomass feedstocks adopted for energy purposes[1]

### 1.3.2 Biomass conversion technologies

Figure 1.5 shows the most common pathways of biomass to energy [6]. Generally, the biomass grows as a result of solar energy, land, water and carbon dioxide in product farming or in energy farming where the goal is to produce biomass for energy purposes.

Biomass is a byproduct of the product farming and it is often used in bioconversion processes suitable for waste and processing biodegradable residues. These processes are divided into three subcategories: extraction, digestion and fermentation/distillation.

Chemical compounds can be obtained by "extraction". The "digestion" generates biogas with approximately 50% of methane [18]. The "fermentation" and "distillation" of biomass generates ethanol which can be used in the chemical industry or/as bio-fuel [19].

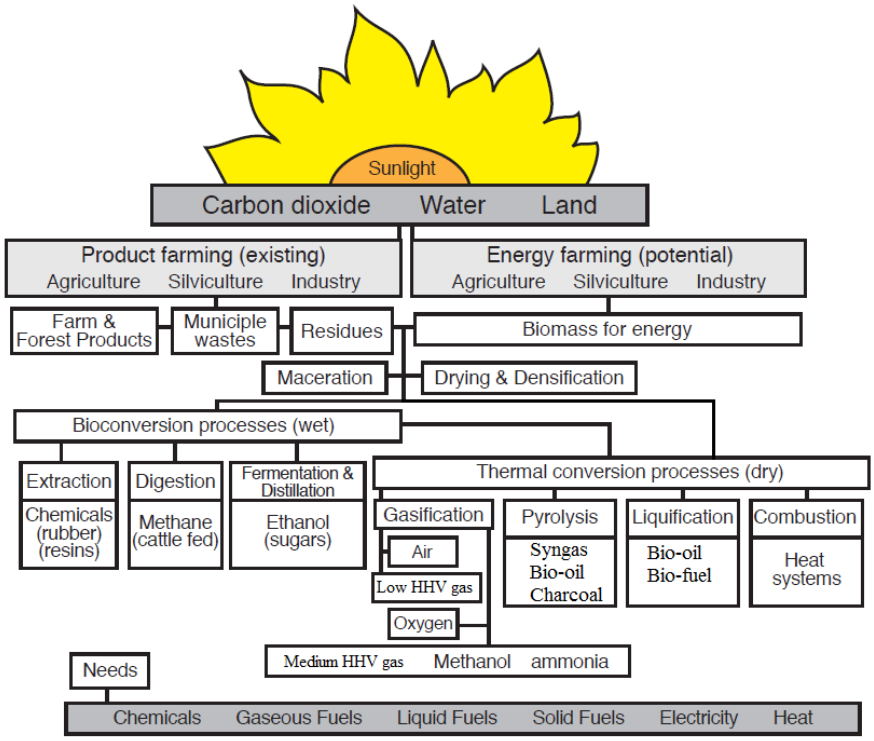


Figure 1.5: Pathways of biomass to energy[6]

The thermal conversion group consists of a group of processes where the heat is key for biomass degradation, conversion and combustion. Depending on the desired effect of the biomass the thermochemical processes are divided into:

- **Gasification:** This is a thermal process that occurs at peak temperatures between 800-1000 $^{o}$C. The gasification process is divided into different phases such as drying, pyrolysis, combustion and reduction [6]. The sequence of these phases depends on the design of the reactor. The gasifier agents which are widely used are air and oxygen. Air gasification generates a low HHV gas (4-5 MJ/Nm$^3$) full of nitrogen. Oxygen gasification is more costly and complicated but the syngas obtained has a medium HHV value of 10-12 MJ/Nm$^3$ [20]. The gas produced through gasification is often called synthesis gas (syngas) which can be used as engine fuel [21], for synthesis of more complex fuels such as ammonia or methanol [22, 5, 23] or burned in order to produce high temperature heat.

- **Pyrolysis:** This transforms biomass into gaseous, liquid and solid compounds. The process can be obtained directly by the under-stoichiometric combustion of biomass or indirectly if the heat is supplied externally. The process temperatures are commonly set between 400 and 800 $^{o}$C [15, 16]. The pyrolysis process can be divided into different types depending on the speed and temperature, such as slow, fast or flash pyrolysis [17]. The products of the pyrolysis can be directly sent to an engine or used as the basis for bio-fuel production. Pyrolysis is also a fundamental part of the gasification process.

- **Liquification:** During this process feedstock macro-molecular compounds are divided into fragments of lighter molecules. This occurs in the presence of a suitable catalyst such as water at a temperature of 525-600 K with a pressure of 5-20 MPa. At the same time, these fragments, which are unstable and reactive, repolymerize into oily compounds called bio-oils which are heavier. The bio-oil can be converted into bio-fuel by specific chemical reactor [24, 25, 26]. There are other processes including the "supercritical water" method for the direct liquefaction of biomass [27].

- **Combustion:** The main product of biomass combustion is heat and during this process the biomass is completely oxidized. Biomass combustion is commonly used for heating, i.e. in stoves, boilers and district heating plants; in addition, it can also be used for power generation in external combustion engines.

This work is focused on wood biomass gasification. Combustion is mentioned in next sub-section in order to identify the most efficient wood to electrical energy process which it is employed in this thesis.

### 1.3.3 Why considering using wood biomass gasification?

The commercial methods to convert the wood biomass into electrical energy are depicted in Figure 1.6. Several technologies for energy production may be considered. These can be divided into two subareas:

- **Gasification based technologies:** Gasification can efficiently convert a solid fuel into syngas which can be burned in internal and external thermal engines [6, 21]. An Internal Combustion (IC) engine cannot be coupled with the gasifier if the syngas is not adequately cleaned [6, 21]. However, this filtering process decreases the heating value of the syngas due to the reduction of its tar content. For this purpose a downdraft gasifier is the best choice due to the low tar and oil content in the produced syngas [6, 21]. Moreover, the "cold gas" efficiency of the gasification process is about 75% [20] because part of the chemical energy of the biomass is lost due to reactor thermal losses or it is disposed as char and tar.

- **Combustion based technologies:** Direct combustion avoids problems related to the char and tar disposal of the gasification plants. The thermal energy obtained in such a way will be easily exploited in an Organic Rankine Cycle (ORC) plant, in an External Firing Gas Turbine (EFGT), in a Stirling engine or in a Turbogas plant [28, 29, 30, 31]. During an Organic Rankine Cycle heat is supplied externally. The cycle uses organic siloxanes as working fluid which operates between lower temperature heat sources compared to the conventional Steam Rankine Cycle (SRC) [28]. A modified version of the Brayton cycle is the EFGT which expands a hot air flow that is heated in a radiant boiler [29]. The Stirling engine is an external combustion reciprocating engine with an ideal high thermodynamic efficiency; however, the real efficiency is lower as IC engine due to thermal and mechanical losses [30]. On the other hand, Stirling engines require less maintenance compared to IC engines [31].

In Reference [32] various scenarios have been analyzed in order to identify the best plant solutions for the energetic use of wood biomass. One of the first topics addressed is the gasification: this technology is needed in plants that work only with syngas, such as

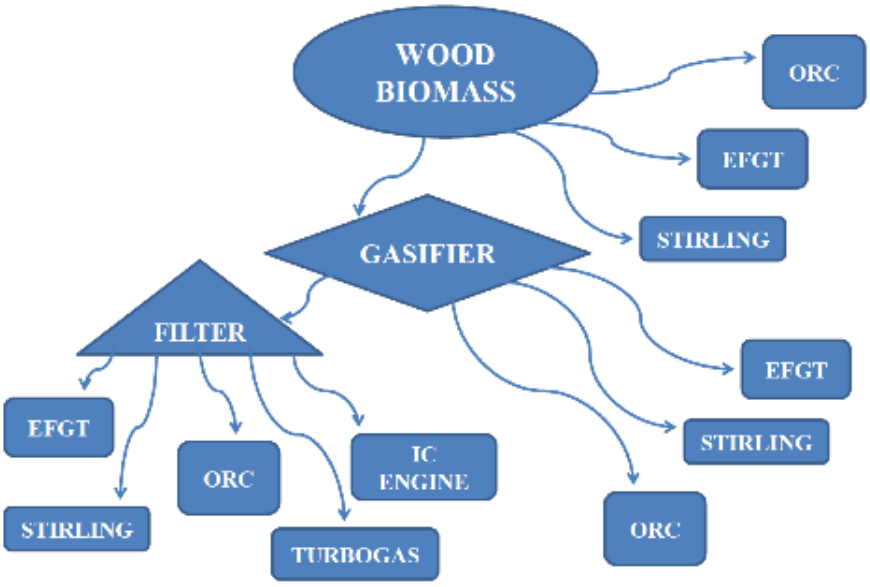


Figure 1.6: Wood to electrical energy conversions pathways [32]

IC engines with diesel cycle or Turbogas. Different scenarios of a hypothetical 250 kWel power plant have been evaluated. Solutions that can use both raw biomass and synthesis gas, such as the ORC turbines or Stirling engines, have been considered.

Table 1.1 summarizes the results of the above comparisons. The IC engine plant working with clean syngas has the best overall calculated efficiency of about 20.2 %, whereby the total biomass consumption of this solution is the lowest as can be seen in Figure 1.7. The annual biomass consumption is the lowest due to the good efficiency of the engine compared with other technologies. However, the disposal or reutilization of the tar and char is required. To overcome this issue, an advance wood to energy system layout is discussed and modeled in Chapter 5. The system proposed is equipped with a filtering system that it is able to reduce the nitrogen of the inlet air. This increases the gasification efficiency and reduces the tar yield. In addition, the IC engine is replaced with a SOFC-MGT generation unit which is able to increase the overall efficiency to 33%.

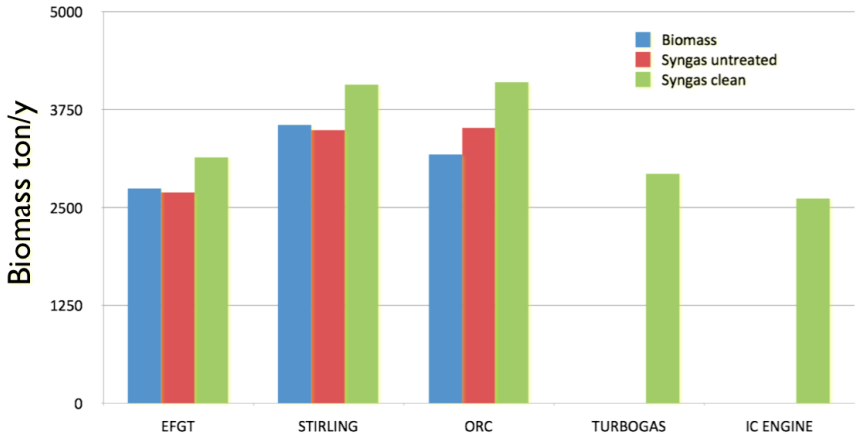


Figure 1.7: Annual biomass consumption of different conversion technologies

Table 1.1: Performance comparison of different conversion technologies

| Plant type | Required biomass [$10^3$ kg/year] | Total electrical efficiency [%] |
|---|---|---|
| ORC with BB | 2785 | 14.6 |
| ORC with CS | 3164 | 12.9 |
| ORC with RS | 3074 | 13.2 |
| Stirling with BB | 3116 | 13.0 |
| Stirling with CS | 3139 | 12.9 |
| Stirling with RS | 3050 | 13.3 |
| EFGT with BB | 2406 | 16.9 |
| EFGT with CS | 2424 | 16.8 |
| EFGT with RS | 2355 | 17.3 |
| Gas Turbine with CS | 2260 | 18.0 |
| IC Engine with CS | 2018 | 20.2 |

Legend: BB = biomass burner; CS = clean syngas; RS = raw syngas.

# Chapter 2

# Wood biomass characterizarion

The wood is part of the category of ligno-cellulosic biomasses. It is typically made of hollow, elongated, spindle-shaped cells arranged parallel to each other [5]. Figure2.1 shows a macroscopic view of a trasverse section of a *Quercus alba* trunk [33]. Beginning at the outside of the tree there is the outer bark (ob). Next is the inner bark (ib) and then the vascular cambium (vc) which is too narrow to see in this magnification. In the interior toward the vascular cambium is the sapwood which is easily differentiated from the heartwood which is closest to the pith (p) in the center.

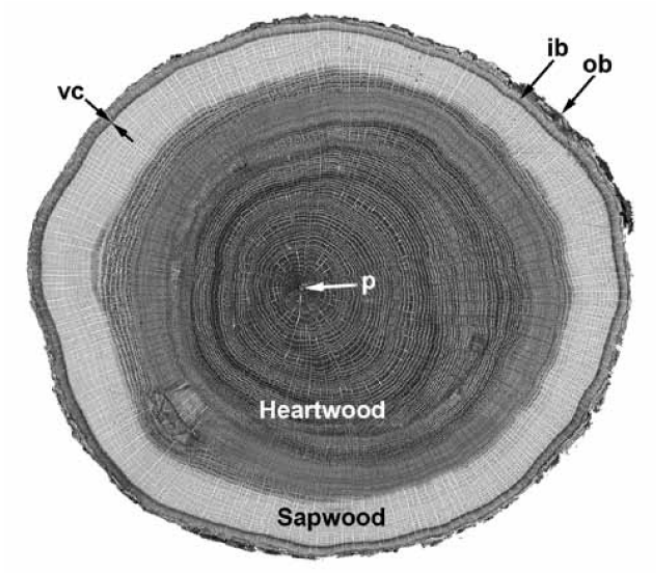


Figure 2.1: Macroscopic view of a trasverse section of a *Quercus alba* trunk [33]

The polymeric composition of the cell walls and other constituents of biomass vary widely [34], but they are essentially made of three major polymers: cellulose, hemicellulose and lignin.

The cellulose is the most common organic compound on Earth and it is the primary structural component of the cell walls in biomass. Its amount varies from 90% (in weight) in cotton to 33% for most other plants. Cellulose is a long chain polymer with a high degree of polymerization and a large molecular weight [35] which is represented by the

generic formula $(C_6H_{10}O_5)_n$.

Hemicellulose is another constituent of the cell walls of a plant. While the cellulose is of a crystalline and strong structure that is resistant to hydrolysis, hemicellulose has a random and amorphous structure with little strength. It is a group of carbohydrates with a branched chain structure and a lower degree of polymerization (100-200), and which is represented by the generic formula $(C_5H_8O_4)_n$ [35].

Lignin is a complex, highly branched polymer of phenylpropane and it is an integral part of the secondary cell walls of plants. The lignin is the cementing agent for cellulose fibers which holds adjacent cells together.

Table 2.1 shows the polymeric composition of some types of wood. Unlike carbohydrates or starch, the ligno-cellulose is not easily digested by humans so these biomasses are not part of the human food chain. For this reason, its use for thermochemical conversion into energy does not threaten the world's food supply.

There is a growing interest in the cultivation of plants exclusively for the production of energy. These crops are ligno-cellulosic and known as SFR [36]. They typically have a short growing period, high yields and require little or no fertilizer, so they provide a quick return on investment. Energy crops are planted more densely than common crops which increase the productivity. For energy production, woody crops such as Miscanthus, Willow, Switchgrass, and Poplar are widely utilized. These plants have a high energy yield per unit area of land and they require much less energy for cultivation [5].

Table 2.1: Commonly ligno-cellulosic woods composition [34]

| Plant | Lignin [% wt] | Cellulose [% wt] | Emicellulose [% wt] |
|---|---|---|---|
| Deciduous | 18-25 | 40-44 | 15-35 |
| Coniferous | 25-35 | 40-44 | 20-32 |
| Willow | 25 | 50 | 19 |
| Larch | 35 | 26 | 27 |

## 2.1 Wood biomass structure

The main components of the plant are "extractives", cell walls and ashes. The "extractives" are substances such as protein, oil, sugar, etc. which cover the vegetable tissue. It is possible to extract this coumpound from the plant using a solvent treatment. The cell wall provides the necessary structural strenght to support the plant. Normally, a cell is made of carbohydrate fibers (mainly cellulose and hemicellulose) and lignine which hold the fibers together.

The ash is the inorganic component of the biomass. The ash content of wood biomass is generally very small (about 1-5 %), but may play a significant role in the utilization of biomass especially if it contains alkali metals such as potassium, or halides such as chlorine.

## 2.2 Classification of wood as fuel

"Atomic ratio", "ratio of ligno-cellulose constituents" and "ternary diagram" are three methods which characterise the biomass as fuel from its chemical composition [5]. Atomic ratio is a useful approach to identify qualitatively the Higher Heating Value $HHV$ [MJ/kg]

of the fuel. As shown in upper part of Figure 2.2, the increase of the oxygen to carbon (O/C) atomic ratio creates a decrease of the $HHV$. In fact, the anthracite has an O/C atomic ratio of 0.1 and its $HHV$ is 38 MJ/kg, whereas the common wood biomass has an O/C atomic ratio of 0.7 and its $HHV$ is 15 MJ/kg. Futhermore, an increase of the hydrogen to carbon (H/C) atomic ratio decreases the $HHV$.

The biomass age influences the O/C ratio, for example the energy content of the oldest coal and anthracite is higher than fresh plant biomass. The high O/C ratio fuel produces high volatile and the high H/C ratio fuel produces a high liquid compost. Unfortunely, high oxygen reacts with hydrogen to produce water so the high H/C content does not translate into a high gas yield [37].

A further biomass classification is based on the relative ratios of cellulose, hemicellulose and lignin. It is possible to estimate the "pyrolysis attitude" of the biomass starting from its polymeric components ratio [37]. Biomasses with similar hemicellulose-lignin and cellulose-lignin ratios have similar physical and chemical properties. For typical biomasses, the cellulose-lignin ratio increases from 0.5 to 2.7, while the hemicellulose-lignin ratio increases from 0.5 to 2.0.

Finally, the ternary diagramm depicted in the lower part of Figure 2.2 is a useful method for analyzing the biomass conversion processes. Each angle of the triangle represents a pure component: the bottom left angle is Carbon, the bottom right angle is Oxygen and the top angle is Hydrogen. Opposite each angle, the concentration of the component is zero. Generally, biomass fuel is closer to the hydrogen and oxygen angles compared to coal, so the biomass contains more hydrogen and oxygen than coal. In the ternary diagramm reported in the lower part of Figure 2.2 some conversion processes are shown: the slow pyrolysis (P) moves the products toward carbon through the formation of solid char; the fast pyrolysis (F) moves the products toward hydrogen and away from oxygen which creates a higher liquid production; Oxygen gasification (O) moves the products toward the oxygen corner; Steam gasification (S) takes the process away from the carbon corner and Hydrogenation process (H) increases the hydrogen and thus it moves the products towards the hydrogen angle.

## 2.3 Thermo-physical properties

The thermo-physical properties of the biomass influence its pyrolysis and gasification behaviour. Permeability is an important factor in pyrolysis, thermal conductivity and diffusivity influence thermochemical conversions.

The composition and the physical proprieties of biomass is often expressed on a different basis depending on the situation. The following conditions are commonly used:

- **As received (as):** The conditions of raw biomass, often with high moisture.
- **Air dry (ad):** The conditions of biomass after a hot air drying treatment where the heart temperature of biomass doesn't reach 100 $^o$C. The total percentage of moisture $M$ [% wt] is given by the sum of two factors: 1) the surface moisture $M_s$ [% wt] and 2) the inherent moisture $M_i$ [% wt]. In this case, the surface moisture $M_s$ is removed while the inherent moisture is retained. To calculate the generic constituent percentage on an air-dry basis starting from an as-received basis, the amount of the constituent is divided by the total mass of the sample minus the surface moisture mass.

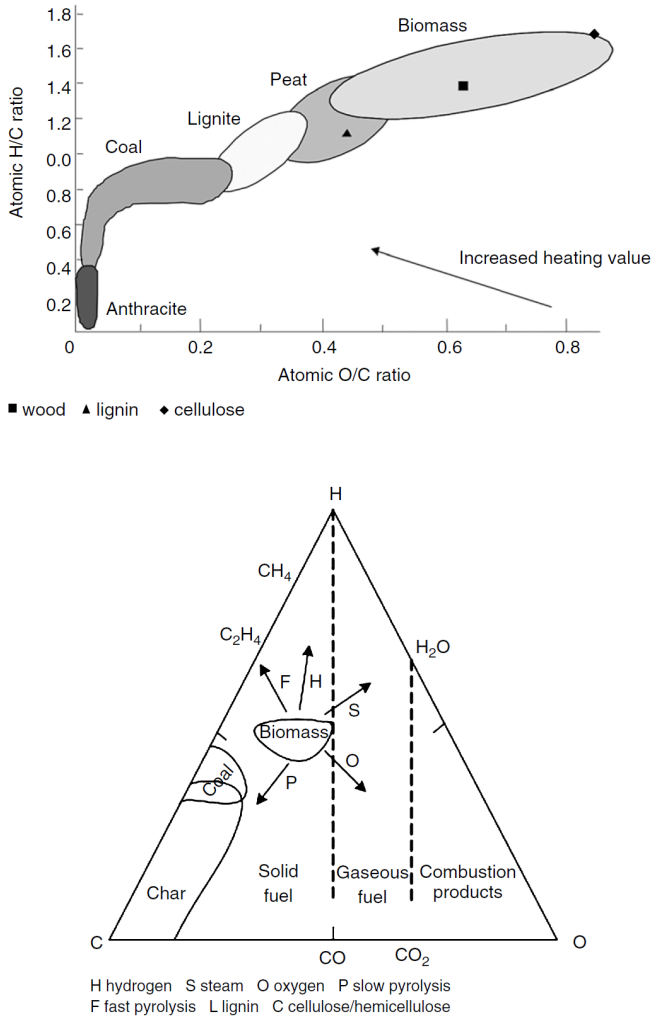


Figure 2.2: Classification of fuel by their H/C and O/C atomic ratios [37] (up) and C-H-O ternary diagramm of biomass showing the gasification process (down) [5, 37]

- **Total dry (db):** The conditions of biomass after a drying treatment with hot air where the heart temperature of biomass exceeds 100 $^o$C. In a such a way, the total moisture percentage $M$ is removed. To calculate the generic constituent percentage in this case, the amount of the constituent is divided by the total mass minus the total moisture mass.

- **Dry ash-free (daf):** Ash is the non organic component of the biomass. To calculate the generic constituent percentage in this case, the amount of the constituent is divided by the total mass minus the total moisture mass and the ash mass.

Taking into account these conditions, some crucial thermo-physical properties are defined and discussed below.

### 2.3.1 Density

The most important physical property to consider is the density $\rho$ [kg/m$^3$]. For granular biomass, three characteristic densities are defined: true, apparent and bulk.

The true density ($\rho_{true}$) is the weight per unit volume occupied by the solid constituent of the biomass. The true density of the most wood cell walls is about 1530 kg/m$^3$. However, the calculation of the true density is difficult because it is hard to measure the true solid volume which can be obtained with a picnometer [5].

It is easy to measure the apparent volume of a sample of biomass and its related apparent density ($\rho_{app}$). This measure includes the internal pores of a biomass particle but not the interstitial volume between biomass particles packed together. For this reason, the bulk density ($\rho_{bulk}$) based on the overall space occupied by an amount or a group of biomass particles is defined. The bulk volume includes interstitial volume between the particles and it depends on how the biomass is packed. The previous densities can be calculated as following:

$$\rho_{app} = \rho_{true}(1 - \epsilon_p) \tag{2.3.1}$$

$$\rho_{bulk} = \rho_{app}(1 - \epsilon_b) \tag{2.3.2}$$

where $\epsilon_p$ [ad] is the void fraction of the biomass particle and $\epsilon_b$ [ad] is the void fraction of particle packing.

### 2.3.2 Thermal conductivity

Biomass particles, however small they may be, are subject to heat conduction along and across their fiber, which in turn influences their pyrolysis behaviour. Conductivity also depends on the biomass moisture content, porosity and temperature. Some of these depend on the degree of conversion, as the biomass undergoes combustion or gasification. Typical wood is made of fiber walls which have channels carrying gas and moisture. Reference [5] reviews some experimental formulas to calculate the thermal conductivity along and across the grains of the wood.

### 2.3.3 Specific heat

The specific heat of biomass is adopted in several model of termochemical conversion such as the pyrolysis and the gasification. The specific heat $C_p$ [kJ $kg^{-1}K^{-1}$] of general wood biomass can be calculated by the Equation 2.3.3 valid in the temperature range between 0 - 106 $^o$C [38]. The inflence of the moisture on the specific heat of the biomass is correlated by the Equation 2.3.4.

$$C_{p,T} = 0.266 + 0.00116T \tag{2.3.3}$$

$$C_p = M_{wet}Cw + (1 - M_{wet})C_{p,T} \tag{2.3.4}$$

where $T$ [$^o$C] is the temperature; $M_{wet}$ [% wt] is the total moisture fraction on wet basis and $C_w$ is the specific heat of water.

### 2.3.4 Heat of formation and heat of reaction

Heat Formation (HF), also known as *Enthalpy Formation*, is the change in the enthalpy change of one mole of a product when it is formed by the reaction of the reagent in its standard state of 25 $^o$C and 1 atm. If the compound is formed through multiple steps, HF is the sum of the enthalpy change in each step of the process. The simplest gases such as $H_2$, $O_2$, $N_2$ etc. are not compounds and the heat of formation for them is zero. To calculate the HF of the biomass, it is necessary to know the Heat Reaction (HR) of the combustion of the biomass. HR is the amount of heat released or adsorbed in a chemical reaction with no change in temperature. Considering the combustion reaction, HR is also known as *heat of combustion* $\Delta H_{comb}$ and can be calculated by the following equation:

$$HR = \Delta H_{comb} = \sum HF_{products} - \sum HF_{reagents} \tag{2.3.5}$$

For example, if we assume $CH_{1.35}O_{0.617}$ as the chemical formula of sawdust, its heat of formation results -80.5 kJ/mol.

### 2.3.5 Ignition

When the fuel is heated by external means, the rate of the exothermic reaction increases with a corresponding increase in the heat generation rate. Above a certain temperature, the rate of heat generation matches or exceeds the rate of heat loss. When this happens, the process becomes self-sustainable and this temperature is knows as the *ignition temperature*.

This temperature is an important property of any fuel because the combustion reaction of the fuel becomes stable only when it is higher than it. The ignition temperature is generally lower for fuel with higher volatile matter. Biomass particles have a higher volatile matter content (about 70%) and therefore they have a significantly lower ignition temperature of about 250 $^o$C [5, 39].

### 2.3.6 Higher and lower heating values

Higher Heating Value (HHV) is defined as the amount of heat released by the unit mass or the volume of fuel which is initially 25 $^o$C when it is combusted and the products have returned to a temperature of 25 $^o$C. HHV includes the latent heat of vaporization

of the water and it can be measured in a Mahler bomb calorimeter [40] where a sample of biomass of known mass is burned in a closed vessel filled with oxygen at 20-25 atm in order to assure the complete combustion of the sample. The reaction at constant volume generates thermal energy equal to the decrease of the internal energy of the system $\Delta U$ [J]. The heat of combustion $\Delta H_{comb}$ is calculated by:

$$\Delta H_{comb} = \Delta U + \Delta nRT \tag{2.3.6}$$

where $\Delta n$ [mol] is the moles variation of the gas, $R$ [J mol$^{-1}$ K$^{-1}$] is the universal gas constant and $T$ [K] is the temperature. The difference between $\Delta H_{comb}$ and $\Delta U$ is small for solid fuel such as biomass (about 0.1 %), so often the $\Delta H_{comb}$ is considered similar to $\Delta U$. The method to evaluate $\Delta U$ is to immerse the "bomb" into a quasi-adiabatic vessel filled with a known amount of water. The combustion increases the water temperature with a specific trend and a graphical method exposed in [40] permits to calculate the average $\Delta T$ of the water. The $\Delta U$ of water is assumed equal to the $\Delta H_{comb}$ and it is evaluated using the equation:

$$\Delta H_{comb} = \Delta U_{water} = K\Delta T \tag{2.3.7}$$

where the calorimeter constant $K$ [J/K] was previuosly calculated through a calibration process described in [40]. Considering the biomass conditions, the HHV can be expressed in three common ways:

$$HHV_{ar} = \frac{Q}{m_f} \tag{2.3.8}$$

$$HHV_{db} = \frac{Q}{m_f - m_M} \tag{2.3.9}$$

$$HHV_{daf} = \frac{Q}{m_f - m_M - m_{ASH}} \tag{2.3.10}$$

where $Q$ [MJ] is the heat of combustion of an amount of "as-received" biomass, $m_f$ [kg] is the "as-received" mass of the feedstock, $m_M$ [kg] is the mass of total moisture in the feedstock and $m_{ASH}$ [kg] is the mass of ash in the feedstock. The $HHV_{daf}$ of soft wood is about 17 MJ/kg and of hard woods is about 20 MJ/kg. A complete database of heating values for widely used biomass and waste is available on the web [41].

Several technologies, such as boilers or conventional heat generators are not able to condensate the steam inside the exhaust gases of combustion. In these cases, the latent heat of the vaporization of water is it not recovered. For this reason, a new heating value need to be considered: the lower heating value (LHV). It is defined by the amount of heat released by the full combustion of a specified quantity of fuel minus the heat of vaporization of the water in the combustion products. The LHV can be evaluated from the HHV by the following equation:

$$LHV = HHV - r\left(\frac{9H}{100} + \frac{M}{100}\right) \tag{2.3.11}$$

where $r$ [kJ/kg] is the the latent heat of water at atmosferic pressure, $H$ and $M$ are the hydrogen and total moisture mass percentage of the "as-received" biomass respectively.

## 2.4 Chemical analysis

Wood biomass contains several complex organic compounds, moisture and a small amount of inorganic impurities. The organic compounds comprise of four principal elements: carbon, hydrogen, oxygen and nitrogen. Some biomasses from agricoltural residues and treated wood such as demolition wood from buildings and structures may contain small amounts of sulfur or chlorine. The composition of the feedstock is vital to simulate and design the conversion processes. Two methods are widely applied to evaluate the composition of biomasses: Proximate and Ultimate analyisis.

### 2.4.1 Proximate analysis

Proximate analysis is a simple and inexpensive process which gives the gross composition of an "as-received" biomass sample. These are: the total moisture ($M$), the volatile matter ($VM$), the ash ($ASH$) and the fixed carbon ($FC$). The $M$ and $ASH$ percentages which are determined by the proximate analysis are the same as that obtained by the ultimate analysis. However, the fixed carbon in proximate analysis is different from the carbon in ultimate analysis because it does not include the carbon in the volatile matter.

The latter is the condensable and noncondensable vapour released when the fuel is heated to a standard temperature of 950 $^o$C for wood biomass and at a standard rate in a controlled environment for seven minutes [5].

The ash is the inorganic solid residue left after the fuel has been completely burned. Its primary ingredients are silica, aluminum, iron, and calcium; small amounts of magnesium, titanium, sodium, and potassium may also be present. The ash content of biomass is generally very low, but may play a significant role in the use of biomass especially if it contains alkali metals such as potassium or halides such as chlorine. Straw, grasses, and demolition wood are particularly susceptible to this problem. These components can lead to serious agglomeration, fouling and corrosion in boilers or gasifiers [42].

A method which evaluates the risk of agglomeration in a type of wood biomass is explained in [43]. A sample of biomass was heated in a kiln for 3 hours at 550 $^o$C in order to reduce it to ashes. Then a parallelepipeon of pressed ashes was tested in an optical vertical dilatometer. The dilatometer was heated to 500 $^o$C and then the ash sample was added considering the flash test mode as suggested by [44]. The temperature of the instrument rose to 850 $^o$C at a rate of 80$^o$ C/minute and then the heaters were turned off, letting the sample cool down. Figure 2.3 reports three different trends: 1) the temperature of the sample from the moment it was inserted in the heated part of the instrument, 2) the percentage of sintering that was evaluated measuring the height variations of the sample and 3) the variation of the crossing area of the sample. The most important trend is that of sintering. A reduction under the 95% range is a consequence of "ash sinterization" and therefore "slagging" is imminent.

The ash obtained from biomass conversion does not necessarily come from the biomass entirely. During collection, biomass is often scraped off the forest floor and then undergoes multiple handlings, during which it can pick up a considerable amount of dirt, rock, and other impurities. In many plants, these impurities constitute the major inorganic component of the biomass feedstock.

A high moisture is ordinary for most common biomass. The moisture can be expressed in the "dry basis" ($M_{dry}$) condition or in the "wet basis" ($M_{wet}$) condition as follows:

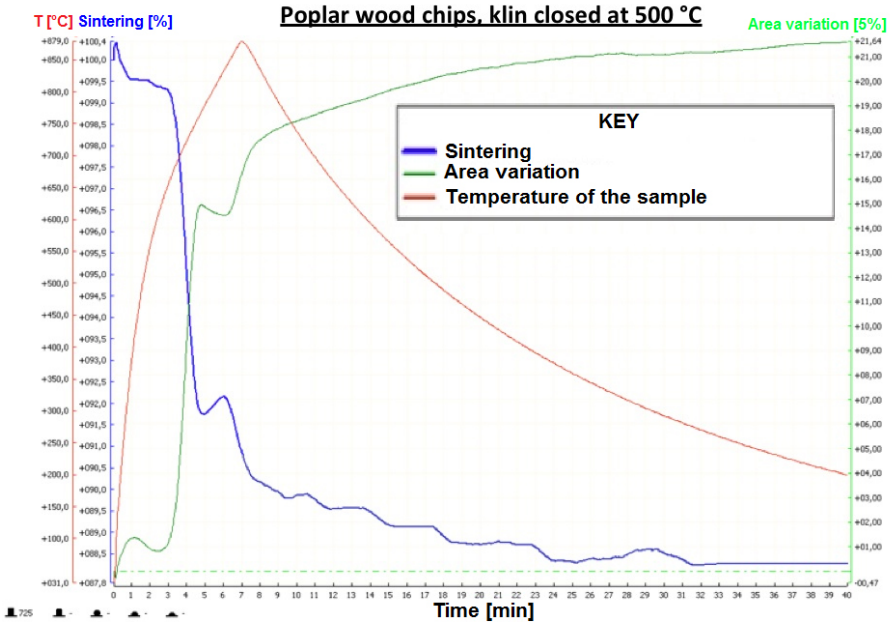


Figure 2.3: Thermal microscophy analysis of a poplar woodchip ash sample

$$M_{dry} = \frac{m_{f,wet} - m_{f,dry}}{m_{f,dry}} \tag{2.4.1}$$

$$M_{wet} = \frac{m_{f,wet} - m_{f,dry}}{m_{f,wet}} \tag{2.4.2}$$

where $m_{f,wet}$ [kg] is the wet mass of feedstock and $m_{f,dry}$ [kg] is the dry mass of feedstock. $M_{wet}$ is considered in composition calculations, instead $M_{dry}$ is used for feedstock trading.

The $M_{dry}$ of the biomass can be as high as 90% [5]. The moisture drains much of the deliverable energy from a gasification plant, as the energy used in evaporation is not recovered. This important input design parameter must be known for the assessment of the cost of the energy required for drying the biomass. For example, the total moisture of most common "as-received" wood chips used as feedstock in gasification power plants is about 40-50 %. In this case, a drying to 10-15 % of $M_{wet}$ is necessary to assure a good efficiency of the gasifier [6, 22, 5, 21].

Finally, the fixed carbon $FC$ of the feedstock represents the solid carbon in the biomass that remains in the char after devolatilization. For gasification analysis, $FC$ is an important parameter because in most gasifiers the conversion of fixed carbon into gases determines the rate of gasification and its yield. This conversion reaction is the slowest and it is used to determine the size of the gasifier. Experimentally, it is obtained by:

$$FC = 100 - M - VM - ASH \tag{2.4.3}$$

### 2.4.2 Ultimate analysis

Ultimate analysis is a complex chemical method to estimate the composition of feedstocks described in terms of its basic elements except for $M$ and $ASH$ [5]. Results of a general ultimate analysis of an "as-received" biomass sample can be summarized as follow:

$$C + H + O + N + S + ASH + M = 100\% \tag{2.4.4}$$

where $C$,$H$,$O$,$N$ and $S$ are the carbon, hydrogen, oxygen, nitrogen, and sulfur weight percentages. Several times, $S$ is not present in the biomass. Moreover, $H$ and $O$ not include the hydrogen and the oxygen of the moisture. With the composition of the feedstock, it is possible to calculate the equivalent chemical formula of as-received biomass ($CH_xO_yN_z$) used into mathematical models by these relation:

$$x = \frac{H * MW_C}{C * MW_H} \tag{2.4.5}$$

$$y = \frac{O * MW_C}{C * MW_O} \tag{2.4.6}$$

$$z = \frac{N * MW_C}{C * MW_N} \tag{2.4.7}$$

where $MW_C$, $MW_H$, $MW_O$ and $MW_N$ [g/mol] are the atomic weights of carbon, hydrogen, oxygen and nitrogen. The feedstock composition can be transposed in the "total dry" conditions using the Equation2.4.8 and in "dry ash-free" conditions using the Equation2.4.9.

$$C_{db} + H_{db} + O_{db} + N_{db} + S_{db} + ASH_{db} = 100\% \tag{2.4.8}$$

$$C_{daf} + H_{daf} + O_{daf} + N_{daf} + S_{daf} = 100\% \tag{2.4.9}$$

Furthermore, the $HHV_{db}$ of the biomass can be estimated with the following relation developed by Channiwala and Parikh [45]:

$$HHV_{db}[kJ/kg] = 349.1C_{db} + 1178.3H_{db} + 100.5S_{db} + 103.4O_{db} + 15.1N_{db} - 21.1ASH_{db} \tag{2.4.10}$$

This equation is generalized for solid, liquid and gas fuel but it is valid in a specific range reported in [45]. Another important information, that can be derived from the composition of the feedstock is the stoichiometric amount of air for the complete combustion fo the biomass. Considering the dry air composed by 23.16 % of oxigen, 76.8% of nitrogen and 0.04% of inert gases, its stoichiometric mass $m_{da}$ $[kJ/kg_{db,fuel}]$ necessary for the complete combustion of 1 kg of biomass is:

$$m_{da} = 0.1153C_{db} + 0.3434(H_{db} + 0_{db}/8) + 0.0434S_{db} \tag{2.4.11}$$

# Chapter 3

# Gasification

Gasification is a thermochemical process which occurs through incomplete oxidation at high temperatures of solid fuels. Usually, the temperature ranges from 600 to 1000 $^o$C and the goal of the process is to produce a low or medium HHV syngas essentialy composed by burner gases as $H_2$, $CO$, $CH_4$ and diluent gases as $N_2$, $CO_2$ and $H_2O$. Gasification occurs also in the combustion of wood biomass. Fox example, in a matchstick reported in Figure 3.1 the gases and the soot generated from the pyrolysis of wood burn and give the heat necessary to pyrolize the volatile matter of the biomass. The heat necessary to start the process is given by the combustion of the tip of sulfur. The flame is composed by different gases and soot burning: the most orange and luminous is the flame generated by the soot, instead the flame of gases and tar burning has a characteristic yellow colour. The exhaust are trasparent, instead the generation of gas of pyrolysis is blue. The wood becomes before charcoal and after ash during the combustion [6].

The syngas combustion has numerous advantages respect the biomass combustion. First of all, the control and regulation of the combustion is much flexible and the exhausts have a high temperature which permits to achieve a great efficiency according to Carnot principle [46]. The syngas combustion is clearer than the biomass combustion in terms of soot, HC and CO emissions. Furthermore, as shows in Introduction, the gasification of wood biomass allows to achieve the highest electrical energy conversion efficiency starting from wood biomass as feedstock.

The syngas is also suitable for synthetic liquids and pyrolysis oil production and for steam generation as shown in Figure 3.2. Air gasifiers generate low $HHV$ gas with about 50% of $N_2$ and this is ideal for power and steam production. Oxygen and hydrogen gasifiers are able to produce medium $HHV$ gas suitable for steam generation, synthetic fuel production and energy vector utilization in pipeline. Pyrolysis gasifiers generated pyrolytic gas, pyrolysis oil and char. A part of the char yield is used to produce the heat necessary to supply the pyrolysis reaction.

In this Chapter, the process of biomass gasification are described, the chemical reactions that occurs are reported and the most common fixed bed gasifier reactors are exposed.

## 3.1 Processes in gasification

A general gasification reaction that occours in gasifiers is a complex mechanism composed by 5 processes whose presence and succession depends on the reactor type as shown in

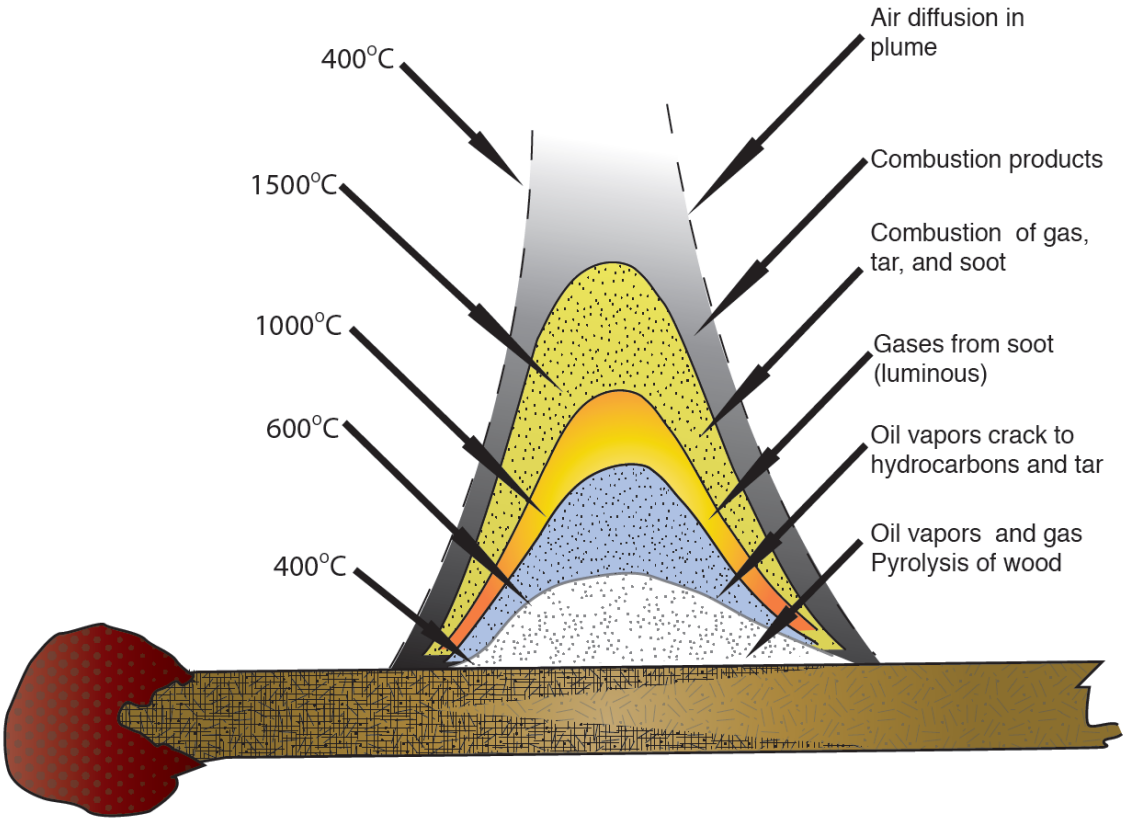


Figure 3.1: Gasification processes in a matchstick combustion [6]

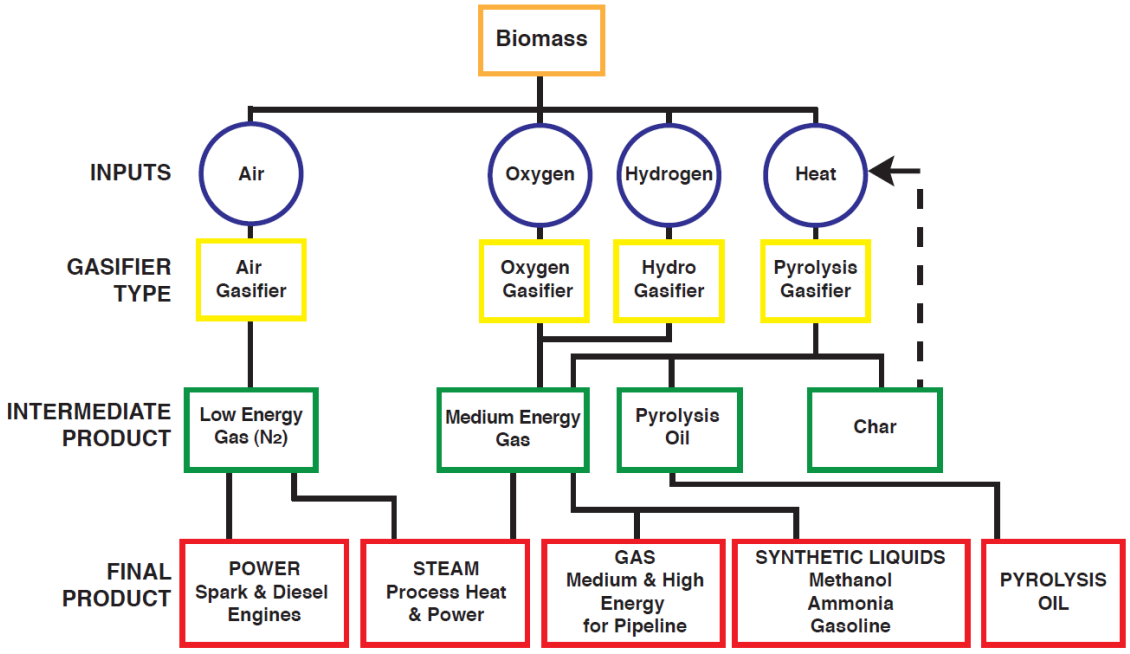


Figure 3.2: The pathways of biomass gasification [6]

Figure 3.3:

- **Drying:** The total moisture of a freshly cut wood ranges between 30 and 60 %. A minimum energy of 2.26 MJ is needed to take away a kilogram of water in the feedstock and it is not recoverable. A pre-drying of wood to 10-20 % of moisture is necessary before gasification. The final drying takes place after the biomass enters into the gasifier, where it receives heat from the hot zone downstream. The surface moisture is removed above 100 $^o$C, over this temperature the VM start volatilizing. The drying zone in the gasifier ends over 200 $^o$C.

- **Pyrolysis:** In gasifiers, the pyrolysis involves the thermal breakdown of larger hydrocarbon molecules of biomass into smaller gas molecules which can be condensable and non condensable. No major chemical gasifying medium such as air or oxygen do not partecipate to the pyrolysis. As shown in Figure 2.2, the slow pyrolysis moves the composition toward to the carbon corner, instead the fast pyrolysis moves toward the C-H axis opposite the oxygen corner so the oxygen decrease and thus we expect more liquid hydrocarbon. In the slow pyrolysis (often called carbonization), the heating time of few days to reach the final pyrolysis temperature of about 400 $^o$C is much higher than the pyrolysis reaction time. The slow pyrolysis has been known since time immemorial for the production of charcoal beehive oven in which large logs were stacked and covered by a clay wall and a small fire at the bottom provided the required heat. In fact, the goal of the fast pyrolysis is to maximize the production of bio-oil. The biomass is heated so rapidly that it reaches the peak of about 800 $^o$C before it decomposes. In gasifiers often occours a sort of conventional pyrolysis which involves the production of gas, char and tar (described below). The dried biomass is heated at a moderate rate and at a moderate temperature ( 600 $^o$C). The products residence time is few minutes.

- **Combustion:** Part of char and tar produced by the pyrolysis is burned with air or oxygen as oxidizing agent. The products of combustion are water and $CO_2$ which react in the reduction zone of the gasifier. The combustion zone is necessary to give the heat for pyrolysis and tar cracking.

- **Cracking:** The tar is a complex mixture of condensable hydrocarbons including, among others, ring aromatic and complex polyaromatic hydrocarbons. It appears such as a thick, black, highly viscous liquid which condenses in the low temperature zones of a gasifier, clogging the gas passage and leading to system disruptions [5, 47, 48]. The tar produced in the pyrolysis process inside the gasifier, also known as tarry gas it is in its gaseous phase and must be cracked in small moleculas such as $H_2$ and $CO$ by the heat coming from the combustion inside the reactor or coming from an external heat source. Furthermore, the syngas produced by the gasifier has a big amount of tar and a possible way to reduce it is an external heating up. Generally, the tar must be heated up to 1200 $^o$ or to 800 $^o$ with a catalyst to crack the tar molecules [5].

- **Reduction:** This process involves chemical reactions among the hydrocarbons, steam, carbon dioxide, oxygen and hydrogen in the reactor, as well as chemical reactions among the evolved gases. Of these, char reduction is the most important. The char produced through pyrolysis of biomass is not necessarily pure carbon. It

contains a certain amount of hydrocarbon comprising hydrogen and oxygen. The char from biomass is generally more porous and reactive than coke. Its porosity is in the range between 40 and 50% while the porosity of the coal ranges between 2 and 18%. Thus, its reaction behaviour is different from coal, lignite or peat. The reduction of the char from biomass involves several reactions between the char and the gasifying mediums. The reduction reactions are generally endothermic, but some of them can be exothermic as well.

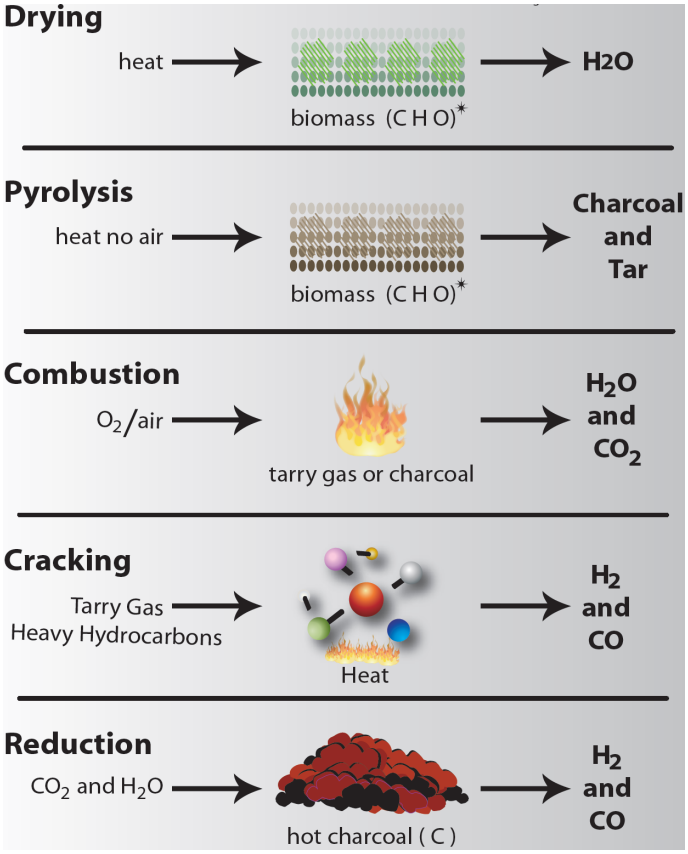


Figure 3.3: Processes in wood biomass gasification

## 3.2 Gasification chemical reaction

Inside gasifier reactors occur several chemical reaction which can be classified in 5 types depending on the reaction mechanims: carbon, oxidation, shift, methanation and steam reforming.

### 3.2.1 Carbon reactions

There are four carbon reaction of interest in gasification [5]:

$$\text{Boudouard: } C + CO_2 \leftrightarrow 2CO + 172kJ/mol \tag{3.2.1}$$

$$\text{Water-gas: } C + H_2O \leftrightarrow CO + H_2 + 131kJ/mol \tag{3.2.2}$$

$$\text{Hydrogasification: } C + 2H_2 \leftrightarrow CH_4 - 74.8kJ/mol \tag{3.2.3}$$

$$\text{Char-oxygen: } C + 0.5O_2 \rightarrow CO - 111kJ/mol \tag{3.2.4}$$

The char-oxygen reaction is the fastes carbon reaction. The water-gas is the most important gasification reaction and its rate is three to five orders of magnitude slower than that the char-oxygen reaction. The presence of hydrogen has a strong inhibiting effect on the water-gas reaction [5].

The Boudouard is six to seven orders of magnitude slower than char-oxygen and it is insignificant below 1000 K. The hydrogasification is the slowest of all and it is important in the production of synthetic natural gas (SNG) [5].

### 3.2.2 Oxidation reactions

Four exothermic oxidation reaction happen in the combustion zone for air and oxygen gasifiers:

$$\text{Char oxydation: } C + O_2 \rightarrow CO_2 - 394kJ/mol \tag{3.2.5}$$

$$\text{Carbon monoxide oxydation: } CO + 0.5O_2 \rightarrow CO_2 - 284kJ/mol \tag{3.2.6}$$

$$\text{Methane oxydation: } CH_4 + 2O_2 \leftrightarrow CO_2 + 2H_2O - 803kJ/mol \tag{3.2.7}$$

$$\text{Hydrogen oxydation: } H_2 + 0.5O_2 \leftrightarrow H_2O - 242kJ/mol \tag{3.2.8}$$

The char, carbon monoxide, methane and hydrogen generated by pyrolysis react with the oxygen of the gasifying agent to generate $CO_2$, water and heat required for heating, drying and pyrolyzing processes. The char oxydation gives the highest amount of heat per mole of carbon consumed, but also char-oxygen is exothermic and produces fuel gas $CO$. When the carbon comes in contact with the oxygen, both char-oxigen and char oxydation can take place, but their extent depends on the temperature. A partition coefficient $\theta$ may be defined to determine the partition of the oxygen between the two reaction. These reaction can be merged togheter:

$$\theta C + O_2 \rightarrow 2\,(\theta - 1)\,CO + (2 - \theta)\,CO_2 \tag{3.2.9}$$

$\theta$ ranges from 1 to 2 and it is influenced by surface temperature of char $T$ [K] [5]:

$$\theta = \frac{[CO]}{[CO_2]} = 2400\exp -(6234/T) \tag{3.2.10}$$

### 3.2.3 Water-gas shift reaction

The water-gas shift reaction is an important gas-phase reaction. It increases the hydrogen content of the gasification product gas at the expense of carbon monoxide:

$$\text{Water-gas shift: } CO + H_2O \leftrightarrow CO_2 + H_2 - 41.2kJ/mol \tag{3.2.11}$$

This is a prestep in syngas production in the downstream of a gasifier where the ratio of hydrogen and carbon monoxide in the product gas is critical. The water-gas shift reaction is slightly exothermic and its equilibrium decreases slowly with temperature. Depending on temperature, it may be driven in either direction. Above 1000 $^o$C it rapidly reaches equilibrium, but at a lower temperature it needs heterogeneous catalysts [5].

### 3.2.4 Methanation reactions

Two methanation reactions are considered in gasification [5]:

$$2CO + 2H_2 \rightarrow CH_4 + CO_2 - 247kJ/mol \tag{3.2.12}$$

$$CO_2 + 4H_2 \rightarrow CH_4 + 2H_2O - 165kJ/mol \tag{3.2.13}$$

### 3.2.5 Steam-Reforming reactions

The methane steam-reforming reactions that occour in gasifiers are the following [5]:

$$CH_4 + H_2O \leftrightarrow CO + 3H_2 + 206kJ/mol \tag{3.2.14}$$

$$CH_4 + 0.5O_2 \rightarrow CO + 2H_2 - 36kJ/mol \tag{3.2.15}$$

## 3.3 Gasifier classification

The gasifiers can be classified following a scheme of 5 phases as shown in Figure 3.4:

1. **Medium**: It rapresent the gasication agent inside the reactor. The widely used are air, steam and oxygen. The air as gasification agent presents two major advantages: it is costless and constantly available. It usually generates a gas with low $HHV$ between 4 to 7 MJ/Nm$^3$ and the reactors work with temperatures around 800-1000 $^o$C [22, 49, 6, 50, 51]. This technology is commonly coupled with fixed bed gasifiers in order to create simple units, but in literature bubbling or fluidized bed gasifiers using air as well can be found [52, 53, 54].

   The gasifiers operating with pure oxygen produce a gas with a heating value higher than the air-blown one, in fact the $HHV$ of the gas can reach 12-28 MJ/Nm$^3$ [55, 6, 50, 5]. Oxygen is highly reactive and it is able to process, through high temperature gasification, a wide range of materials. Oxygen-blown gasifiers were also used for pure carbon monoxide production using coke as fuel [56]. The carbon monoxide and hydrogen content in an oxygen blown gasifier can reach the 90% [50]. There are cases

of study where it is sufficient to add oxygen to air in order to increase the gasifier performance [57, 58, 59].

In steam gasifier, a rich gas with a $HHV$ between 10 and 18 MJ/Nm$^3$ was created but the reactions which take place are strongly endothermic. On the other hand, it does not need an oxygen generator which is complex and it consumes much energy. Before entering the reactor, the water passes through a steam generator that consist basically in a pressurized boiler [5, 50, 60, 61]. The steam gasification is used for synthesis of methanol and other chemicals due to the costs and the characteristics of the produced gas [62, 63, 64].

2. **Heat source**: As discussed above, the most important reduction reactions are endothermic, whereby it is need some heat to balance the reactions. This heat can be given by exothermic oxidation reaction inside the reactor (auto-thermal) or outside the reactor (allo-thermal).

3. **Design**: The design of the reactor is based on gas-solid contacting mode. There are three types: fixed bed, fluized bed and entrained flow. The fixed gasifiers are further subdivided into specific types as shown in Figure 3.5. There is an appropriate range of application for each. For example, the fixed-bed (updraft and downdraft) type is used for smaller units from 10 $kW_{th}$ to 10 $MW_{th}$; the fluidized-bed type is more appropriate for intermediate units from 5 $MW_{th}$ to 100 $MW_{th}$; entrained-flow reactors are used for large-capacity units over 50 $MW_{th}$.

4. **Purpose**: the syngas can be used for heat production i.e. in a furnace or used as engine fuel for electrical power production or used for the production of bio-fuels or SNG or ammonia. It is important to underline that there are some external combustion power systems, i.e. EFGT [65] that make this classification difficult to set properly.

5. **Scale**: Large scale plants over 1 $MW_{el}$ or 3 $MW_{th}$ were first designed for coal gasification [66, 6]. During the last decades, different attempts to design or convert big installation for power production were made [67, 68, 69, 70]. The power is generated with a steam ranking cycle or a gas turbine for large application, in some cases the presence of a second fuel for co-firing is reported [49, 71]. Installations with power output of about 1-5 $MW_{el}$ can work with IC engines [72, 73, 74, 75] or ORC turbines [76, 77, 78].

   Medium scale plants range from 0.3 $MW_{th}$ to 3 $MW_{th}$ and they work normally with IC engines, EFGT, Stirling, SOFC or MGFC units [20, 79, 80, 81, 82, 83, 84, 85, 86].

   The diffusion of small power plants below 0.3 $MW_{th}$ has increased in recent years [87, 88, 89, 90, 91, 92] due to fossil fuel cost and increasing energy demand even in emerging countries.

   Finally, for the comprehension of kinetics, the effect of different parameters on gasification outputs and effectiveness of hypothesis for reactor design, it is possible to use lab scale gasifiers where there is an optimum control on the process [93, 94]. It is fundamental to understand the limits of this approach, were the down-scaling effect is ruled by equations and hypothesis [95, 96, 97].

This thesis concerns the following type: air-blown, auto-thermal, fixed-bed, downdraft gasifiers for medium and small electrical power production. A brief description of fixed bed reactor design is reported below.

## 3.4 Fixed bed gasifier

Also called moving bed, these gasifiers have been developed in many different designs and sizes. Most of them are used to gasify coal, waste or biomasses with medium-big particle size such as wood chips, wood blocks, nut shells, corn cobs, wood pellet or briquettes [6, 21]. In these gasifiers, the biomass flows from top to the bottom where it is discharged as char and ash. In literature, fixed bed reactors are classified as a function of the direction of gas flow:

- **Updraft gasifiers:** These are considered the simplest type of gasifiers [22]. The biomass enter from the top while the air intake is situated at the bottom of the reactor. This solution creates a distribution of different layers as reported in Figure 3.5. This reactor is simple and has been built in many size, from small to large scale plants [98, 99, 100, 101, 102]. The fuel is dried using the sensible heat of the gas flowing up in the reactor, this creates a syngas with low temperature but high tar and moisture content up to 60% (wet basis). The amount of tar and moisture in the produced gas makes this reactor more suitable for heat production instead of electrical power generation, but in literature it is possible to find few plants working with updraft gasifier coupled with a robust gas cleaning apparatus [103, 104].
- **Downdraft gasifiers:** in these reactors the air and biomass flow in the same direction. Depending on the geometry and the air intake position, these reactors can be further subdivided into:
  - *Single and double throat gasifiers:* These gasifiers became common during WWII for automotive applications. The Imbert industries were so famous that now many manuals and articles refer to this type of gasifier as Imbert [105, 106, 107]. This reactor has the air intake situated in an intermediate height, below the throat as sketched in Figure 3.5. The throat is the core feature of these gasifiers. It accelerate the flow increasing the hearth load and creates a uniform combustion zone. Increasing the dimension of the reactor means a higher air speed and a higher number of nozzles necessary to create a combustion zone uniform enough. The same concept can be applied to the reduction of bed material size: the smaller the fuel size the harder it is for the air to spread properly inside the biomass bed. For this reason, reactors designed to operate with small fuels have a narrow throat and a long cone with high slope in order to prevent bed bridging [108], but different manuals in literature advise against this reactor design for sawdust or fine fuel processing [109, 110, 6, 50].
  - *Open core:* The open core reactor tries, with design simplification, to reduce the problem related to fuel size limitations reported in the Imbert gasifiers discussion. This gasifier, also known as "open top", is basically a cylindrical reactor, the air and the biomass enter from the top and uniformly move down to the bottom where the char and ash are discharged and the syngas is drawn.

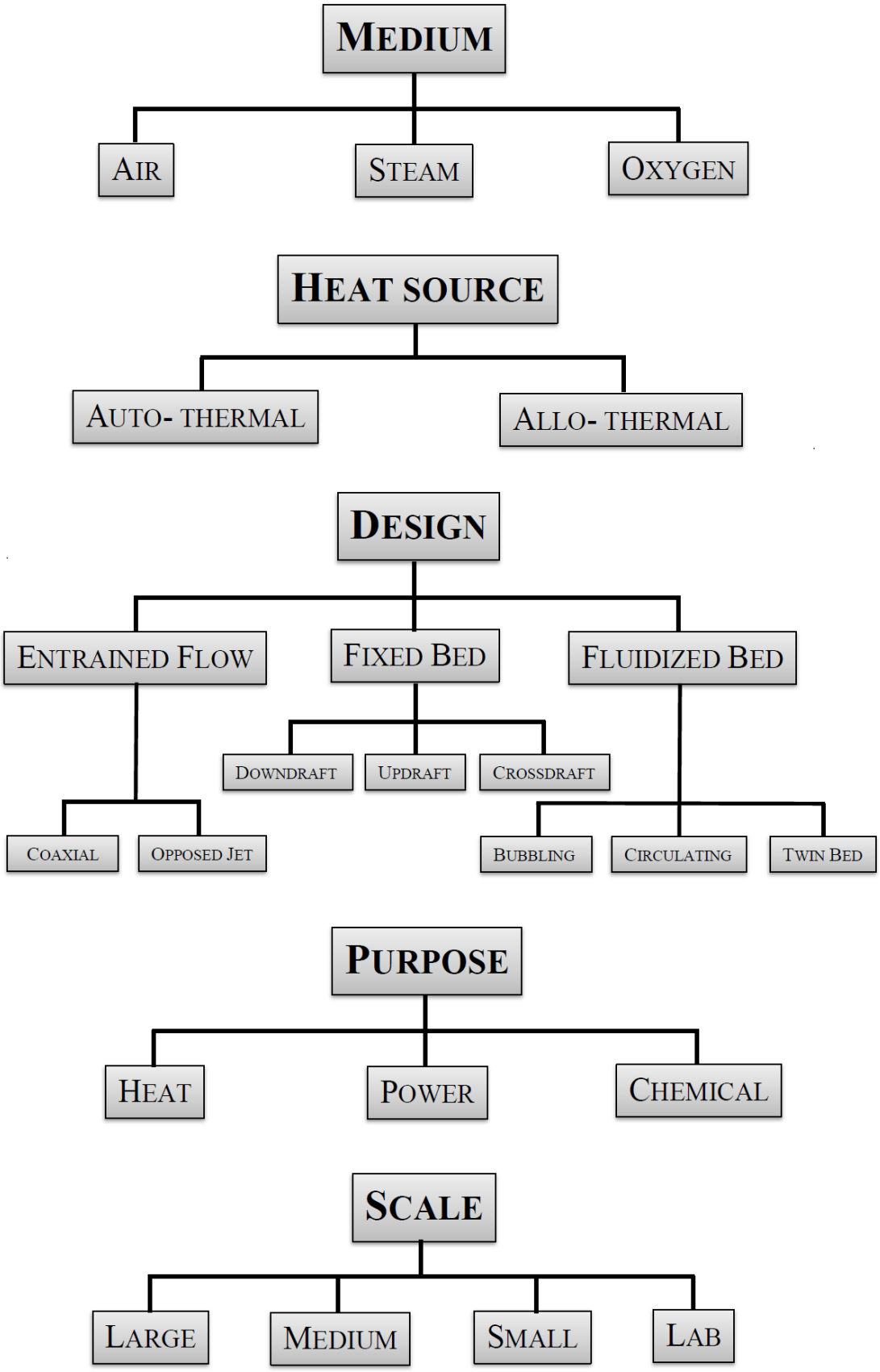


Figure 3.4: Classification of the gasifier

Because all the biomass particles move uniformly down, the reactor presents a stratification into different zones, therefore these reactors are also known as "downdraft stratified". Because the air enters from the top is less of the stoichiometric amount required for complete combustion of the fuel, the flame that is created on the top layer of the gasifier (sometimes covered by a thin drying zone) is called "flaming pyrolysis". This zone generates the major part of the gases of the gasification process, these gases are then forced to pass in the char reduction zone where gaseous tar can be cracked and $CO_2$ and $H_2O$ gases can be reduced thanks to the superficial reaction of high temperature char. The reduction reactions subtract sensible heat to the gases and continue until the temperature is too low (about 600 $^oC$) then it stops. The rest of the gasifier is composed of inert char that wait to be discharged from the bottom of the reactor. This zone acts as a buffer for reactions and temperature fluctuations in the zones above. This reactor design presents different advantages if compared with the Imbert:

1. The stratified reactor is more simple than the Imbert one, there are no nozzles or throats.
2. The open top is a perfect point for measurements and monitoring of the reactor. Imbert gasifiers, when working in depression needs to be properly sealed in order to prevent combustion zone rising.
3. This reactor is more flexible to fuel size variations

On the other hand, there are many disadvantages that have limited the spread of this kind of reactor, some of them are investigated in Chapter 4.

Because the pyrolysis zone of downdraft gasifiers is situated before the oxidation one (in the stratified reactor the two zones coexist in the flaming pyrolysis one), the tar content is low as reported in Table 3.1. This feature makes downdraft gasifiers more suitable for engine applications. However, the proximity of the combustion zone to the gas exit in the single or double throat gasifiers creates a gas with more particles and high temperature.

- **Crossdraft gasifiers:** These gasifiers were first designed for charcoal gasification, they can operate in a very small scale but they have different issues related to high temperatures. If a good quality charcoal is used, small gasifiers can be suitable for micro-power production because the gas produced is clean enough to apply a cyclone and a packed filter only before the engine [111, 112, 113].

A comparison between different fixed bed gasifiers is reported in Table 3.1, while design differences are reported in Figure 3.5.

### 3.4.1 Gasification parameters

#### Cold gas efficiency

The first parameter used for monitor the gasifier performance is the "cold gas" efficiency, it is used for the technical and the economic feasibility of a gasifier system.

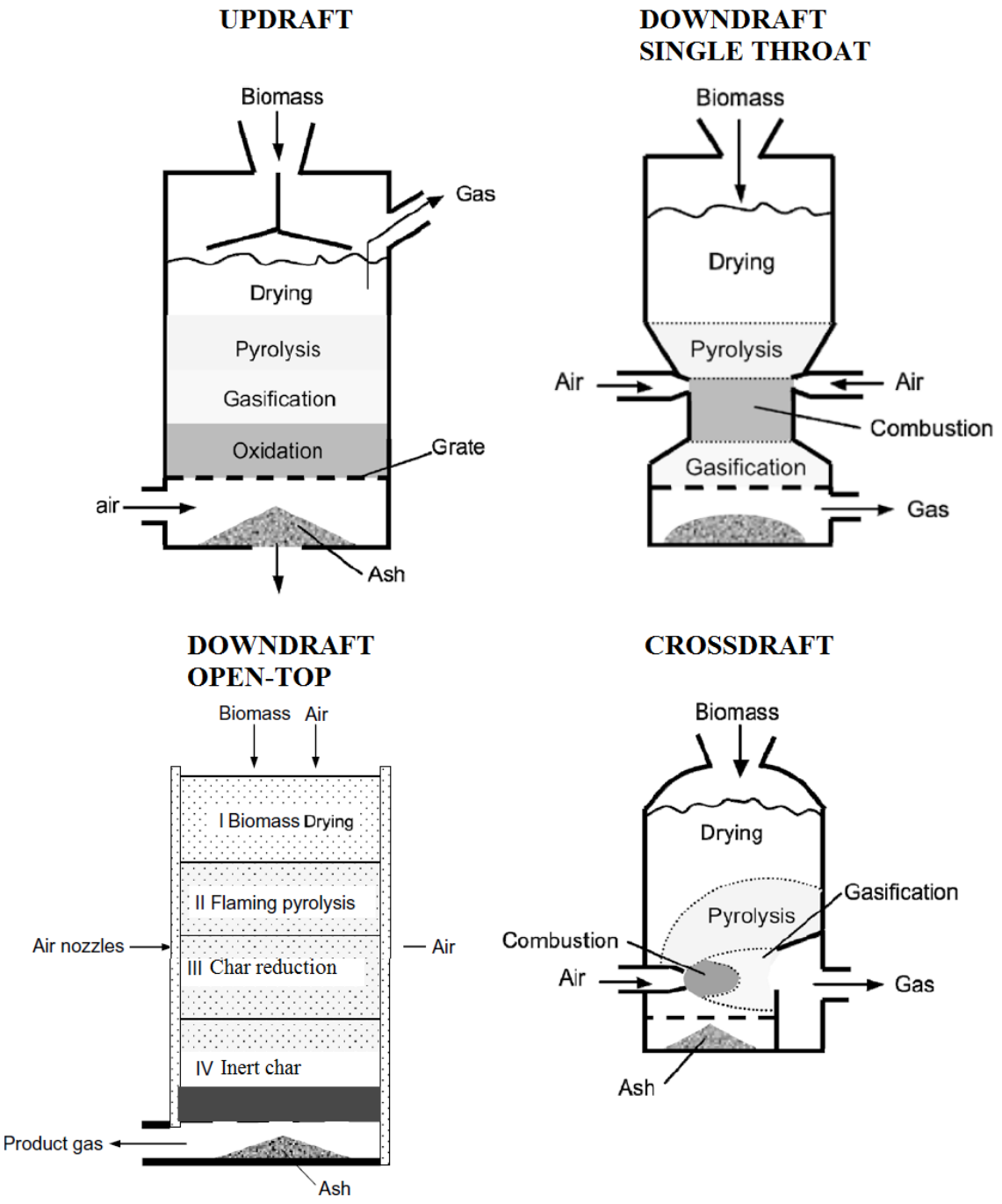


Figure 3.5: Fixed bed gasifiers design

Table 3.1: Comparison between fixed bed gasifiers [22]

| Parameter | Downdraft | Updraft | Crossdraft | Open top |
|---|---|---|---|---|
| Fuel moisture [% wt] | 12 (max 25) | 43 (max 60) | 10-20 | 7-15 |
| Fuel ash content [% db] | 0.5 (max 6) | 1.4 (max 25) | 0.5-1.0 | 1-2 (max 20) |
| Fuel size [$mm$] | 20-100 | 5-100 | 5-20 | 1-5 |
| Gas exit temperature [$^o$C] | 700 | 200-400 | 1250 | 250-500 |
| Tar [g/Nm$^3$] | 0.015-0.5 | 30-150 | 0.01-0.1 | 2-10 |

$$\eta_{g,cold} = \frac{\text{chemical energy of gas}}{\text{chemical energy content in the biomass}} = \frac{\dot{V}_g HHV_{syngas}}{\dot{m}_f HHV_{bio,ar}} \tag{3.4.1}$$

It represents the amount of energy converted into gaseous fuel divided by the chemical energy content of biomass. In literature, there are many works that use the gasifier efficiency as the main parameter for reactor monitoring [114, 21, 6, 115, 116, 5]. The Higher Heating Value of the syngas $HHV_{syngas}$ [MJ/Nm$^3$] can be evaluated by calorimetric approach [117, 118, 119, 120] or using its chemical composition by the following equation:

$$HHV_{syngas} = x_{H_2} HHV_{H_2} + x_{CO} HHV_{CO} + x_{CH_4} HHV_{H_4} \tag{3.4.2}$$

where $x_{H_2}$, $x_{CO}$, $x_{CH_4}$ [% vol] are the volumetric fraction of $H_2$, $CO$, $CH_4$ in the dry syngas and $HHV_{H_2}$, $HHV_{CO}$, $HHV_{CH4}$ [MJ/Nm$^3$] are the Higher Heating Values of $H_2$, $CO$ and $CH_4$.

### Equivalence Ratio

The second parameter that classifies the auto-thermal gasifiers is the equivalence ratio $ER$ defined as the ratio between the oxygen used in the gasifier and the oxygen necessary for the complete combustion of the biomass [5, 121].

$$ER = \frac{\text{oxygen used}}{\text{oxygen necessary for complete combustion}} \tag{3.4.3}$$

The literature reviews show that, depending on the gasifier, ER normally ranges between 0.2 and 0.35. High equivalence ratios result in lower concentrations of $H_2$ and CO, decreasing the heating value of the gas. Low equivalence ratios brings to high tar production [6, 5, 47, 122, 22]. The ER of the reactors analyzed in this thesis have been set between 0.25 and 0.35 as suggested by Reference [6].

### Superficial velocity

The superficial velocity is the ratio between the syngas volumetric flow rate and the cross section area. In literature, it is possible to find a different definition that uses the biomass consumption rate instead of the gas flow rate [21].

$$SV = \frac{\text{Gas Production Rate}}{\text{Cross Sectional Area}} = \frac{\frac{m^3}{s}}{m^2} = m/s \tag{3.4.4}$$

It depends on the gas flow and on the geometric properties of the gasifier. It is representative of the rate at which air, then gas, passes through the reactor [97, 6, 21].

A low SV means that occours slow pyrolysis and high char and tar production. On the other hand, high SV causes very fast pyrolysis, low heating gas and low char production [123, 124].

### Tar and particulate content

As previously reported, gasifiers have two major byproducts: tar and char. The amount of these products need to be monitored because the higher the tar content, the less energy is converted into gas, moreover the high tar content does not allow the use of the produced syngas into IC engines or gas turbines [125]. Hasler and Nussbaumer in 1999 proposed the results reported in Table 3.2 about the different tar and particulate content into the syngas generated by fixed and fluidized bed gasifiers:

Table 3.2: Gas quality of raw producer gas from atmospheric, air blown biomass gasifiers [126]

| Component | Downdraft | Updraft | CFB gasifier |
|---|---|---|---|
| Fuel moisture [% wt] | 6-25 | Nd | 13-20 |
| Particles [mg/Nm$^3$] | 100-8000 | 100-3000 | 8000-100000 |
| Tar [mg/Nm$^3$] | 10-6000 | 10000-150000 | 2000-30000 |

Depending on the application, there are maximum levels of tar and particulate content which need to be taken into account, some of these limits are summarized in Table 3.3.

Table 3.3: Gas quality limits [125]

| Component | IC Engines | Gas Turbine | Methanol synthesis |
|---|---|---|---|
| Particles [mg/Nm$^3$] | $< 50$ | $< 30$ | $< 0.02$ |
| Particle size [$\mu$m] | $< 10$ | $< 5$ | - |
| Tar [mg/Nm$^3$] | $< 100$ | - | $< 0.1$ |

## 3.4.2 Gas cleaning

The tar control in gasification systems is obtained using primary and/or secondary methods [47]. Primary methods are all the thermal or catalytic treatments that occur inside the reactor while the hot gas cleaning processes belong to the secondary methods. There are cases in which it is easier and cheaper to produce a gas rich of tar and proceeding then with thermal or catalytic tar cracking [47, 127, 49]. If the tar content is not too high, but it exceeds the limit for a specific application, the easier solution consists of gas cleaning processes. The first step for hot gas cleaning process is to force the gas to pass into one or more cyclones. The cyclones separate the dust and char from the gas but it is fundamental to keep the cyclones as close as possible to the reactor in order to avoid local condensation. Moreover, in some cases it is necessary to cover the cyclones with insulating material or heating tapes [21, 128, 129]. If the syngas speed is not too high and the particles size is over 1 $\mu$m, it is possible to use gravitational methods, such as sedimentation tanks instead of cyclone separators. These separators occupy a higher volume and are not highly efficient. For this reason they are not common in industrial power plants [130].

The "dry methods" discussed above are only able to separate solid particles with a defined size. For tar and small particles separation it is possible to use electrostatic filters or a scrubber working with water or diesel-oil [22, 131]. Some gasifiers use bio-filters with the main advantage of gasificability of the filtering bed material once it needs to be changed, but on the other hand there are many issues related with these filters: the gas temperature needs to be controlled in order to prevent biofilter pyrolysis, moreover the filtering effectiveness change during the life span of the filtering bed [132, 133, 87]. A complete review of the filtering matter can be found in References [134, 131].

# Chapter 4

# Modeling fixed bed gasifier reactors

Mathematical modeling of a gasifier can provide a qualitative guidance on the effect of design and operation with different types of feedstocks. Simulations allow the designer or the plant engineer to reasonably optimize the design or the operation of the plant. In commercial plants, the optimum operating conditions are often derived through trials on the unit or by experiments on pilot plants. Even though expensive, the experiments can give more reliable design data than can be obtained through modeling and simulation. Modeling may provide a less expensive means to assest the benefits and the associated risk. Simulations can also identify operating limits and hazardous or undesirable operating zones, if they exist. Gasifier models can be based on the following approaches:

- Thermodynamic equilibrium.
- Kinetic of the reaction.
- Computational fluid dynamics (CFD).
- Artificial neural networks.

Only thermodynamic and kinetic models are discussed in this thesis. Thermodynamic equilibrium models predict the maximum achievable yield of a desired product from a reacting system [5]. Equilibrium model concerns the reaction alone without taking into account the geometry of the gasifier. In practice, only a finite time is available for the reactant to react into the gasifier.

For practical applications, kinetic models are used to predict the products of a gasifier which provides a certain time for reaction. A kinetic model studies the progress of reactions in the reactor itself and it gives the syngas compositions at different positions along the gasifier. It takes into account the reactor's geometry as well as its hydrodynamics.

In literature it is possible to find several works about gasification models. Because the great number of reactor typologies and variations, it is possible to find specific models on a particular gasifier, fixed bed or fluid bed, or generical models that tries to predict the behavior of a type of gasifiers [108, 135, 136, 137, 138, 139, 140, 141].

There are also commercial models or features included in several chemical engineering softwares such as ASPEN Plus$^{TM}$ [83, 142, 143]. Moreover, there are models which treat only a part of the reactor, such as the char reduction [144, 145, 146, 147] or the pyrolysis [148, 149, 150] and models that investigates the fluid dynamic of reactors such as the multiphase flow in fluidized and bubble bed gasifiers [151, 152, 153, 154].

## 4.1 Thermodynamic equilibrium models

In this section, two mathematical approach based on the thermodynamic equilibrium are discussed and improved. The first is taken from Reference [135] and it is calibrated using experimental data from a lab-scale gasifier.

The second is derived from [137] where the tar yield is calculated considering it a linear function of the biomass consumption. In this thesis, an improvement of the model with a variable tar yield is reported.

### 4.1.1 Thermodynamic equilibrium tar free model

In Reference [135] is reported a thermodynamic study of the equilibrium constants of water-gas shift and hydrogasification reactions in order to find the syngas composition in fixed bed gasifiers. The following hyphothesis are taken into account:

- Steady state conditions.
- Constant pressure and temperature inside the reactor.
- No tar and char production.

The model is divided in two parts: the chemical balance and the termodynamic balance. The overall air gasification reaction considered for the first balance is:

$$\begin{aligned} CH_xO_yN_z + wH_2O + m\,(O_2 + 3.76N) \rightarrow n_{H_2}H_2 + n_{CO}CO \\ +n_{CO_2}CO_2 + n_{H_2O}H_2O + n_{CH_4}CH_4 + (z/2 + 3.76m)\,N_2 \end{aligned} \tag{4.1.1}$$

where $CH_xO_yN_z$ is the equivalent chemical formula of the "as-received" biomass; the constant $w$ $[mol/mol_{bio}]$ is the specific molar amount of the biomass moisture; the constant $m$ $[mol/mol_{bio}]$ is the specific molar amount of the oxygen in the inlet air; $n_{H_2}$, $n_{CO}$, $n_{CO_2}$, $n_{H_2O}$, $n_{CH_4}$ $[mol/mol_{bio}]$ are the specific molar amount of $H_2, CO, CO_2, H_2O, CH_4$ of the syngas. The values of $w$ and $m$ are given by the following equations:

$$w = \frac{MW_{bio} * M\,(100 + ASH)}{100 * [MW_{H_2O}\,(1 - M/100)]} \tag{4.1.2}$$

$$m = ER * (1 + x/4 + y/2) \tag{4.1.3}$$

$$MW_{bio} = MW_C + x + MW_O * y + MW_N * z \tag{4.1.4}$$

where $M$ [%] is the total moisture; $ER$ [ad] is the equivalence ratio; $MW_{bio}$, $MW_C$, $MW_O$ and $MW_N$ [g/mol] are the molecular or atomic weight of biomass, carbon, oxygen and nitrogen.

The reaction 4.1.1 can be multiplied by the molar biomass flow in "daf" conditions $\dot{n}_{bio,daf}$ $[mol_{bio}/s]$ in order to assess the molar flow of each component of the syngas and the syngas composition in wet and dry conditions:

$$\dot{n}_{bio,daf} = \dot{m}_{bio,as} * (1 - M/100 - ASH/100) \tag{4.1.5}$$

$$\dot{m}_{air} = m * \dot{n}_{bio,daf} \tag{4.1.6}$$

$$\dot{n}_{H_2} = n_{H_2} * \dot{n}_{bio,daf} \tag{4.1.7}$$

$$\dot{n}_{CO} = n_{CO} * \dot{n}_{bio,daf} \tag{4.1.8}$$

$$\dot{n}_{CO_2} = n_{CO_2} * \dot{n}_{bio,daf} \tag{4.1.9}$$

$$\dot{n}_{H_2O} = n_{H_2O} * \dot{n}_{bio,daf} \tag{4.1.10}$$

$$\dot{n}_{CH_4} = n_{CH_4} * \dot{n}_{bio,daf} \tag{4.1.11}$$

$$\dot{n}_{N_2} = (z/2 + 3.76m) * \dot{n}_{bio,daf} \tag{4.1.12}$$

- **Wet syngas conditions**:

$$\dot{n}_{tot,wet} = \dot{n}_{H_2} + \dot{n}_{CO} + \dot{n}_{CO_2} + \dot{n}_{H_2O} + \dot{n}_{CH_4} + \dot{n}_{N_2} \tag{4.1.13}$$

$$x_{H_2} = \dot{n}_{H_2}/\dot{n}_{tot,wet} \tag{4.1.14}$$

$$x_{CO} = \dot{n}_{CO}/\dot{n}_{tot,wet} \tag{4.1.15}$$

$$x_{CO_2} = \dot{n}_{CO_2}/\dot{n}_{tot,wet} \tag{4.1.16}$$

$$x_{H_2O} = \dot{n}_{H_2O}/\dot{n}_{tot,wet} \tag{4.1.17}$$

$$x_{CH_4} = \dot{n}_{CH_4}/\dot{n}_{tot,wet} \tag{4.1.18}$$

$$x_{N_2} = \dot{n}_{N_2}/\dot{n}_{tot,wet} \tag{4.1.19}$$

- **Dry syngas conditions**:

$$\dot{n}_{tot,dry} = \dot{n}_{H_2} + \dot{n}_{CO} + \dot{n}_{CO_2} + \dot{n}_{CH_4} + \dot{n}_{N_2} \tag{4.1.20}$$

$$x_{H_2} = \dot{n}_{H_2}/\dot{n}_{tot,dry} \tag{4.1.21}$$

$$x_{CO} = \dot{n}_{CO}/\dot{n}_{tot,dry} \tag{4.1.22}$$

$$x_{CO_2} = \dot{n}_{CO_2}/\dot{n}_{tot,dry} \tag{4.1.23}$$

$$x_{CH_4} = \dot{n}_{CH_4}/\dot{n}_{tot,dry} \tag{4.1.24}$$

$$x_{N_2} = \dot{n}_{N_2}/\dot{n}_{tot,dry} \tag{4.1.25}$$

Furthermore, it is possible to calculate the normal volumetric flow of wet and dry syngas assuming the syngas components as ideal gases:

$$\dot{V}_{syngas,wet} = \dot{n}_{tot,wet} * 0.022414 \tag{4.1.26}$$

$$\dot{V}_{syngas,dry} = \dot{n}_{tot,dry} * 0.022414 \tag{4.1.27}$$

With Equations 3.4.1 and 3.4.2, it is possible to calculate the "cold gas" efficiency of the gasifier and the $HHV$ of the dry syngas. However, the molar specific amount of the syngas components have to be estimated. The algorithm depicted in Figure 4.1 is adopted.

First step is to choose an initial temperature $T$ [K] and calculate the equilibrium constant of the following reactions:

- **K1:** Water-gas shift $CO + H_2O \leftrightarrow CO_2 + H_2$
- **K2:** Hydrogasification $C + 2H_2 \leftrightarrow CH_4$

The formulas reported in Reference [155] are used:

$$K_1 = e^{\frac{4276}{T} - 3.961} \tag{4.1.28}$$

$$\begin{aligned} ln(K_2) = \frac{7082.842}{T} - 6.567 * ln(T) + \frac{7.467 * 10^{-3} * T}{2} \\ - \frac{2.167 * 10^{-6} * T^2}{6} + \frac{0.702}{2 * T^2} + 32.541 \end{aligned} \tag{4.1.29}$$

Subsequently, the system 4.1.30 must to be solved using the Newton-Raphson method [135]:

$$\begin{cases} \text{Carbon balance } \rightarrow n_{CO} + n_{CO_2} + n_{CH_4} - 1 = 0 \\ \text{Hydrogen balance } \rightarrow 2n_{H_2} + 2n_{H_2O} + 4n_{CH_4} - x - 2w = 0 \\ \text{Oxygen balance } \rightarrow n_{CO} + 2n_{CO_2} + n_{H_2O} - w - 2m - y = 0 \\ \text{Water-gas shift equilibrium constant } \rightarrow K_1 = \frac{n_{CO_2} * n_{CO_2}}{n_{CO_2} * n_{CO_2}} \\ \text{Hydrogasification equilibrium constant } \rightarrow K_2 = \frac{n_{CH_4} * \frac{\dot{n}_{tot,wet}}{\dot{n}_{bio,daf}}}{n_{H_2}^2} \end{cases} \tag{4.1.30}$$

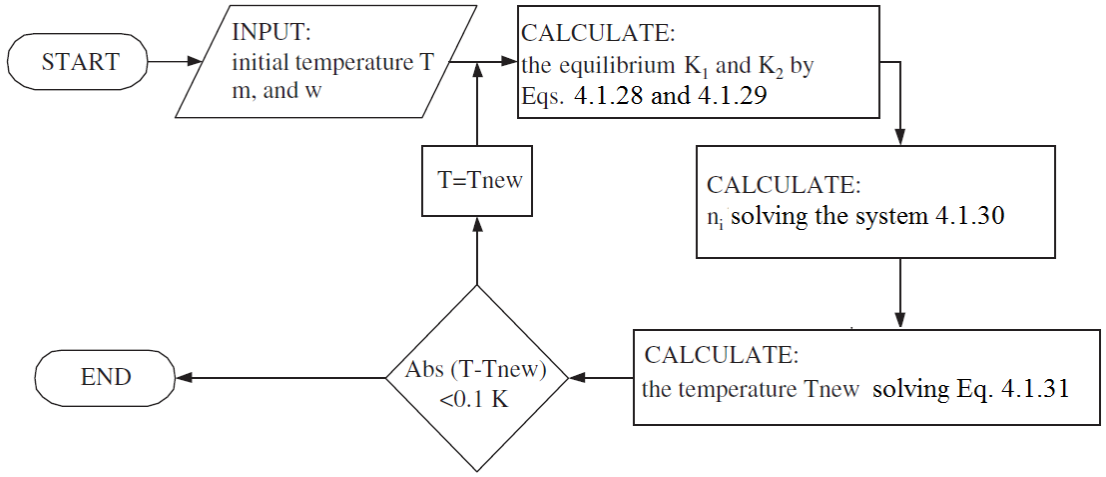


Figure 4.1: Calculation algorithm of the equilibrium models [135]

Obtained the molar specific amount of the syngas species, it is possible to solve the thermodynamic energy balance of the system, reported in Equation 4.1.31, assuming adiabatic conditions in order to find the equilibium temperature $T_{new}$. In this case, adiabatic conditions are assumed and the Newton-Raphson method is applied to solve the problem.

As shown in Figure 4.1, if $abs(T - T_{new}) < 0.1K$ then the calculated equilibium temperature and molar specific gases amounts are the final results; instead, a new iteration is done in order to satisfy the previuous condition.

$$\sum_{j=react} n_j * HF_j^0 = \sum_{i=prod} n_i * \left(HF_i^0 + \Delta H_{T,i}\right) \tag{4.1.31}$$

where $n_j$ [moles] and $HF_j^0$ [kJ/kmol] are the specific moles amount and standard heat formation of the j-th reagent (biomass, air and moisture); $n_i$ [moles] and $HF_i^0$ [kJ/kmol] are the specific moles amount and the standard heat formation of the i-th product ($H_2$, $CO$, $CO_2$, $H_2O$ ,$CH_4$ and $N_2$) and $\Delta H_{T,i}$ is the enthalphy difference between any given state and the standard state for the i-th product. $\Delta H_{T,i}$ can be calculted starting from the specific heat of the product:

$$\Delta H_{T,i} = \int_{298.15}^{T} C_p(T)\, dT = \left| aT + b\frac{T^2}{2} + c\frac{T^3}{3} + d\frac{T^4}{4} \right|_{298.15}^{T} \tag{4.1.32}$$

where the coefficient a,b,c and d are tabuled of each gas in [135]. The standard heat formation of moisture, reactant and product gases are reported in [135], instead the standard heat formation of the biomass fuel is calculated by the following equation [135]:

$$HF_{fuel}^0 = LHV_{bio,daf} + \sum_{k=prod} n_k HF_k^0 \tag{4.1.33}$$

where $HF_k^0$ [kJ/kmol] is the heat formation of product k under combustion of the solid fuel and $LHV$ [kJ/kmol] is the lower heating value of the solid fuel.

The model was implemented into Phyton$^{TM}$ programming languages in order to validate the mathematical method and simulate different gasification conditions. First of all, a comparison with the experimental data reported in Reference [108] was made. Table 4.1 shows a good validation with the RMS error of the syngas composition below 2.2% within the application of two calibration steps:

- An increased value of $m$ respect experimental data.
- Two multipliers applied to the equilibrium constant: $c_{K_1}$ for the water-gas shift reaction and $c_{K_2}$ for the hydrogasification reaction.

A further comparison with the experimental data obtained from a medium scale power plants working with poplar wood chips [156] is reported in Table 4.2. Finally, a comparison with a sunflower-pellets gasification in a micro stratified downdraft gasifier [157] is given in Table 4.3.

Table 4.1: Syngas composition comparisons between the experimental data from a rubber wood gasification (Table 3 of [108]) and the equilibrium no tar model outputs

| **Run no.1** with $w$=0.185, $m$=0.4466, $c_{K_1}$=1.5 and $c_{K_2}$=40 | | |
|---|---|---|
| Gas | Experimental [% vol] | Model [% vol] |
| $H_2$ | 17.2 | 16.2 |
| $CO$ | 19.6 | 18.5 |
| $CO_2$ | 9.90 | 11.7 |
| $CH_4$ | 1.40 | 1.10 |
| $N2$ | 51.9 | 52.5 |
| RMS | 1.1 % | |
| Average gasification temperature $T$ | 1238 K | |
| **Run no.7** with $w$=0.147, $m$=0.4092, $c_{K_1}$=1.5 and $c_{K_2}$=11.28 | | |
| Gas | Experimental [% vol] | Model [% vol] |
| $H_2$ | 15.5 | 18.7 |
| $CO$ | 19.1 | 19.4 |
| $CO_2$ | 11.4 | 11.5 |
| $CH_4$ | 1.10 | 1.10 |
| $N2$ | 52.9 | 49.3 |
| RMS | 2.16 % | |
| Average gasification temperature $T$ | 1119 K | |
| **Run no.9** with $w$=0.125, $m$=0.5192, $c_{K_1}$=1.5 and $c_{K_2}$=300 | | |
| Gas | Experimental [% vol] | Model [% vol] |
| $H_2$ | 13.0 | 11.3 |
| $CO$ | 19.1 | 17.8 |
| $CO_2$ | 10.7 | 11.2 |
| $CH_4$ | 1.20 | 1.00 |
| $N2$ | 56.0 | 58.6 |
| RMS | 1.53 % | |
| Average gasification temperature $T$ | 1460 K | |

Table 4.2: Syngas composition comparison between the experimental data from a medium scale power plants working with poplar wood chips [156] and the equilibrium no tar model outputs

| Conditions: $w$=0.0093, $m$=0.45, $c_{K_1}$=1.5 and $c_{K_2}$=40 | | |
|---|---|---|
| Gas | Experimental [% vol] | Model [% vol] |
| $H_2$ | 12.3 | 11.6 |
| $CO$ | 17.9 | 18.3 |
| $CO_2$ | 10.4 | 12.2 |
| $CH_4$ | 2.80 | 2.20 |
| $N2$ | 56.6 | 55.6 |
| RMS | 1.0 % | |
| Average gasification temperature $T$ | 1347 K | |

Table 4.3: Syngas composition comparison between the experimental data from a sunflower-pellets gasification in a micro downdraft stratified gasifier [157] and the equilibrium no tar model outputs

| Conditions: $w$=0.138, $m$=0.45, $c_{K_1}$=1.5 and $c_{K_2}$=300 | | |
|---|---|---|
| Gas | Experimental [% vol] | Model [% vol] |
| $H_2$ | 17.4 | 15.4 |
| $CO$ | 19.5 | 18.0 |
| $CO_2$ | 11.5 | 12.4 |
| $CH_4$ | 1.58 | 0.97 |
| $N2$ | 50.0 | 53.3 |
| RMS | 1.9 % | |
| Average gasification temperature | 1329 K | |

A positive factor which emerges from the previous validations, beyond the quality of the results obtained, is no divergence of the model for the given inputs. Furthermore, the calculations converge in few iteration for several types of feedstocks. However, the gasification temperature is higher than experimental data due to increased value of $m$.

### 4.1.2 Thermodynamic equilibrium model with tar calculation

The work exposed in [137] is a thermodynamic equilibrium model which take into account the tar production and it considers three reactions: water-gas shift, hydrogasification and methane steam reforming. In the original model the tar yield depends linearly on the biomass consumption. An improvement of the model with a variable tar yield is reported. The model is able to find the syngas composition in fixed bed gasifiers setting the gasification feedstock and the gasification conditions in terms of $m$ and $w$. The following hyphothesis are taken into account:

- Steady state conditions.
- Constant pressure and temperature inside the reactor.
- No char production.
- Constant chemical tar composition.

The modified model is divided in two parts: the chemical balance and the termodynamic balance. The overall air gasification reaction considered for the first balance is:

$$\begin{aligned} CH_xO_yN_z + wH_2O + m\left(O_2 + 3.76N\right) \rightarrow n_{H_2}H_2 + n_{CO}CO + n_{CO_2}CO_2 \\ + n_{H_2O}H_2O + n_{CH_4}CH_4 + \left(z/2 + 3.76m\right)N_2 + n_{tar}CH_pO_q \end{aligned} \tag{4.1.34}$$

where $CH_xO_yN_z$ is the equivalent chemical formula of "as-received" biomass; $CH_pO_q$ is the equivalent chemical formula of tar [158]; $w$ $[mol/mol_{bio}]$ in the specific molar amount of the biomass moisture; $m$ $[mol/mol_{bio}]$ in the specific molar amount of oxygen in the inlet air; $n_{H_2}, n_{CO}, n_{CO_2}, n_{H_2O}, n_{CH_4}$, $n_{tar}$ $[mol/mol_{bio}]$ are the specific molar amount of $H_2, CO, CO_2, H_2O, CH_4, tar$ of the syngas. The values of the inputs $w$ and $m$ are given by Equations 4.1.2 and 4.1.3.

The reaction 4.1.34 can be multiplied by the molar biomass flow in "daf" conditions $\dot{n}_{bio,daf}$ $[mol_{bio}/s]$ in order to assess the molar flow of each component of the syngas and the syngas composition in wet and dry conditions. The molar flow of tar is given by Equation 4.1.35, the tar production Vs. the "daf" biomass input $x_{tar}$ [% wt. "daf" biomass] is calculated by Equation 4.1.36. Furthermore, Equation 4.1.37 can be used to evaluate the specific volumetric tar amount $m_{tar,vol}$ [g/Nm$^3$] in the syngas in order check the gas quality limits reported in Table 3.3 .

$$\dot{n}_{tar} = n_{tar} * \dot{n}_{bio,daf} \tag{4.1.35}$$

$$x_{tar} = \frac{n_{tar} * MW_{tar}}{MW_{bio}} \tag{4.1.36}$$

$$m_{tar,vol} = \frac{n_{tar} * MW_{tar}}{\frac{\dot{n}_{tot,dry}}{\dot{n}_{bio,daf}} * 0.022414} \tag{4.1.37}$$

$$MW_{tar} = MW_C + x + MW_O * p + MW_N * q \tag{4.1.38}$$

Furthermore, assuming the syngas components as ideal gases it is possible to calculate the normal volumetric flow of wet and dry syngas. Equations 3.4.1 and 3.4.2 allow to estimate the "cold gas" efficiency of the gasifier and the $HHV$ of the dry syngas. However, the molar specific amount of the syngas components have to be estimated. An algorithm similar to that reported in Figure 4.1 is adopted. The first step is to choose an initial temperature $T$ [K] and calculate the equilibrium constant of the following reactions:

- **K1:** Water-gas shift $CO + H_2O \leftrightarrow CO_2 + H_2$
- **K2:** Hydrogasification $C + 2H_2 \leftrightarrow CH_4$
- **K3:** Methane steam reforming $CH_4 + H_2O \leftrightarrow CO + 3H_2$

Equations 4.1.27 and 4.1.29 are used to calculate $K_1$ and $K_2$ [155] and Equation 4.1.39 is used to evaluate $K_3$ [159]:

$$K_3 = 1.198 * 10^{13} * e^{\frac{-26830}{T}} \tag{4.1.39}$$

Subsequently, the system 4.1.40 must to be solved with the Newton-Raphson method:

$$\begin{cases} \text{Carbon balance } \rightarrow n_{CO} + n_{CO_2} + n_{CH_4} + n_{tar} - 1 = 0 \\ \text{Hydrogen balance } \rightarrow 2n_{H_2} + 2n_{H_2O} + 4n_{CH_4} + pn_{tar} - x - 2w = 0 \\ \text{Oxygen balance } \rightarrow n_{CO} + 2n_{CO_2} + n_{H_2O} + qn_{tar} - w - 2m - y = 0 \\ \text{Water-gas shift equilibrium constant } \rightarrow K_1 = \frac{n_{CO_2} * n_{CO_2}}{n_{CO_2} * n_{CO_2}} \\ \text{Hydrogasification equilibrium constant } \rightarrow K_2 = \frac{n_{CH_4} * \frac{\dot{n}_{tot,wet}}{\dot{n}_{bio,daf}}}{n_{H_2}^2} \\ \text{Methane steam reforming equilibium constant } \rightarrow K_3 = \frac{n_{CO} * n_{H_2}^3}{\left(\frac{\dot{n}_{tot,wet}}{\dot{n}_{bio,daf}}\right)^2 n_{H_2O} n_{CH_4}} \end{cases} \tag{4.1.40}$$

Obtained the molar specific amount of the syngas species, it is possible to solve the thermodynamic energy balance of the system, reported in Equation 4.1.41, assuming adiabatic conditions in order to find the equilibium temperature $T_{new}$. In this case, adiabatic conditions are assumed and the Newton-Raphson method is applied to solve the problem.

As shown in Figure 4.1, if $abs(T - T_{new}) < 0.1K$, the calculated equilibium temperature and molar specific gases amounts are the final results; instead, a new iteration is done in

order to satisfy the previuous condition. Now, there is the tar in the products, so the standard heat formation of the tar is calculated by the following equation [135]:

$$HF^0_{tar} = LHV_{bio,daf} + \sum_{k=prod} n_k HF^0_k \tag{4.1.41}$$

where $HF^0_k$ [kJ/kmol] is the heat formation of product k under the combustion of the tar and $LHV$ [kJ/kmol] is the lower heating value of the tar. The model was implemented into the Phyton$^{TM}$ programming language in order to validate the mathematical method and simulate different gasification conditions. First of all, a comparison with the experimental and numerical data reported in [108, 135, 137] was made. Table 4.4 shows a good validation with RMS error of the syngas composition Vs. experimental data [108] below 4.5%.

The predicted average temperature of gasification is 918 K (645 $^o$ C) similar to 915 K and 923 K obtained from the model of Reference [160] and Reference [137] for gasification on untreated wood. The present model is stable for a wide ranges of the given input $m$ and $w$. Furthermore, the calculations converge in few iteration. Figure 4.2 shows some 3D plots which illustrates the influence of $m$ and $w$ on the syngas composition and on the tar production considering. The tar production is low at high $m$ values over 0.35, instead the moisture of biomass do not infuence the tar and the $CH_4$ production. The rising of the term $m$ increases $H_2$ production and decrease $CO$, $N_2$ and $CO_2$ production. The rising of the term $w$ increases $CO$, $CO_2$ and $CH_4$ production and decrease $H_2$ and $N_2$ production.

## 4.2 Kinetic modeling

### 4.2.1 Downdraft stratified reactor modeling

Many works can be found in literature about mathematical modeling of gasifiers, however stratified open core downdraft gasifiers raise less interest compared to other reactors. This lack of interest has resulted in fewer works published on the chemical and thermal modeling about this configuration. The first author that needs to be cited is Thomas Reed. He represents the major landmark for stratified reactors, during his work different models have been developed [161, 162, 93].

These models proposed are "black box" approach to gasification modeling. Other equilibrium models are the Altafini model proposed in Reference [163]. A very effective model, that takes into account the kinetic of reduction reactions, is proposed by Wang and Kinoshita [164]. This model is able to predict the char reduction zone using a kinetic approach where reactions between char particle surfaces and gas are modeled.

More complex models for char reduction have beed proposed by Chen [165, 166]. His model is divided into two part with the main goal of creating a tool for gasifier design. Others char reduction models focused on stratified reactors are reported in References [144, 147]. More complex work is the equilibrium model proposed by Di Blasi in References [138, 167].

In this thesis, a mathematical model has been adapted from two different literature models with appropriate modifications and improvements [168, 43]. The first model was developed by Reed and Markson [162]. It predicts the flaming pyrolysis zone length $l_p$ and the char reduction zone length $l_c$ starting from the biomass properties and the gasifier dimensions. The model is composed by the following equations:

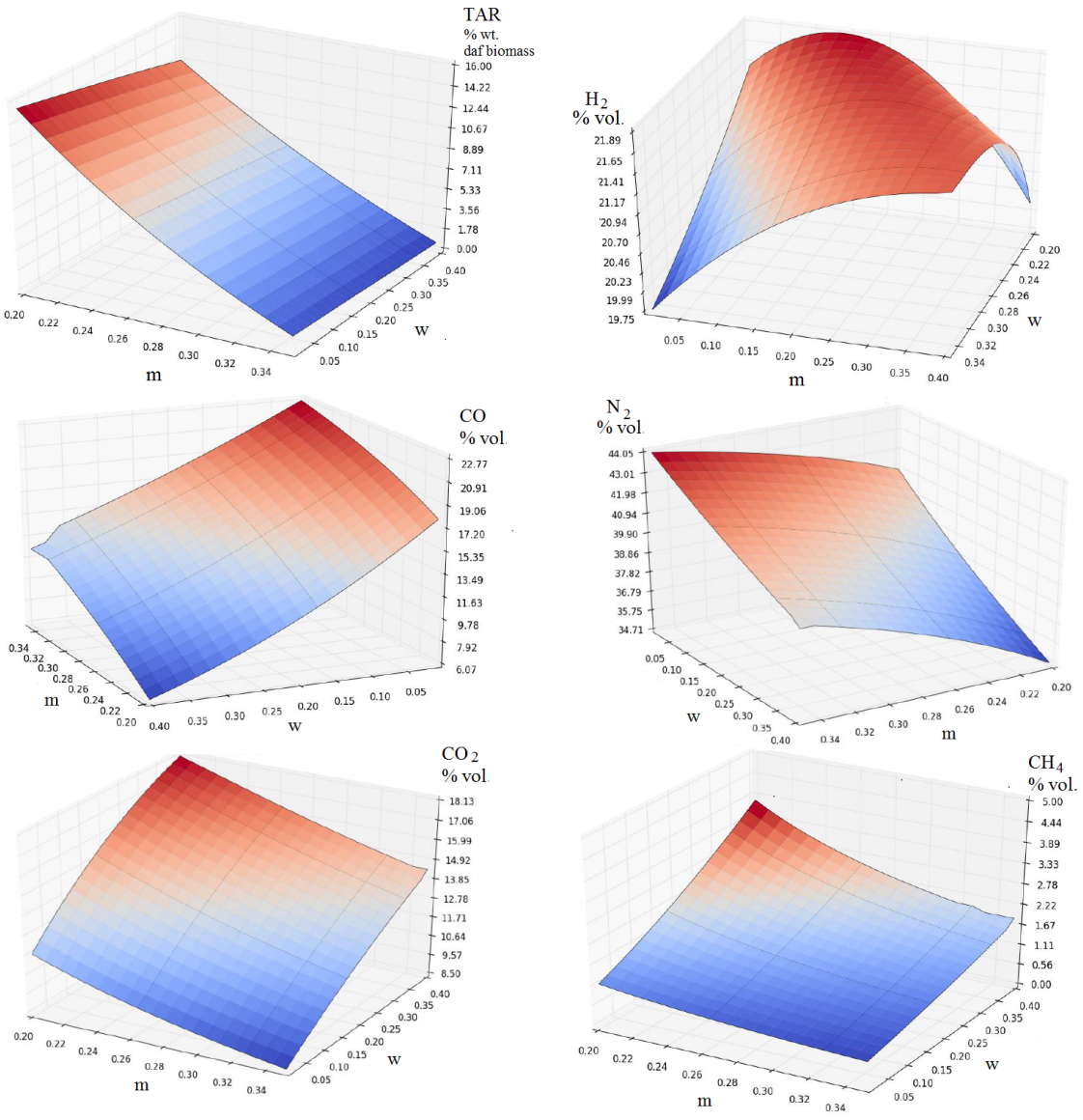


Figure 4.2: $m$ and $w$ influence on the syngas composition and the tar production of rubber wood gasification [108]

Table 4.4: Syngas composition comparison between the experimental data [108], the numerical results of [135], the numerical results of [137] and the equilibrium tar model outputs

| Conditions: $w$=0.16, $m$=0.33 | | | | |
|---|---|---|---|---|
| | Experimental [108] [% vol] | Present model [% vol] | [137] model [% vol] | [135] model [% vol] with $m = 0.4647$ |
| $H_2$ | 17.0 | 22.5 | 16.2 | 18.0 |
| $CO$ | 18.4 | 19.4 | 17.3 | 17.9 |
| $CO_2$ | 10.6 | 12.2 | 12.3 | 11.9 |
| $CH_4$ | 1.3 | 1.15 | 1.06 | 0.11 |
| $N2$ | 52.7 | 44.7 | 53.1 | 52.15 |
| Tar [% wt.] | Np. | 2.29 | 5 | Np. |
| RMS of the syngas composition predicted by the present model Vs. the experimental data | | | | 4.4 % |
| Average gasification temperature | | | | 918 K |

$$l_p = V_f t_p \tag{4.2.1}$$

$$l_c = V_f t_c \tag{4.2.2}$$

$$V_f = \frac{\dot{m}_{bio}\left[A_g F_d (1 - F_v)\right]}{A_g} \tag{4.2.3}$$

where $V_f$ [m/s] is the fuel velocity, $t_p$ [s] is the pyrolysis time, $t_c$ [s] is the char reduction time, $M$ [kg/h] is the input biomass flow in "daf" conditions, $A_g$ [$m^2$] is the area of the gasifier, $F_d$ [$kg/m^3$] is the density of the biomass and $F_v$ [ad] is the void fraction in the biomass.

The pyrolysis time $t_p$ is obtained by the following equation [5]:

$$t_p = \frac{F_d V (h_p + F_m h_w)}{Aq} \tag{4.2.4}$$

where $V$ [$m^3$] is the volume of the biomass particle, $A$ [$m^2$] is the surface area of the biomass particle, $h_p$ [kJ/kg] is the heat per unit mass released by the pyrolysis process at the temperature $T_s$, $h_w$ [kJ/kg] is the water latent of vaporization of water and $q$ [$kW/m^2$] is the heat transfer rate per unit area in the flaming pyrolysis by radiation. The values of $h_p$ and $h_w$ were tabulated by Reed and Markson [162] starting from Huff data [169]. The heat transfer rate $q$ can be obtained with a weighted average calculation from the data reported in [162]. In this calculation, the weight of the terms depends on the moisture of the biomass, on the surface temperature and on the surface area of the biomass particle. The char reduction time was calculated assuming a constant height $H$ [m] of the fixed bed from the following equation:

$$t_c = (H - l_p)/V_f \tag{4.2.5}$$

From the previous equations, it is possible to calculate the layers height, the time of the pyrolysis and char reduction assuming a constant pyrolysis surface temperature and a constant biomass consumption.

An additional approach, presented by Wang and Kinoshita [164], was used to estimate the syngas composition, the air inlet flow, the syngas output flow and the charcoal and water production. This model does not consider the tar production, furthermore the temperature of the reduction zone and the equivalence ratio are fixed parameters. It is based on the following general reaction of gasification [164]:

$$\begin{aligned} CH_\alpha O_\beta + wH_2O + m\left(O_2 + 3.76N_2\right) \rightarrow \phi_1 C + \phi_2 H_2 \\ +\phi_3 CO + \phi_4 H_2O + \phi_5 CO_2 + \phi_6 CH_4 + \phi_7 N_2 \end{aligned} \tag{4.2.6}$$

where $CH_\alpha O_\beta$ is the equivalent chemical formula of "as-received" biomass without nitrogen; $w$ [$mol/mol_{bio}$] in the specific molar amount of biomass moisture; $m$ [$mol/mol_{bio}$] is the specific molar amount of oxygen in the inlet air; $\phi_i$ [$mol/mol_{bio}$] is the specific molar amount of the i-th product of gasification. The values of the inputs $w$ and $m$ are given by Equations 4.1.2 and 4.1.3.

Equation 4.2.6 can be multiplied by the molar biomass flow in "daf" conditions $\dot{n}_{bio,daf}$ $[mol_{bio}/s]$ in order to assess the molar flow of each component of the syngas and the syngas composition in wet and dry conditions. The variables $\phi_i$ are the unknowns of the problem. At the end of the flaming pyrolysis zone (subscript 0) these variables are calculated solving the linear system below [164] assuming $\phi_{2,0} = 0$, $\phi_{3,0} = 0$ and $\phi_{7,0} = z$:

$$\phi_{1,0} + \phi_{5,0} + \phi_{6,0} = 1 \tag{4.2.7}$$

$$2\phi_{4,0} + 4\phi_{6,0} = \alpha + 2w \tag{4.2.8}$$

$$\phi_{4,0} + 2\phi_{5,0} = 2y + \beta + w \tag{4.2.9}$$

$$\phi_{4,0} = \lambda\phi_{5,0} + w \tag{4.2.10}$$

where $\lambda = 1$ is the ratio between the water vapor and the carbon dioxide formation [164]. In the reduction zone the temperature ranges from 1200 K to 1000 K. In this zone, the char is consumed gradually as the result of the following chemical reactions [164]:

1. Boudouard: $C + CO_2 \rightleftarrows 2CO$
2. Water-gas: $C + H_2O \rightleftarrows H_2 + CO$
3. Hydrogasification: $C + 2H_2 \rightleftarrows CH_4$
4. Methane steam reforming: $CH_4 + H_2O \rightleftarrows CO + 3H_2$

Surface reactions 1 and 2 involve single gas molecules, while two molecules are involved in surface reactions 3 and 4. The Langmuir-Hinshelwood mechanism [170] is applied to calculate the net rate for reactions 1 and 2 given by Equations 4.2.11 and 4.2.12 and the Langmuir-Rideal mechanism [170] is adopted to calculate the net rate for reactions 3 and 4 given by Equations 4.2.13 and 4.2.14.

$$v_1 = -k_{a1}\frac{\phi_5 - \phi_3^2/(P_\phi K_{p1})}{\sum_{i=2}^{7}(K_i + 1/p)\phi_i}\left(\frac{\phi_{1,0}}{\phi_i}\right)^{1/3}\left(\frac{\phi_i}{\rho d_p}\right) \tag{4.2.11}$$

$$v_2 = -k_{a2}\frac{\phi_4 - \phi_2\phi_3/(P_\phi K_{p2})}{\sum_{i=2}^{7}(K_i + 1/p)\phi_i}\left(\frac{\phi_{1,0}}{\phi_i}\right)^{1/3}\left(\frac{\phi_i}{\rho d_p}\right) \tag{4.2.12}$$

$$v_3 = -k_{a3}\frac{\phi_2^2 - \phi_6 P_\phi/K_{p3}}{P_\phi K_{p1}\sum_{i=2}^{7}(K_i + 1/p)\phi_i}\left(\frac{\phi_{1,0}}{\phi_i}\right)^{1/3}\left(\frac{\phi_i}{\rho d_p}\right) \tag{4.2.13}$$

$$v_4 = -k_{a4}\frac{\phi_4\phi_6 - \phi_3\phi_2^2/(P_\phi^2 K_{p4})}{\sum_{i=2}^{7}(K_i + 1/p)\phi_i}\left(\frac{\phi_{1,0}}{\phi_i}\right)^{1/3}\left(\frac{\phi_i}{\rho d_p}\right) \tag{4.2.14}$$

$$P_\phi = \frac{1}{p}\sum_{i=2}^{7}\phi_i \tag{4.2.15}$$

where $v_i$ [mol/s] is the net veleocity of the i-th reaction, $k_{ai}$ [1/s] is the apparent rate constant of the i-th reaction, $K_{pi}$ [ad] is the equilibrium constant and $K_i$ [ad] is the

adsorption constant of the i-th reaction, $p$ [atm] is the pressure in the gasifier, $P_\phi$ [ad] is the pressure constant, $\phi_{1,0}$ $[mol/mol_{bio}]$ is the specific molar number of carbon at the beginning of the reduction zone, $\rho$ [kg/m$^3$] is the density of the carbon, $d_p$ [m] is the equivalent diameter of the char particle. The equilibrium constants $K_{pi}$ are calculated by JANAF thermochemical tables [144] and the adsorption constants $K_i$ are taken from Reference [171] at a fixed reduction temperature $T$. The apparent rate constants are calculated by the following Arrhenius equation [172]:

$$k_{ai} = A_i \exp\left(\frac{-E_{ai}}{RT}\right) \tag{4.2.16}$$

where $A_i$ [1/s] is the pre-exponential factor of the i-th reaction, $E_{ai}$ [KJ/mol] is the activation energy of the i-th reaction, $T$ is the reduction temperature and $R$ [KJ K$^{-1}$ mol$^{-1}$] is the universal gas constant. $A_i$ and $E_{ai}$ of each reaction were taken from the regression reported in Reference [164]. The specific molar amount of the products at the end of the reduction zone is obtained integrating the following differential equations system from zero to $t_c$:

$$\begin{cases} \frac{d\phi_1}{dt} = v_1 + v_2 + v_3 \\ \frac{d\phi_2}{dt} = -v_2 + 2v_3 - 3v_3 \\ \frac{d\phi_3}{dt} = -2v_1 - v_2 - v_4 \\ \frac{d\phi_4}{dt} = v_2 + v_4 \\ \frac{d\phi_5}{dt} = v_1 \\ \frac{d\phi_6}{dt} = -v_3 + v_4 \end{cases} \tag{4.2.17}$$

The molar flow rate of syngas, char, and water at the end of the reduction zone is assested multipling the specific molar amount of the product for the molar biomass flow in "daf" conditions $\dot{n}_{bio,daf}$ $[mol_{bio}/s]$. The syngas is considered an ideal gas and its $HHV_{syngas}$ is calculated using Equation 3.4.2. An alternative method to calculate the tar mass flow is using the following equation which considers some experimental data:

$$\dot{m}_{tar} = \frac{HHV_{syngas}\dot{V}_{syngas} - \dot{V}_{syngas,exp}HHV_{syngas,exp}}{HHV_{tar,exp}} \tag{4.2.18}$$

where $HHV_{syngas}$ [MJ/Nm$^3$] is the calculated higher heating value of the syngas, $\dot{V}_{syngas}$ [Nm$^3$/s] is the normal volumetric flow rate of the syngas obtained by Equation 4.1.27, $\dot{V}_{syngas,exp}$ is the normalized volumetric flow rate obtained by experimental measures, $HHV_{syngas,exp}$ [MJ/kg] is the experimental syngas higher heating value obtained by gas cromatography analysis and $HHV_{tar,exp}$ [MJ/kg] is the experimental higher heating value of the tar obtained by Mahler bomb analysis.

## 4.3 An application of downdraft stratified modeling

This section investigates two important phenomena related to each other in fixed bed reactors: 1) the influence of biomass loading operations on the reactions of gasification and 2) the presence of the "channels" that modify the gasification conditions.

Since the first utilization of the gasification technology for power production, most gasifiers have been designed to work with continuous loading, but the filling method actually discretizes the charge in a series of small batches. The loading frequency of these batches, as well as other control variables, can deeply influence the gasifier performance and, in particular, the syngas $HHV$ and the tar and water production. Downdraft stratified gasifiers seem to be the most influenced reactors by the loading conditions. This phenomenon is due to the limited thickness and to the superficial placement of the flaming pyrolysis layer in this kind of gasifiers.

This part of the thesis is aimed at investigating the influence of loading conditions on a 250 $kW_{el}$ gasification power plant. Results have shown great variations in most of the plant outputs acquired during the experimental campaign rapresented by five days of tests for each loading condition of 4-second-long and of 15-second-long. The 15-second loading tests showed some scattered results that suggested the coexistence of pyrolysis and combustion zones in the reactor. These phenomena have been explained by the parallel running of two modified mathematical models that were obtained by coupling two kinetical models of gasification describe below. Models results confirmed the presence of "channels" or "chimneys" where the majority of the air passes.

### 4.3.1 Definition of channeling and loading frequency

It is proven that continuous loading of a gasifier reactor avoids strong fluctuations of the gasification performance [6]. These fluctuations are common in batch-working gasifiers as result of the continuous change of the reaction conditions [174]. Unfortunately, the continuous feeding does not guarantee the complete absence of those oscillations. In concrete terms, most of the applications approximate the continuous feeding through a series of small batch loads. Every small load causes a pressure or temperature drop in the reactor and it changes its internal conditions.

The gasifier design influences its sensitivity to operating conditions [21, 5]. The more distant the combustion zone is from the loading one, the less heavily the combustion reactions are influenced by the loading operations.

Stratified downdraft gasifiers are characterized by the proximity of the flaming pyrolysis zone to the top surface; moreover, the drier the biomass is, the thinner the drying zone is [6]. This presumes a higher sensitivity of stratified downdraft gasifiers performance to the variations of loading operations compared to other typologies of reactors.

This part of the thesis is aimed at investigating the influence of the loading frequency on the performance of a stratified downdraft gasifier operating with a very dry biomass. The system analyzed is a 800 $kW_{th}$ power plant able to produce up to 250 $kW_{el}$. The plant has two IC engines which use the filtered syngas as fuel.

During the experimental campaign, the plant was run for five days forcing the auger to load the reactor for 15 seconds every time the laser-meter gave the signal of low bed height. After three days the test was repeated reducing the charging time to 4 seconds. The power output was setted to 160 kWe in order to slow down the loading operations from

the nominal power conditions. Running the plant at partial power output allows precise monitoring of the following parameters: biomass consumption; tar, water and charcoal production; superficial and inner temperatures; impellers spinning velocities and engines power output. Moreover, the $HHV$ of tar and charcoal were evaluated by experimental analysis for both the operating conditions.

Results showed that the loading frequency strongly infleunces the gasifier behaviour. Reciprocal effects between operating variables and loading frequency were observed. A possible explanation of the observed phenomena can be given after looking locally at the processes that occur on the reactor surface when the fresh biomass is loaded. A large amount of biomass can choke the flaming pyrolysis preventing the correct air flux to the zone. The air entering into the reactor is diverted to preferential paths.

The previous phenomenon, well known as "channeling", has been reported in literature [12, 172] and it has been implemented in a model specifically set up for assuming the gasifier composed of two zones with different reaction conditions. The experimental data about water, tar and charcoal were compared with model outputs in order to find out the reaction conditions of the two zones.

### 4.3.2 Materials and methods

The experimental campaign was run on a full scale gasification power plant consisting of a 800 $kW_{th}$ stratified downdraft reactor coupled with two IC engines with power output set to 160 $kW_{el}$. The system was fed with poplar wood chips which are dried with both the exhaust and the cooling air coming from the engines. In order to obtain enough clean gas to avoid frequent maintenance of the engines, the syngas is forced to pass through a cyclone, a water scrubber and a battery of 24 electrostatic filters. The system is the same reported in Chapter 5.

#### Experimental campaign

The whole gasifier-filters-engines system is characterized by a high inertia: the gasifier takes hours to heat up properly and the filtering system discharges the tar produced hours later. For this reason the experimental campaign was done separating the measurements into two different categories: those obtained from the steady state plant (i.e. biomass consumption, syngas flow, temperatures, water production, impellers spinning velocities and power output) and those obtained from the whole experimental campaign (i.e. char and tar productions). The campaign lasted five days for every loading condition. Every day, the steady state measurements were taken after 4 hours from the plant start-up.

#### Measurements

The gas flow rate was measured by a Pitot tube flow-meter inserted in the pipe which connect the filtering system to the engines. The measuring point was placed about the length of 30 diameters of rectilinear pipe away from the closest curve. In this case, the average velocity in the pipe ensures a fully developed turbulent flow of syngas, this guarantees the good reliability of the measurements.

For a precise measurement of the biomass consumption, the tests were started after 4 hours from the plant start-up. During the tests, the dryer was stopped and the reactor was fed with a known quantity of biomass previously dried and weighed.

The average mass of poplar wood chips used for every steady-state test was about 420 kg. In order to maintain the moisture level under control, three samples of biomass were tested for every plant run using a PCE - MB 200 moisture meter. All the tested biomass samples had a moisture content under 10%. The water yield was collected in the settling tank of the water scrubber, then it was discharged to a storage tank with a volume of 1 $m^3$. After every test, the water level was measured and the storage tank was weighed.

The temperatures of the upper zone of the reaction bed were obtained with three N type thermocouples with 6 mm of thickness. The thermocouples were placed 10, 20 and 30 cm from the top of the reaction bed, the thermocouple tips were placed about 3 cm inside the reactor. The top surface temperature in the reactor was measured continuously with a dual laser infrared (IR) thermometer. It has a focus of 50:1 inches and it was fixed on the air inlet passage. The thermometer placement was chosen pointing at the reacting surface and focusing the lasers on the top surface of the reactor for a bed height of incipient loading signal from the laser meter.

The tar and char yields were collected at different points of the filtering system. The charcoal was discharged from the bottom of the reactor and cyclone, while the tar was collected from: 1) the recovery tank of the electrostatic filters and 2) the settling tank of the water scrubber by floating or sinking. These processes of separation and collection avoid an instantaneous monitoring of tar and char yields. For this reason, acquired data about these byproducts refer to five days of experimental campaign. The instantaneous power output as well as impellers spinning velocities were obtained from the software which control the plant operation.

### Modeling

A Matlab$^{TM}$script was used to implement the kinetic mathematical model discussed below. The biomass used was poplar wood chips and Table 4.5 collects its chemical, physical and geometrical properties.

A heuristic upgrading of the model was applied to consider the presence of channels in the 15-second-long loading condition. The channels were modeled considering them as a part of the reactor an they have a total crossing area $A_1$, while the rest of the reactor bed was assumed to have a total crossing area $A_2 = A - A_1$. The biomass consumption in each sub-reactor was considered proportional to its area. A schematical explanation of this concept is reported in Figure 4.3. Each part was simulated with different boundary conditions:

- $ER_1$, $\dot{m}_1 = \dot{m}A_1/A$ for the first part.
- $ER_2$, $\dot{m}_2 = \dot{m}A_2/A$ for the second part.

A method that randomly changed the boundary conditions was applied to verify if the channelling theory could explain both the high water and tar production. Table 4.6 shows the model input parameters adopted in the simulation. Table 4.10 and Table 4.11 show the comparison between experimental data and model outputs and it collects the boundary conditions that better fit with experimental data.

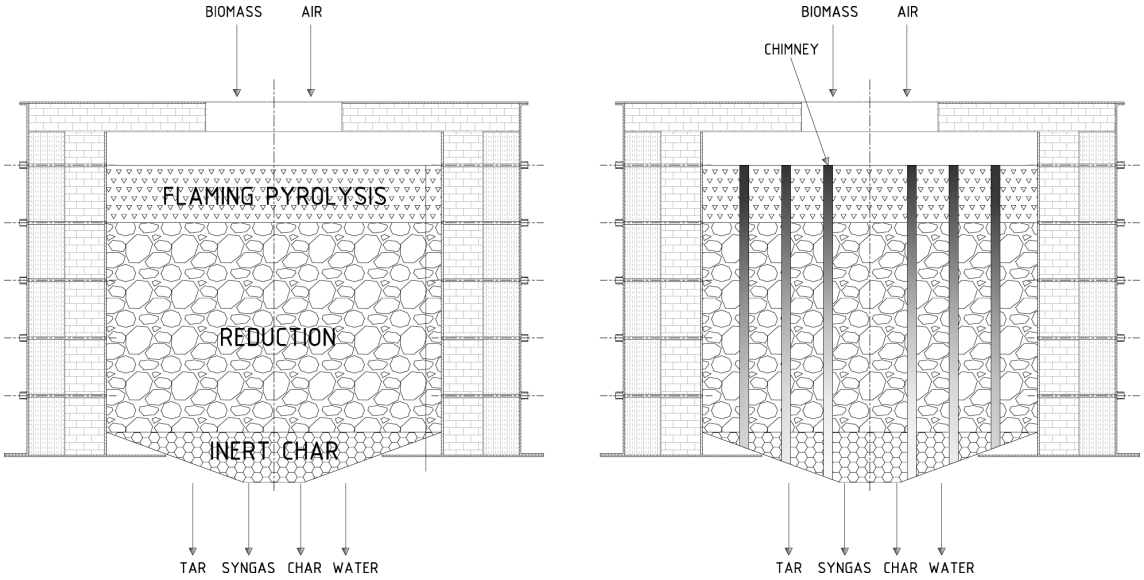


Figure 4.3: Reaction bed condition in the 4-second-long loading test (left) and in the 15-second-long loading test (right)

Table 4.5: Biomass properties

| Poplar wood chip | Proximate analysis (%wt) | | | Composition (%wt) | | |
|---|---|---|---|---|---|---|
| | VM | FC | ASH | $C$ | $H$ | $O$ |
| | 79.1 | 18.1 | 2.75 | 45.1 | 5.74 | 45.63 |
| Chip equivalent diameter | $d_p$ | 0.0156 | $m$ | | | |
| Biomass density | $F_d$ | 0.4 | $kg/m^3$ | | | |
| Biomass void fraction | $F_v$ | 0.63 | - | | | |
| Biomass moisture | $F_m$ | 0.03 | - | | | |

Table 4.6: Model parameters

| Parameter | Symbol | Value | Unit |
|---|---|---|---|
| Gasifier area | $A_g$ | 0.668 | $m^2$ |
| Flaming pyrolysis temperature | $T_s$ | 1173.5 | K |
| Fixed bed height | $H$ | 0.6 | m |
| Biomass coefficient | $\alpha$ | 1.52 | - |
| Biomass coefficient | $\beta$ | 0.67 | - |
| Equivalence ratio | $ER$ | 0.3 | - |
| Reduction temperature | $T$ | 1073.5 | K |
| Pressure in the gasifier | $p$ | 1 | atm |

### 4.3.3 Results and Discussion

#### Temperatures

The thermal stratigraphy of the top part of the gasifier is reported in Figure 4.4. The temperatures are lower than what literature suggests in both the loading conditions. The temperature in the center of the reactor should be higher than what was attained by the thermocouples because the reactor diameter is big and the biomass cannot properly reach the peripheral part of the gasifier. Here the biomass creates a small ash annulus that protects the thermocouples from the higher temperatures in the center of the gasifier. During the plant maintenance operations, the ash layer was measured an it was about 4 cm thick. The small thickness signifies that this phenomenon is neglected in the model.

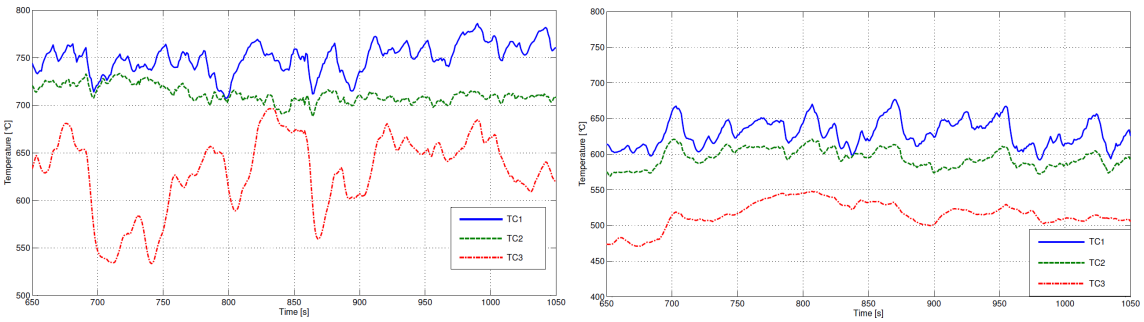


Figure 4.4: Thermal stratigraphy in the 4-second-long loading test (left) and in the 15-second-long loading test (right)

Figure 4.4 shows the different temperature trends of the top of the reactor for the two loading conditions. In the 15 second load feed, the large amount of biomass for every "batch" decreases the reactor temperature as result of the sensible heat adsorbed by the biomass. This chokes the flaming pyrolisys on the top surface of the reactor bed.

The 15-second-long loading test shows lower temperatures and small fluctuations, especially for the thermocouple placed under the flaming pyrolysis zone (TC-3). In fact, the reactor is not able to recover the high temperature suggested by literature for these zones.

The 4-second-long loading condition creates high temperatures and great fluctuations even for the deeper thermocouple. These variations are related to an irregular gasification zone: the peaks width is about 60 seconds. This is the stand-by period for every 5 second run of the mixer.

In the 15-second test, the thermal substratum has a low temperature and it is quite homogeneous. For this reason the mixer does not create significant variations, but during the 4-second test this substratum is characterized by higher temperatures between 500 and 700 $^{o}$ C. These are the extreme temperatures of gasification reactions as reported by Reed and Das [6].

Figure 4.5 shows two trends obtained acquiring the superficial temperature of the reaction bed by the IR thermometer.

The differences between the left part of Figure 4.5 and the right part of Figure 4.5 consist in the maximum temperature reached by the surfaces, moreover the recovery of the temperature after the charge is slower in the 15-second loading condition. This shows 9 big peaks during the 1000 seconds of the screenshot, it results in 15-seconds long loads

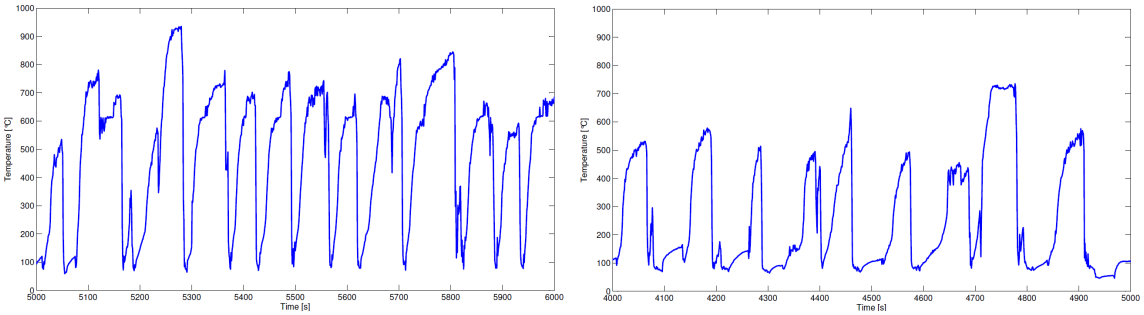


Figure 4.5: The superficial temperature in the 4-second-long loading test (left) and in the 15-second-long loading test (right)

every 111 seconds. This value decreases to an average value of 77 seconds in the 4-seconds loading condition.

In order to estimate the amount of time in which the combustion reactions are locally choked, the temperature trends have been divided in two zones: above and below 250 $^o$C. This value is the average autoignition temperature for wood [39]. For this reason, during the periods with a reactor surface temperature above 250$^o$ C, a wood parcel on the top surface can start its flaming pyrolysis if it is able to reach the right amount of oxidant.

Results of this analysis are reported in Table 4.7. The 4-second loading tests had a surface reactor temperature above the autoignition for 67% of time. During the 15-second loading tests this value was lower (about 39% of time). A lower value can be related to a higher tar production because temperatures under 250 $^o$ C, associated with the choking effect of long loading, generate a reaction more similar to the torrefaction or slow pyrolysis than flaming pyrolysis [175].

Table 4.7: Comparison of the superficial temperatures of the reacting bed

| Variable | Symbol | 4 sec load | 15 sec load | Unit |
|---|---|---|---|---|
| Fraction time over 250$^o$ C | $t_{hot}$ | 67.89 | 38.6 | % |
| Min. average temperature | $T_{min}$ | 42.6 | 31.8 | $^o$ C |
| Max. average temperature | $T_{max}$ | 896 | 739 | $^o$ C |
| Average temperature | $T_{mean}$ | 422 | 259 | $^o$ C |

### Power output and propellers frequencies

The power plant is controlled by a power output basis. Once the power output is set, the controller changes the impellers frequencies in order to maintain the fixed power generation. The controller increases or decreases the amount of syngas drawn from the reactor and sent to the engines. Changing the syngas flow, constantly modifies the reaction conditions. This phenomenon creates oscillations in the propellers frequency and in the instantaneous power output. These oscillations are registered from the controller data logger.

In order to quantify differences of these oscillations under the two loading conditions, the instantaneous values of the impellers spinning frequencies and power output were acquired. The mean value and the standard deviation were calculated and reported in Table 4.8. For the 15-second loading condition, the impellers spin faster on average. This

can be related to a poorer quality of syngas because a grater amount of gas is necessary for the same power output. Moreover, the standard deviation of the spinning frequency is higher in this case and this suggests that the great thermal and physical oscillations on the top of the reactor influence the behavior of the propellers.

Table 4.8: Propellers frequencies comparison

| Variable | Symbol | 4 sec load | 15 sec load | Unit |
|---|---|---|---|---|
| Min. average propellers frequencies | $f_{min}$ | 21.4 | 21.3 | Hz |
| Max. average propellers frequencies | $f_{max}$ | 37.8 | 38.9 | Hz |
| Average propellers frequencies | $f_{mean}$ | 29.9 | 30.78 | Hz |
| St. dev. of the propellers frequencies | $std, f_{mean}$ | 2.71 | 3.08 | Hz |

The result obtained for the power output is different. Table 4.9 shows a lower standard deviation of this parameter in the 15-second loading condition. This phenomenon can be explained looking at the temperature trends in Figure 4.5: during this loading condition the temperatures rise slowly after every reactor fill. For this reason, the impellers are forced to greatly change their spinning velocities as result of the large changes in reactor conditions. Even if the impellers can properly "follow" the changes, they maintain a constant power output.

Table 4.9: Engines power output comparison

| Variable | Symbol | 4 sec load | 15 sec load | Unit |
|---|---|---|---|---|
| Min. average electrical power | $P_{min}$ | 119.5 | 116.6 | kW |
| Max. average electrical power | $P_{max}$ | 207.7 | 204.6 | kW |
| Average electrical power | $P_{mean}$ | 158.2 | 158.5 | kW |
| St. dev. of the electrical power | $std, P_{mean}$ | 4.79 | 4.17 | kW |

### Model and experimental outputs

Table 4.10 and Table 4.11 collect the main outputs for the two different loading conditions compared with the analogous simulated system outputs. The amount of biomass consumed per hour seems to not be influenced by the loading conditions and it depends only on the set power output of the whole system.

The second important group of data acquired is the charcoal production which is similar in the two conditions. This is somehow an unexpected result, because a higher amount of energy was presumed to be discharged by the char in the 15-second loading case. For this reason, the different charcoals had been tested in a bomb calorimeter in order to estimate their higher heating value. The charcoal produced during the 15-second loading tests has a $HHV$ of 24.87 MJ/kg, higher than 17.89 MJ/kg obtained testing the charcoal produced during the 4-second-loading tests. This phenomenon is caused by the discharging system of char which works maintaining a fixed pressure drop at the bottom of the reactor. This method ignores the fact that the char had or had not finished to react.

The water production data can be considered in contrast to the tar data, because a higher equivalence ratio brings to low tar and high water productions due to the preponderance of the combustion reactions. The opposite condition is related to a low equivalence ratio which it produces more tar compared to water. The 15-second loading campaign resulted

in a high production of both water and tar. The scientific explanation results from the "inception" model of the reactor which it simulates a reactor characterized by the coexistence of combustion "channels" in the reactor and the rest of the reactor is at low equivalence ratio conditions.

Table 4.10: Comparison between model outputs and 4-second-long loading experimental data

| Variable | Symbol | Model | Exp. data | Unit |
|---|---|---|---|---|
| Biomass consumption | $\dot{m}_{bio}$ | 519 | 519 | $g/s$ |
| Syngas higher heating value | $HHV_{syngas}$ | 4.99 | 5.25 | $MJ/Nm^3$ |
| Syngas volumetric flow rate | $\dot{V}_{syngas}$ | 112 | 103 | $l/s$ |
| Air volumetric flow rate | $\dot{V}_{air}$ | 80.6 | 91.2 | $l/s$ |
| Char flow rate | $\dot{m}_{char}$ | 5.00 | 6.90 | $g/s$ |
| Tar+water flow rate | $\dot{m}_{tar+water}$ | 11.9 | 12.7 | $g/s$ |
| Cold gas efficiency | $\eta_{gas}$ | 66.5 | 66.6 | % |

Table 4.11: Comparison between model outputs and 15-second-long loading experimental data

| Parameter | Symbol | Value | Unit | |
|---|---|---|---|---|
| Chimney area | $A_1$ | 0.318 | $m^2$ | |
| ER of the chimney area | $ER_1$ | 0.667 | - | |
| Pyrolysis area | $A_2$ | 0.350 | $m^2$ | |
| ER of the pyrolysis area | $ER_2$ | 0.048 | - | |
| Variable | Symbol | Model | Exp. data | Unit |
| Biomass consumption | $\dot{m}_{bio}$ | 531 | 531 | $g/s$ |
| Syngas higher heating value | $HHV_{syngas}$ | 4.22 | 3.97 | $MJ/Nm^3$ |
| Syngas volumetric flow rate | $\dot{V}_{syngas}$ | 122 | 103 | $l/s$ |
| Air volumetric rate | $\dot{V}_{air}$ | 87.9 | 91.2 | $l/s$ |
| Char flow rate | $\dot{m}_{char}$ | 6.80 | 7.77 | $g/s$ |
| Tar+water flow rate | $\dot{m}_{tar+water}$ | 17.3 | 21.8 | $g/s$ |
| Cold gas efficiency | $\eta_{gas}$ | 62.1 | 66.6 | % |

### 4.3.4 Summary

The experimental campaign showed a deep relation between the loading parameters and the performance of the gasifier. Subdividing the loading in small amounts reduces the tar and the water production in the reactor. The results obtained from a 15 second-long loading condition founded a theoretical structure thanks to an "inception" mathematical model. This model, based on the coupled Reed-Wang models, explains the effect of large loads to choke the superficial reactions and to force the air to run through few paths in the reacting bed. This phenomenon creates "channels" with a high equivalence ratio where most of the water is produced, while the rest of the reactor runs with a low equivalence ratio producing a great amount of tar. These observations outline the importance of control parameters and modeling into the design process of gasifier reactors and power plants.

# Chapter 5

# Modeling and simulation wood gasification power plants

Chapter 1 introduces the advantages of gasification applied to electrical power production. However, some aspects decrease the gasifier efficiency together with some issues related to the power plant that can nullify the advantages previously discussed. For these reasons it is vital to monitor how the power plants run in order to keep the efficiency, tar and char disposal under control.

Some problems occurs when the power plant monitored has not been designed for a complete acquisition of the necessary thermochemical variables. Especially for medium or large scale plants, every hour of plant stoppage is paid in terms of loss of earnings. For this reason, the experimental campaign needs to be carried out when the plant working without interfering with the routine operations if possible. Moreover, the larger the plant is the higher the inertia of the whole system is. This forces an adoption of investigation methods that take into account this peculiarity. In this Chapter the modeling and the simulation of conventional and advanced $250kW_{el}$ biomass power plants is discussed.

## 5.1 A conventional medium scale downdraft stratified power plant modeling and comparison with experimental results

The plant investigated consists of a stratified downdraft gasifier coupled with two diesel IC engines. As previously discussed in Chapter 3, these engines require a tar-free gas which avoids fouling problems in the compressor, valves, combustion chambers and turbine. For this purpose, a downdraft gasifier is the best choice due to the low tar content in its syngas [6]. The stratified gasifier represents the simplest design for a downdraft reactor. It consists in a refractory cylinder with no nozzles and no reduction of diameters. Both air and wood fuel enter from the open top and pass through different zones of reaction as illustrated in Figure 5.1. Several researches [21, 176, 161, 162, 93, 144, 177] suggest different approaches to the stratified downdraft gasifier modeling. A simple model of the process has been set up starting from energy balances as reported by [21]. The model implemented in this section is based on energy and mass balance equations and it is able to predict some of the thermochemical variables which can be measured in situ. The analyzed power plant is depicted in Figure 5.2 and consists of a stratified downdraft gasifier designed to produce up to 800 $kW_{th}$ which is fed with poplar wood chips. Two diesel engines connected to

the gasifier produce up to 125 $kW_{el}$ each. A cylindrical dryer is used to reduce the total moisture of the biomass to a value of 10-15 % using the exhaust and the cooling air of the engines. Before reaching the engines, the syngas is cleaned by a cyclone, a water scrubber and a battery of 24 electrostatic filters. The engines need 4 to 8 l/h of diesel each to ensure the ignition of the whole fuel mixture. This fuel fraction can be switched to vegetable oil after a start-up period. The gasifier is affected by an excessive production of tar and charcoal, these are removed during the gas purifying process. In spite of the presence of the cleaning phases described above, a part of the tar pass through the filters and go into the engines. This phenomenon decreases the durability of the engines and causes the frequent shutdowns of the plant, this put in place frequent cleaning operations. In order to investigate the overproduction of tar, the first step taken was to measure the thermochemical variables of the process. The efficiency of the gasifier was calculated via experimental analysis setting the electrical power output to 200 $kW_{el}$ and the experimental variables were compared with the outputs of the model.

The obtained results were used to find better operating conditions related to low tar production. Results can also be used as the basis for future reactor design improvements. Some data (i.e. biomass consumption) was calculated in different ways, such as: model prediction, experimental campaign and mass balance equation. Differences between these values are being used for validating the effectiveness of the experimental procedures outlining the parameters that need to be acquired with an alternative method.

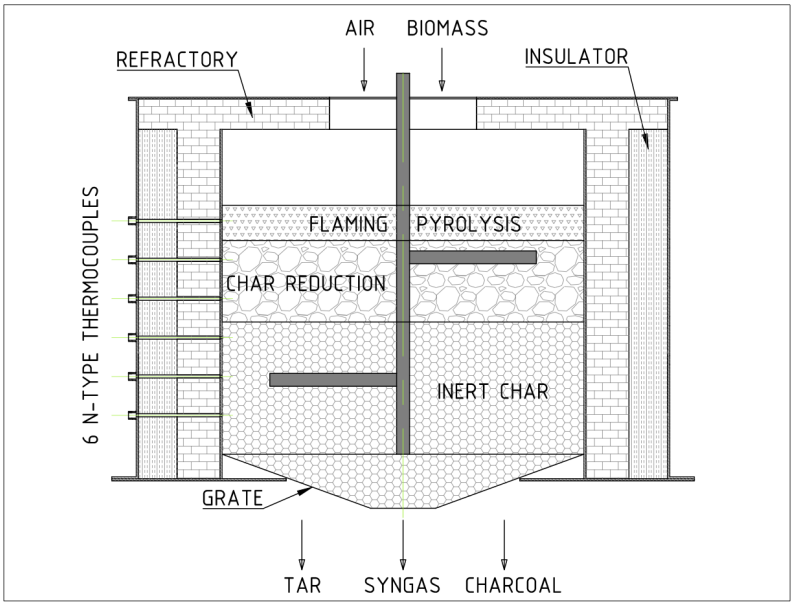


Figure 5.1: Stratified downdraft reactor

### 5.1.1 Energy and mass balance model

#### The power generation unit model

This section describes the mathematics of the internal combustion engines connected to the alternators in order to produce electrical energy. The thermal power going into the engines is calculated by Equation 5.1.1:

$$\dot{Q}_{eng} = \frac{P_{el}}{\eta_{eng}\eta_{alt}} \tag{5.1.1}$$

The engines are supplied by the syngas and diesel oil. The thermal power generated by the syngas combustion is given by Equation 5.1.2 and the thermal power generated by the diesel oil combustion is given by Equation 5.1.3.

$$\dot{Q}_{syngas} = \dot{Q}_{eng} - \dot{Q}_{oil} \tag{5.1.2}$$

$$\dot{Q}_{oil} = \dot{m}_{oil} HHV_{oil} \tag{5.1.3}$$

The volumetric flow rate of the syngas and the mass flow rate of the diesel oil are calculated using their higher heat of combustion as follows:

$$\dot{V}_{syngas,dry} = \frac{\dot{Q}_{syngas}}{HHV_{syngas,dry}} \tag{5.1.4}$$

$$\dot{m}_{oil} = \rho_{oil}\dot{V}_{oil} \tag{5.1.5}$$

Moreover, the air/fuel mixture flow rate which go into the engines is calculated as follows [21]:

$$\dot{V}_{engine} = \frac{NVn}{120} \tag{5.1.6}$$

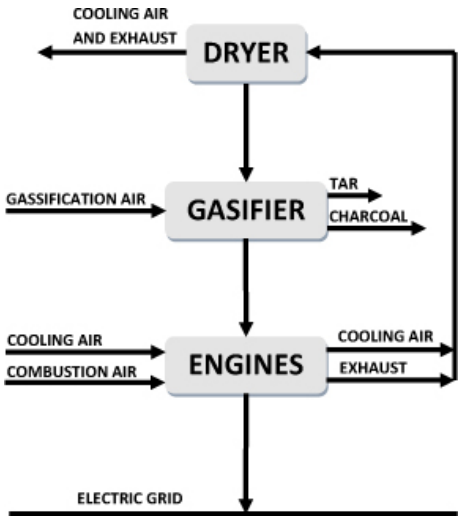


Figure 5.2: Power plant basic layout

The volumetric efficiency of the engines can be obtained combining Equation 5.1.4 and Equation 5.1.7. The air flow rate to the engines are calculated by Equation 5.1.8:

$$\dot{V}_{syngas} = \frac{\dot{V}_{engine}\eta_{vol}}{1+\phi_{eng}} - \dot{V}_{oil} \tag{5.1.7}$$

$$\dot{V}_{air,engine} = (\dot{V}_{oil} + \dot{V}_{syngas})\phi_{eng} \tag{5.1.8}$$

Table 5.1 reports the design parameters of the power generation unit.

Table 5.1: Power plant parameters

| Description | Symbol | Value |
|---|---|---|
| Number of engines | N | 2 |
| Displacement | $V_{eng}$ | 0.0129 $m^3$ |
| Nominal rpm | n | 1 500 rpm |
| Air to fuel ratio | $\phi_{eng}$ | 1.10 |
| Nominal volumetric efficiency | $\eta_{vol}$ | 1.11 |
| Maximum electrical power | $P_{max}$ | 320 kW |
| Nominal electrical power | $P_{nom}$ | 250 kW |
| Engines nominal efficiency | $\eta_{eng}$ | 29.4% |
| Alternator efficiency | $\eta_{alt}$ | 0.95 |
| Diesel oil higher heat of combustion [178] | $HHV_{oil}$ | 42 MJ/N$m^3$ |
| Diesel oil density [178] | $\rho_{oil}$ | 830 kg/$m^3$ |
| Diesel oil volumetric flow rate | $\dot{V}_{oil}$ | 8 l/hour |

### Gasifier Model

The biomass consumption is calculated as follows:

$$\dot{m}_{bio} = \frac{\dot{Q}_{syngas}}{\eta_{gas} HHV_{bio,ar}\phi_{eng}} \tag{5.1.9}$$

The higher heating value of biomass is calculated by the following equation, which takes the total moisture percentage ($M$) of the feedstocks into account [179]:

$$HHV_{bio,ar} = HHV_{bio,db}(1 - M/100) - r * M \tag{5.1.10}$$

The ultimate analysis of the biomass, reported in Table 5.2, was used to obtain the $HHV_{bio,db}$ by the Equation 2.4.10.

Table 5.2: Biomass ultimate analysis

| Element | C | H | S | O | N | M | Ash |
|---|---|---|---|---|---|---|---|
| Weight fraction% | 46.0 | 5.86 | 0.00 | 44.03 | 0.58 | 1 | 2.75 |

The mass flow rate of the air entering into the gasifier is given by Equation 5.1.11 derived by [6, 21]:

$$\dot{m}_{air,gas} = m_{da} * \dot{m}_{bio} * ER \tag{5.1.11}$$

For these kind of reactors, the mass of charcoal discharged can be assumed to be equal to 10% of the entering biomass [6, 21] and the tar production can be calculated assuming that 2 g of tar are contained into each N$m^3$ of syngas generated [6, 21]. Poplar wood chips are used in this study. Table 5.3 summarizes the design parameters of the gasifier.

Table 5.3: Gasifier design parameters

| Description | Symbol | Value |
|---|---|---|
| Gasifier nominal cold gad efficiency | $\eta_{gas}$ | 80% |
| Internal diameter | D | 0.92 m |
| Gasifier bed height | H | 0.6 m |
| Biomass higher heating value, dry based | $HHV_{bio,db}$ | 19.33 MJ/N$m^3$ |
| Biomass total moisture | $M$ | 1% (very dry) |
| Water latent heat [46] | $r$ | 2.257 MJ/kg |
| Stoichiometric air-biomass ratio [6] | $m_{st}$ | 6.36 $kg_{air}/kg_{bio}$ |
| Equivalence ratio [128, 6] | $ER$ | 0.3 |

### 5.1.2 Experimental analysis

At the beginning of the project, the thermochemical data were largely insufficient. For this reason the power plant was equipped with instruments measuring the air and gas flow rates, the biomass consumption, reactor temperatures, tar and charcoal productions. All of these measurements permit a more controllable gasification process. Moreover, they can also be used to compare ideal model results to the system values.

#### Gas flow rate

The gas flow rate was measured by introducing a Pitot tube in the syngas intake pipe of each engine. The data logger, connected to the Pitot, was calibrated by syngas density and temperature. The Pitot acquires pressure values from the center of the gas pipe. More than 30 diameters of rectilinear pipe separate the acquiring section from the closer bent. For common spinning values of the fans moving the syngas, the average velocity in every pipe ranges between 3.6 m/s and 15.8 m/s which corresponds to Reynolds values ranging between 2.1x$10^4$ and 7.6x$10^4$. This ensures a fully developed turbulent flow of syngas at 310 K.

#### Air flow rate

The air intake is composed of different parts connected to a central pipe. This architecture creates several secondary air intake, i.e. the chimney, the auger feeder and the hole for the laser meter. A proper assessment of the pressure drop from the outside to the inside of the reactor is not possible. The air intake has a large diameter and is short in length. Taking this into account, the choice of Venturi or diaphragms for the flow rate measurement are avoided. In addition, the high temperatures, dust and continuous biomass crossover can interfere with ultrasonic flowmeters.

When the gasifier is running, the reactor produces syngas and the mass flow changes passing through the reactor. Problems related to the inlet flow measurements can only be

solved by correlating the inlet pressure drop to the analogous flow data, acquired by the Pitot, when the gasification process is turned down.

Once the reactor had been turned off, it can be considered cold two days later. A differential manometer is plugged into the air inlet duct. Fans draw air from the outside through the gasifier and the filters, then the air is sent to the engines. Since the gasifier is cold, no gas is produced in the reactor, therefore the air drawn in the gasifier and the air flow rate sent to the engines is the same. This procedure allows us to correlate every pressure drop to a flow rate value. Once the system is turned on, the correlation continues and indicates the actual air flow rate entering the reactor. Figure 5.3 shows the correlation between the pressure drop and the flow rate at the air inlet duct, the value related to the 200 $kW_{el}$ is indicated.

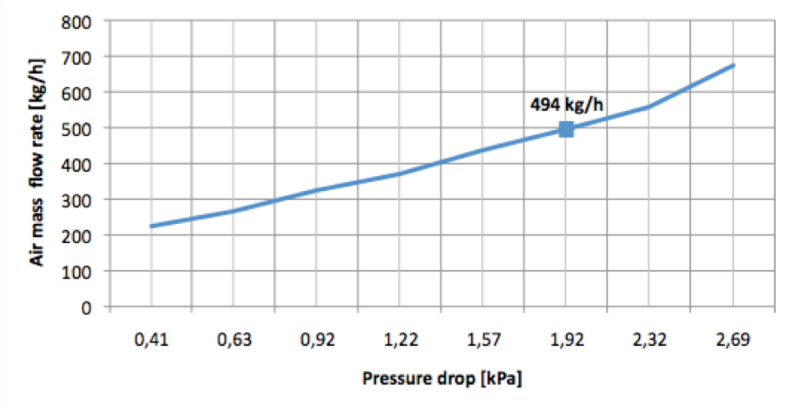


Figure 5.3: The air pressure-flow correlation

### Biomass consumption and moisture content

When the steady-state is reached about four hours after the plant start-up, the volume of biomass entering and exiting the dryer is the same assuming that the drying process reduce the water content of the fuel without reducing the particle volume. The mass flow rate of the biomass is obtained calculating the time spent $t$ [s] to consume an amount of wet biomass $m_{in}$ [kg] charged in the dryer under steady-state operating conditions.

A sample of this fuel amount is analyzed using a PCE - MB 200 moisture meter for calculating the initial moisture content. Once the biomass starts exiting the dryer, another sample is tested. The mass flow rate can be calculated as follows:

$$\dot{m}_{bio} = m_{fin}/t \tag{5.1.12}$$

$$m_{fin} = \frac{m_{dry}}{1 - \theta_{fin}} \tag{5.1.13}$$

$$m_{dry} = m_{in}(1 - \theta_{in}) = m_{fin}(1 - \theta_{fin}) \tag{5.1.14}$$

where $\theta$ indicates the moisture, the subscript $in$ indicates "initial" (before the drying process) and the subscript $fin$ indicates "final" (after the drying process).

### Temperatures

The reactor was equipped with six N type thermocouples with a diameter of 3 mm. A data logger was used in order to constantly record the six different temperatures plus the ambient temperature during the tests. The thick diameter of thermocouples guaranteed a good mechanical resistance, even in the high temperature zones. The thermal stratigraphy is used to control the process and to indicate the thickness and placement of the different zones in the reactor. The temperature data will be used in more detailed models to specify the different reactions taking place in the gasifier.

### Tar and charcoal

For a complete understanding of the process, an assessment of all byproducts is needed. The char is discharged from the bottom of the gasifier as well as from the cyclone. The tar is discharged by the filtering system. If the reactor starts to produce more tar, the excessive production will be read minutes after when the tar is collected by the filters and sent to the discharge tank.

All of these systems are electronically controlled, therefore they work discontinuously. For this reason, a real time control of the tar and charcoal production is not possible. The simplest solution consists in measuring the total amount of products generated during an entire test.

### Syngas composition

For the entire power output range from 40 $kW_{el}$ to 250 $kW_{el}$, a syngas sample has been analyzed. The gas samples were taken using vacuum cylinders connected to the gas pipe through a glass tank. The tank was pre-filled with syngas coming from the plant. This procedure avoids the possibility of the air contamination into the syngas sample. The gas-chromatography results of the 200 $kW_{el}$ sample are reported in Table 5.6. The $HHV$ of the syngas has been obtained from Equation 3.4.2

## 5.1.3 Results

The system was set at 200 $kW_{el}$ and the simulated results were compared to the experimental data. Two different tests were implemented:

- The model was set with the experimental values of $HHV_{syngas}$ and $\eta_{gas}$. The model results are reported in Table 5.4 and are compared to the experimental data.
- The model was set with the design $HHV_{syngas}$ and $\eta_{gas}$. Table 5.5 shows the model results and the experimental data are compared to these results.

The "gas cold" efficiency of the gasifier calculated by experimental data is about 38.3 %. In Table 5.4, $\Delta$ [%] is the model percentual error related to experimental data. The experimental value of the $HHV_{syngas}$ was calculated considering the syngas composition and the $HHV$ values of every combustible component as shown in Table 5.6.

Table 5.4: Energy balance modeling predictions Vs. experimental data

| Variable | Model | Experimental | Δ |
|---|---|---|---|
| $\eta_{gas}$ [%] | 38.3 | 38.3 | 0 |
| $HHV_{syngas}$ [MJ/N$m^3$] | 4.59 | 4.59 | 0 |
| $\dot{m}_{bio}$ [kg/h] | 311 | 261 | +16% |
| $\dot{V}_{air}$ [kg/h] | 555 | 468 | +19% |
| $\dot{V}_{syngas}$ [kg/h] | 496 | 417 | +19% |

Table 5.5: Design-based model Vs. experimental data

| Variable | Model | Experimental | Δ |
|---|---|---|---|
| $\eta_{gas}$ [%] | 80 | 38.3 | -52% |
| $HHV_{syngas}$ [MJ/N$m^3$] | 5 | 4.59 | -8% |
| $\dot{m}_{bio}$ [kg/h] | 149 | 261 | +75% |
| $\dot{V}_{air}$ [kg/h] | 237 | 468 | +97% |
| $\dot{V}_{syngas}$ [kg/h] | 455 | 417 | -8% |

Table 5.6: Syngas composition

| GAS | %Vol. | HHV[MJ/N$m^3$] [173] |
|---|---|---|
| $CO$ | 17.9 | 12.62 |
| $H_2$ | 12.3 | 12.75 |
| $CH_4$ | 2.80 | 39.72 |
| $N_2$ | 55.6 | / |
| $CO_2$ | 10.54 | / |
| $O_2$ | 1 | / |

### 5.1.4 Summary

The proposed model is able to predict the behavior of a gasifier with a maximum error of 19%. This error cannot be reduced due to the initial hypothesis of low tar and charcoal production as suggested by [6, 21, 22, 128]. The tar overproduction involves a discharge of not reacted chemical energy. This phenomenum reduces the $HHV$ of the syngas causing the decrease of the "cold gas" efficiency. Comparing the results of the model set with the design inputs ($HHV_{syngas}$ and $\eta_{gas}$) to the real experimental data, it can be noted that the system is far from its optimal conditions. The experimental $HHV_{syngas}$ is lower than the design one, this occurs because part of the chemical energy of the biomass is discharged in tar and charcoal as previously described, furthermore the air excess (97%) dilutes the syngas and increases the combustion reactions. The experimental $\eta_{gas}$ is lower than the design one because the $HHV_{syngas}$ and the syngas flow rate decrease (8%) and the biomass consumption increases (75%).

Both sensitivity analysis and model versus experimental comparisons are significantly influenced by the reliability of the experimental data. The main errors in the air and gas flow rate analysis come from acquiring the single values of fluctuating variables instead of taking the average one. The main errors in the biomass flow rate are caused by the intermittent operation of the dryer. The dryer contains a volume of biomass several times greater than the amount used for the single tests.

Moreover, the rheology of wet and dry biomass is different. Due to the control method of the dryer, very big batches of wet biomass is charged into it. The biomass creates a compact pile interrupting the charging even if the rest of the dryer is not full. For these reasons the charging and discharging of the dryer are intermittent. This reduces the reliability of the method adopted for biomass consumption measurement. For a better control of the process, a new dryer has been designed. The plant can be easily switched from the main dryer to the new one. The new machine processes small amounts of biomass, about 1 $m^3$. The speed of the spinning plates and the hot air flow rate can be controlled to reach the desired moisture content. The biomass consumption will be obtained calculating the time spent to consume all the cubic meters of biomass charged in the dryer. The major advantages of using this model include the possibility to monitor the system under different conditions, i.e. by changing the power output of the engines. For every condition, the model indicates how far the system is running away from the theoretical conditions.

If the optimum working point identified will not coincide with the condition of nominal power output, the system will be forced to run with limited power. A possible solution for running the engines with full power adding more diesel or vegatable oil without demanding more syngas from the reactor, consists of installing an extra throttle between the reactor and the engine. The engine compressor draws both air and syngas, so the throttle could modify the air-gas ratio.

The tar overproduction could be related to the air excess due to the biomass size. The system uses wood chips with a high content of very small pieces similar to sawdust. The air hardly penetrates the compact biomass bed. When it finds preferential passages the stoichiometric conditions may differ from zone to zone.

The reactor dimensions, reported in Table 5.3, indicate very large and thin zones. Due to these dimensions, there is a risk that some of the biomass reagents will mix with another zone. Moreover, the intermittent loading of the biomass in the reactor can temporarily extinguish the flaming pyrolysis every time the fresh fuel hits the reaction bed.

These phenomena have inspired the "inception" code reported in Chapter 4. This mathematical model has been designed in order to predict the presence of channels in the biomass reacting bed. In addition, the study reported in Chapter 4 investigated the influence of the charging time on the performance of the reactor.

## 5.2 Modeling and simulation of a DG-SOFC-MGT hybrid system

Most of gasifiers for electrical and CHP applications are commonly coupled with Organic Rankine Cycle (ORC) systems, IC engines, turbogas, EFGT or Stirling engines [6, 21, 29, 30, 180]. However, the efficiency of these systems is lower compared to some advanced power generation systems such as Molten Carbonate Fuel Cells (MCFC) [20, 79], Solid Oxide Fuel Cells (SOFC) [80, 181, 182] or SOFC coupled with Micro Gas Turbine (MGT) [183, 84, 85, 86, 184, 81, 82, 185, 186, 187]. For this kind of systems, downdraft gasifiers are very suitable because creates a syngas with low tar and particulate content compared to updraft, crossdraft or fluized bed gasifiers [6, 21, 47].

This feature optimizes the performance and the reliability of the SOFC-MGT subsystem that operates properly with a clean syngas fuel [188]. The syngas obtained from the gasification process is stored and used in the SOFC-MGT unit able to produce electrical and thermal energy. On one hand, the syngas storage tanks allow to all the subsystems to operate in their optimal point, on the other hand it avoids to switch off the power production every time the maintenance operations of the gasifier are required.

This management preserves SOFC and MGT reliability. However, it is difficult to size the storage, infact an oversized storage volume rises the systems costs and an undersized storage volume reduces or nullifies the time available for the maintenance and the advantages of the subsystems operation at a fixed point. For this reason, the storage has been designed taking into account the tank pressure, the electrical power production of SOFC-MGT unit and the time required for the scheduled stops of the gasifier for maintenance operations.

The mathematical model of the gasifier was developed and it was validated using the experimental data acquired from a DG power plant with nominal power of 250 kW [168]. The mathematics of the SOFC-MGT unit and auxiliary subsystems was taken from literature. The overall model was implemented in Matlab Simulink$^{TM}$ software environment in order to simulate the operation of the hybrid system over a year long period. The efficiency of every subsystem was calculated, in addition the electrical conversion performance of the whole system was estimated under different conditions of biomass choice and moisture content from 5 to 30%. The following types of wood biomasses was considered: poplar wood chips, peach tree wood chips and vineyard prunings. For every simulations, the annual energy production was estimated. Furthermore, the behaviour of the storage sub-system has been investigated.

### 5.2.1 System modeling and simulation

The system layout is reported in Figure 5.4. The most important components are:

- **Dryer:** In this device, the moisture of the inlet biomass is reduced using the sensible heat of the syngas.

- **Downdraft gasifier:** The gasifier is equipped with a subsystem for the syngas treatment composed by a cyclone, an heat exchanger, a scrubber and an electrostatic filters.
- **Syngas storage:** There is 5 tanks for a total volume of 500 $m^3$.
- **SOFC-MGT unit:** This subsystem is connected to the electrical grid by an inverter and an alternator.

The humid biomass is introduced in the dryer where a heat exchanger heats the biomass even it reach the desidered value of moisture. This device allows to increase the gasifier efficiency and it cools down the syngas. After the moisture reduction, the biomass reacts inside the gasifier with the inlet air.

The raw syngas has a temperature of about 600 $^o$C, it is dusted in the cyclone then it is cooled in a heat exchanger and in a scrubber until it reaches a temperature of about 50 $^o$C. In the scrubber subsystems, the water and tars inside the syngas are discharged. An electrostatic filter purifiers furthermore the syngas which it goes first into the compressor 1 and then into the storage system. This one is composed of an inlet manifold, 5 storage tanks and an outlet manifold.

The compressor 2 sends the syngas to the SOFC stack. In this device, the fuel reforming occurs at the anode and there is a recirculation of the 20% of the anode exhaust to increase the fuel reforming performance. The anode exhaust is used to preheat the syngas inlet flow then it is finally burned in the MGT burner together with the cathode exhaust. The air required for the electrochemical reaction is compressed and preheated in the recuperator of the MGT and in the air preheater of the SOFC.

The SOFC stack generates DC current which it is converted in AC current by the inverter and it is sent to the electrical grid. The MGT drags the air compressor and the remaining mechanical energy is converter in electrical energy by an alternator.

### Gasifier modeling

The kinetic model explained in Chapter 4 was applied to simulate the gasifier. Table 5.7 resumes the parameters of the gasifier model. Tables 5.8, 5.9 and 5.10 present the proprieties of poplar wood chips, peach tree wood chips and vineyard prunings. These parameters are obtained by experimental analysis. The maintenance of the DG has taken into account setting it to 12 hours every 120 hours of operation. With these conditions, the DG works about 8000 hours a year. Further assumptions of the model are: fixed tar production and the sensible heat of the syngas is sufficient to properly dry up the biomass. Other features of the model adopted and plant investigated are reported in [168] and [156].

### Compressor and storage system modeling

To compress the syngas produced by the gasification, a polytropic compression is considered. The electrical power required for compression given by [189]:

$$P_{comp} = \frac{\dot{n}_{gas} L_{comp,is}}{\eta_{comp}} = \frac{\dot{n}_{gas}}{\eta_{comp}} \frac{mRT_{in}}{m-1} \left[ 1 - \left( \frac{p_{out}}{p_{in}} \right)^{\frac{m-1}{m}} \right] \tag{5.2.1}$$

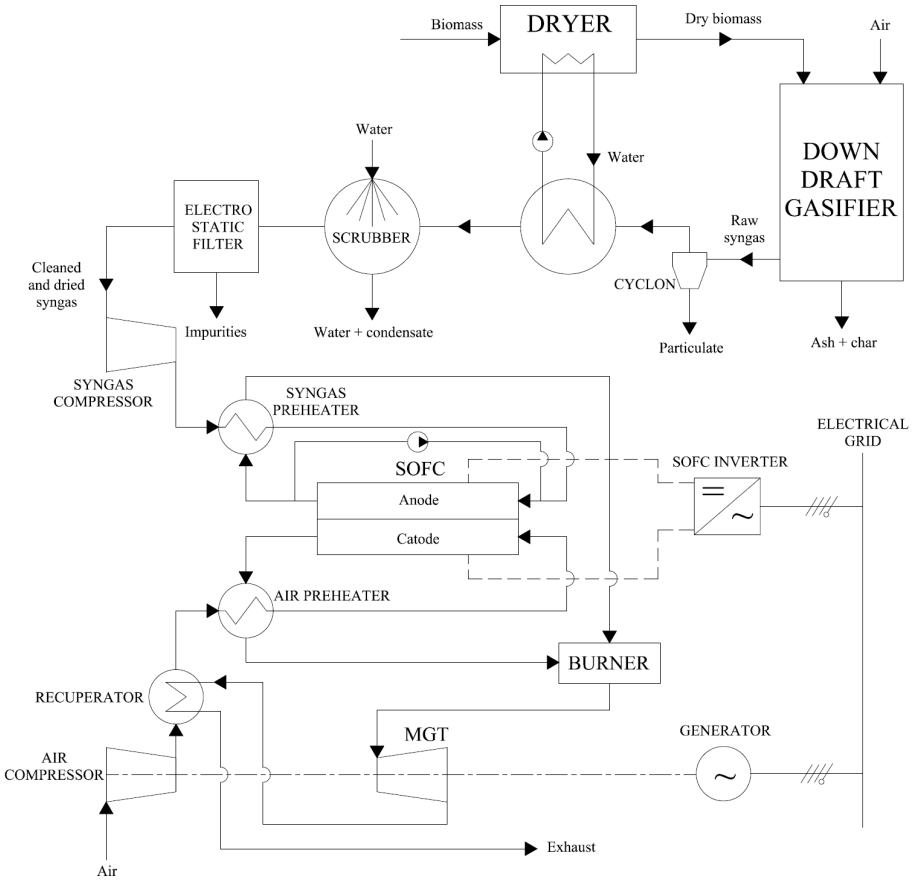


Figure 5.4: Basic layout of the DG-SOFC-MGT system

Table 5.7: Gasifier model parameters

| Description | Symbol | Value |
|---|---|---|
| Biomass consumption | $\dot{m}_{bio}$ | 187 kg/h |
| Gasifier cross area | $A_g$ | 0.668 $m^2$ |
| Flaming pyrolysis temperature | $T_p$ | 1173.5 K |
| Char reduction temperature | $T_c$ | 1073.5 K |
| Fixed bed height | H | 0.6 m |
| Pressure | p | 1 atm |
| Equivalence ratio | ER | 0.25 |
| Gasifier and filters self consumption | $P_{DG,self}$ | 12.5 kW |
| Cyclic operation hours | $h_{operation}$ | 120 h |
| Cyclic maintenance hours | $h_{maintenance}$ | 12 h |

Table 5.8: Poplar wood chips proprieties

| Description | Symbol | Value |
|---|---|---|
| Bulk density | $F_d$ | 0.4 kg/m$^3$ |
| Void fraction | $F_v$ | 63 % |
| Total moisture | $M$ | 5-30 % |
| Chip length | $L_{chip}$ | 0.02 m |
| Chip width | $W_{chip}$ | 0.02 m |
| Chip height | $H_{chip}$ | 0.005 m |
| Carbon content (dry basis) | $C_{db}$ | 46.4 % |
| Hydrogen content (dry basis) | $H_{db}$ | 5.90 % |
| Nitrogen content (dry basis) | $N_{db}$ | 0.58 % |
| Oxygen content (dry basis) | $O_{db}$ | 44.4 % |
| Ash content | $ASH$ | 2.75 % |
| Higher heating value (dry basis) | $HHV_{db}$ | 15.7 MJ/kg |

Table 5.9: Peach tree wood chips proprieties

| Description | Symbol | Value |
|---|---|---|
| Bulk density | $F_d$ | 0.4 kg/m$^3$ |
| Void fraction | $F_v$ | 63 % |
| Total moisture | $M$ | 5-30 % |
| Chip length | $L_{chip}$ | 0.02 m |
| Chip width | $W_{chip}$ | 0.02 m |
| Chip height | $H_{chip}$ | 0.005 m |
| Carbon content (dry basis) | $C_{db}$ | 43.2 % |
| Hydrogen content (dry basis) | $H_{db}$ | 4.98 % |
| Nitrogen content (dry basis) | $N_{db}$ | 0.60 % |
| Oxygen content (dry basis) | $O_{db}$ | 47.49 % |
| Ash content | $ASH$ | 3.72 % |
| Higher heating value (dry basis) | $HHV_{db}$ | 15.4 MJ/kg |

Table 5.10: Vineyards prunings proprieties

| Description | Symbol | Value |
|---|---|---|
| Bulk density | $F_d$ | 0.4 kg/m$^3$ |
| Void fraction | $F_v$ | 63 % |
| Total moisture | $M$ | 5-30 % |
| Chip length | $L_{chip}$ | 0.02 m |
| Chip width | $W_{chip}$ | 0.02 m |
| Chip height | $H_{chip}$ | 0.005 m |
| Carbon content (dry basis) | $C_{db}$ | 44.2 % |
| Hydrogen content (dry basis) | $H_{db}$ | 4.88 % |
| Nitrogen content (dry basis) | $N_{db}$ | 1.03 % |
| Oxygen content (dry basis) | $O_{db}$ | 46.58 % |
| Ash content | $ASH$ | 3.28 % |
| Higher heating value (dry basis) | $HHV_{db}$ | 17.9 MJ/kg |

where $m$ is the polytrophic coefficient, $R$ is the universal gas constant equal to 8.314 J mol$^{-1}$ K$^{-1}$, $T_{in}$ is the gas inlet temperature assumed to be equal to 50 $^{o}$C, $p_{in}$ and $p_{out}$ [atm] are the gas inlet and outlet pressures, $\dot{n}_{gas}$ [mol/s] is the gas molar flow and $\eta_{comp}$ is the compressor efficiency available from manufacturer's data. The maximum pressure value inside the storage system is necessary to design properly the tanks and the compressor. Assuming ideal gas hyphotesis and a constant temperature $T_s$ of the storage of 25 $^{o}$C, the pressure inside the tanks is calculated by the ideal gas law:

$$p_s = \frac{nRT_s}{V} \tag{5.2.2}$$

where $n$ [mol] are the moles of syngas inside the tanks and $V$ [m$^3$] is the storage total volume. Assuming a value of the initial syngas moles $n_{in}$ inside the storage, the moles of syngas at the time $T$ [s] is given by:

$$n = n_{in} + \int_0^T \left(\dot{n}_{in,s}(t) - \dot{n}_{out,s}(s)\right) dt \tag{5.2.3}$$

where $\dot{n}_{in,s}(t)$ and $\dot{n}_{out,s}(t)$ [mol/s] are the inlet and the outlet molar flow at the istantaneous time $t$ [s]. Table 5.11 reports the parameters of the storage and compressor models adopted in the simulations.

Table 5.11: Storage and compressor model parameters

| Description | Symbol | Value |
|---|---|---|
| Politropic exponent of the syngas | $m$ | 1.33 |
| Syngas compressor efficiency | $\eta_{comp}$ | 92 % |
| Tanks temperature | $T_s$ | 298.15 K |
| Initial syngas amount in the tanks | $n_{in}$ | $3x10^4$ mol |
| Number of tanks | $N$ | 5 |
| Total tanks volume | $V$ | 500 m$^3$ |

### SOFC modeling

The SOFC model was developed by Bang-Møller and Rokni [85]. This model do not take into account the recirculation of the exhaust in the anode. To overcome this issue, the reforming model presented by Rami Salah El-Emam et al. [82] was applied. The syngas refoming occurs near the anode where it take place the reforming of the methane (Equation 5.2.4) and the water-gas shift of the carbon monoxide (Equation 5.2.5). The electrochemical reaction takes place both in the anode and in the cathode.

At the anode, the hydrogen reacts with the oxigen ions to form water and electrons following the Equation 5.2.6. At the cathode, the oxigen of the inlet air reacts with the electrons from the anode (Equation 5.2.7) to form oxygen ions that are direct to the anode through the solid oxide electrolyte. Equation 5.2.8 resumes the overall electrochemical reaction.

$$CH_4 + H_2O \rightarrow CO + 3H_2 \tag{5.2.4}$$

$$CO + H_2O \rightarrow CO_2 + H_2 \tag{5.2.5}$$

$$H_2 + O^{2-} \rightarrow H_2O + 2e^- \tag{5.2.6}$$

$$\frac{1}{2}O_2 + 2e^- \rightarrow O^{2-} \tag{5.2.7}$$

$$H_2 + \frac{1}{2}O_2 \rightarrow H_2O \tag{5.2.8}$$

The mathematical modeling of reforming and electrochemical reactions are explained in References[82] and [85]. Using these models, it is possible to calculate the electrical power production and the electrical conversion efficiency for a given syngas inlet flow with a specific composition. The SOFC model parameters adopted in the simulations are reported in Table5.12.

### MGT modeling

Modeling of gas turbines is well described in literature. The reader is referred to Bang-Møller and Rokni [85] for details. Characteristics of the turbine and others components connected to the MGT are listed in Table 5.13.

Table 5.12: SOFC model parameters

| Description | Symbol | Value |
|---|---|---|
| Fuel utilization factor | $U_f$ | 0.75 |
| Recirculation factor | $r$ | 0.2 |
| Operating temeprature | $T_{sofc}$ | 1073.15 K |
| Anode pressure loss | $\Delta p_a$ | 500 Pa |
| Cathode pressure loss | $\Delta p_c$ | 1000 Pa |
| Anode pressure loss | $\Delta p_a$ | 500 Pa |
| Current density | $i$ | 300 mA/cm$^2$ |
| Active cell area | $A_cell$ | 81 cm$^2$ |
| Cells for each stack | $n_{cell,stack}$ | 75 cells |
| Number of stacks | $n_{stack}$ | 145 stacks |
| Cathode air excess | $vent$ | 1.4 |
| Pressure ratio | $PR$ | 2.5 |
| Steam to carbon coefficient | $STC$ | 2.5 |
| Electrochemical parameters taken from [85] | | |

## 5.2.2 Simulation results

The SOFC-MGT unit has a constant energy production during the year of simulation in order to preserve the stability of the cells and gaskets which are very sensible to the thermal stresses [190]. Starting from that, the syngas molar flow consumed by the SOFC-MGT unit is calculated by the following equation which it considers the cycling operation of the DG:

$$\dot{n}_{syngas-SOFC} = \frac{h_{operation}\dot{n}_{DG}}{h_{operation} + h_{maintenance}} \tag{5.2.9}$$

Table 5.13: MGT model parameters

| Description | Symbol | Value |
|---|---|---|
| Politropic exponenet of the air | $m$ | 1.33 |
| Turbine isoentropic efficiency | $\eta_{is,turb}$ | 84 % |
| Air compressor isoentropic efficiency | $\eta_{is,comp}$ | 75 % |
| Turbine mechanical efficiency | $\eta_{mec,turb}$ | 99 % |
| Air compressor mechanical efficiency | $\eta_{mec,comp}$ | 98 % |
| Recuperator effectiveness | $\eta_{rec}$ | 85 % |
| Burner efficiency | $\eta_{eff,burner}$ | 99 % |
| MGT generator efficiency | $\eta_{alt,MGT}$ | 95 % |
| Pressure ratio | $PR$ | 2.5 |

Figure 5.5 depicts the overall model implemented in Matlab Simulink$^TM$ software. Tables 5.14, 5.15 and 5.16 show the results of the simulations for the three biomass considered with a moisture of 10%. Figure 5.6 reports a comparison between the system performances varying the type of biomass.

Figure 5.7 resumes the net electrical power production ($P_{el,tot}$), the power generated by the SOFC-MGT unit ($P_{el,SOFC+MGT}$) and the power self consumed ($P_{el,self}$) for each type of biomass.

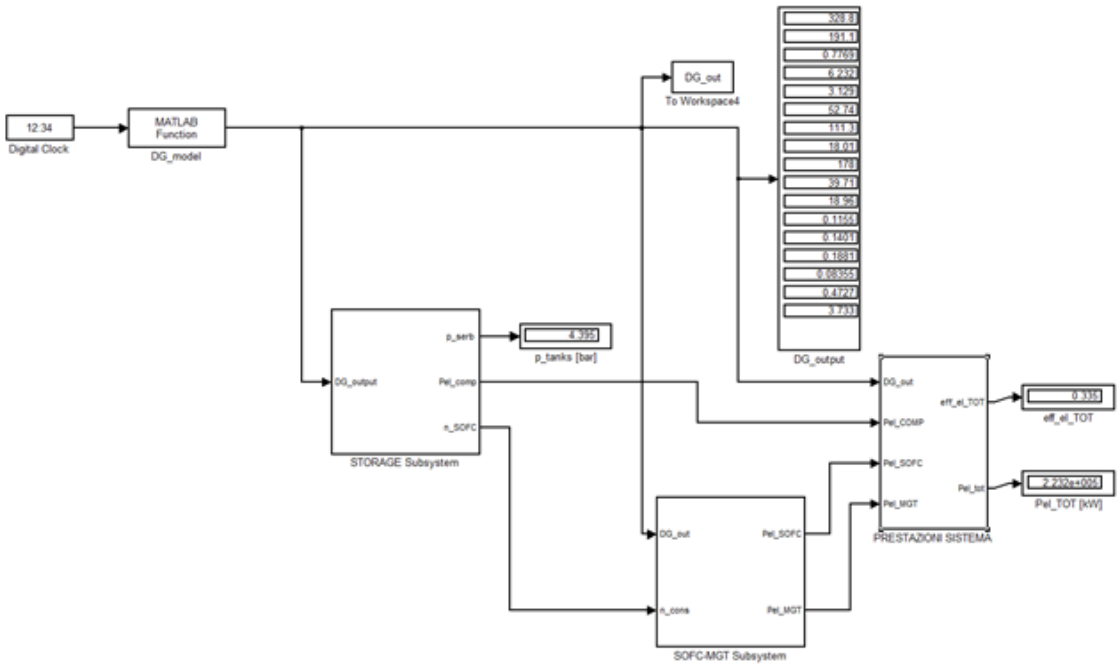


Figure 5.5: System in Matlab Simulink$^TM$

The influence of moisture of poplar wood chips on the performance of the system is reported in Figures 5.8 and 5.9. The moisture level do not influence the total efficiency while an increase of moisture causes a sensible decrease of the power production with the same biomass consumption. The overall electrical efficiency is about 33.5%, it is a good

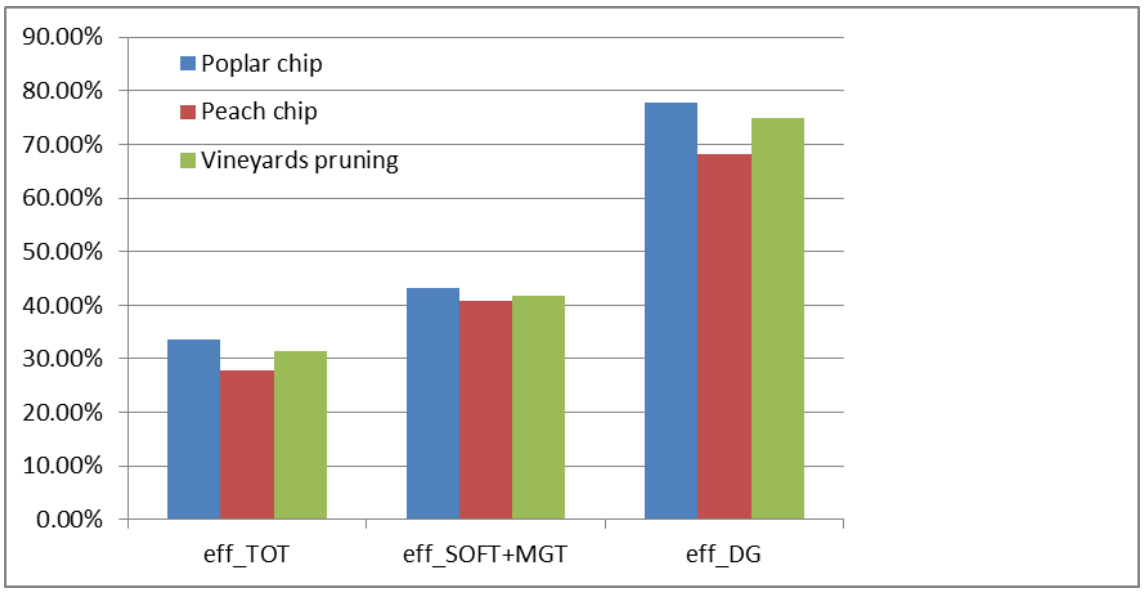


Figure 5.6: Performance of the system varying the biomass

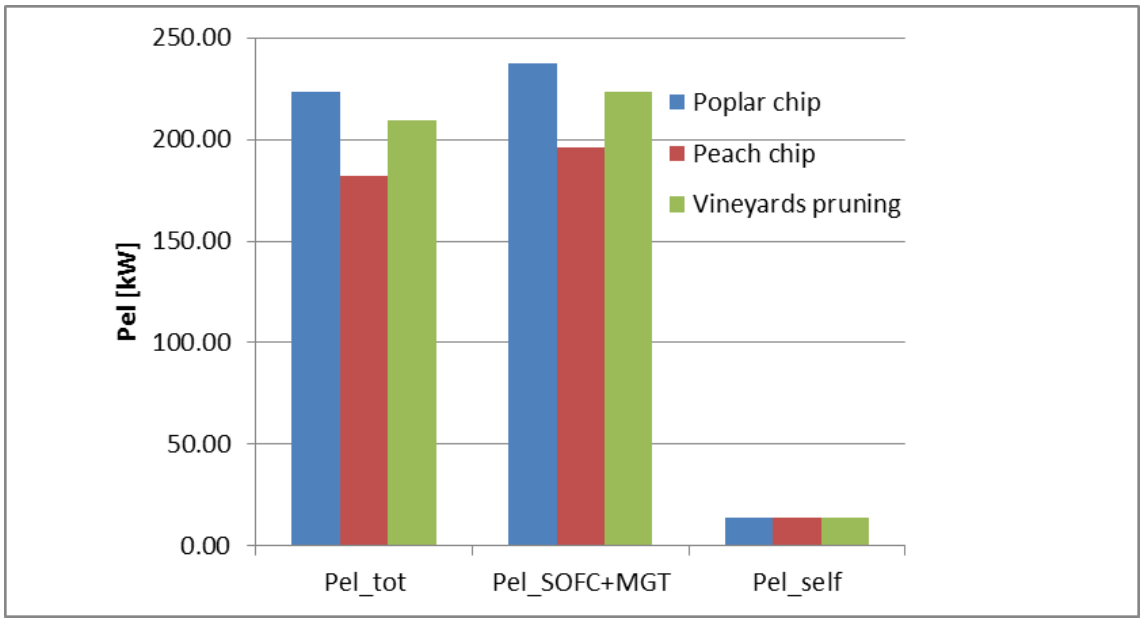


Figure 5.7: Electrical powers of the system varying the biomass

Table 5.14: Simulation results for poplar wood chips at 10 % of moisture

| Description | Value |
|---|---|
| $H_2$ fraction in the dry syngas | 11.5 % vol. |
| $CO$ fraction in the dry syngas | 14.0 % vol. |
| $CO_2$ fraction in the dry syngas | 18.8 % vol. |
| $CH_4$ fraction in the dry syngas | 8.3 % vol. |
| $N_2$ fraction in the dry syngas | 47.3 % vol. |
| Molar flow of dry syngas | 3.73 mol/s |
| Gasifier cold efficiency | 77.7 % |
| Specific tar production | 2 g/Nm$^3$ |
| Tanks pressure range | 1.49-8.76 bar |
| Molar flow of dry syngas to the SOFC-MGT unit | 3.39 mol/s |
| SOFC+MGT power production | 237.4 $kW_{el}$ |
| Average self consumption | 14.1 $kW_{el}$ |
| Average total power production | 223.3 $kW_{el}$ |
| Average SOFC+MGT electrical efficiency | 43.2 % |
| Average total electrical efficiency | 33.5 % |

Table 5.15: Simulation results for peach tree wood chips at 10 % of moisture

| Description | Value |
|---|---|
| $H_2$ fraction in the dry syngas | 12.8 % vol. |
| $CO$ fraction in the dry syngas | 15.8 % vol. |
| $CO_2$ fraction in the dry syngas | 20.4 % vol. |
| $CH_4$ fraction in the dry syngas | 6.3 % vol. |
| $N_2$ fraction in the dry syngas | 44.7 % vol. |
| Molar flow of dry syngas | 3.39 mol/s |
| Gasifier cold efficiency | 68.1 % |
| Specific tar production | 2 g/Nm$^3$ |
| Tanks pressure range | 1.49-8.09 bar |
| Molar flow of dry syngas to the SOFC-MGT unit | 3.08 mol/s |
| SOFC+MGT power production | 195.9 $kW_{el}$ |
| Average self consumption | 13.9 $kW_{el}$ |
| Average total power production | 182.0 $kW_{el}$ |
| Average SOFC+MGT electrical efficiency | 40.9 % |
| Average total electrical efficiency | 27.8 % |

Table 5.16: Simulation results for vineyard pruning at 10 % of moisture

| Description | Value |
|---|---|
| $H_2$ fraction in the dry syngas | 10.1 % vol. |
| $CO$ fraction in the dry syngas | 12.2 % vol. |
| $CO_2$ fraction in the dry syngas | 19.1 % vol. |
| $CH_4$ fraction in the dry syngas | 8.9 % vol. |
| $N_2$ fraction in the dry syngas | 49.7 % vol. |
| Molar flow of dry syngas | 3.73 mol/s |
| Gasifier cold efficiency | 74.9 % |
| Specific tar production | 2 g/Nm$^3$ |
| Tanks pressure range | 1.49-8.09 bar |
| Molar flow of dry syngas to the SOFC-MGT unit | 3.39 mol/s |
| SOFC+MGT power production | 223.2 $kW_{el}$ |
| Average self consumption | 14.1 $kW_{el}$ |
| Average total power production | 209.1 $kW_{el}$ |
| Average SOFC+MGT electrical efficiency | 41.9 % |
| Average total electrical efficiency | 31.4 % |

results compared to the maximum efficiency of about 20% of conventional biomass power plants [32]. In addition, the total electrical energy production during the year of simulation is about 1956 MWh obtained by a power of about 223 kW constantly transferred to the electrical grid. Figure 5.10 depicts the overall energy balance of the system using poplar wood chips with 10% of moisture as fuel. 42% of the energy is lost in the SOFC+MGT unit, while the self consumption of the system is only 2%. Finally, Figure 5.11 reports the pressure inside the storage tanks during the year of simulation using poplar wood chips with 10% of moisture as fuel. The storage volume is appropriate because the pressure is low and ranges between 1.49 and 8.76 bars.

### 5.2.3 Summary

The hybrid system reaches a high electrical efficiency also with a biomass of medium quality such as vineyard prunings. This occurs because the SOFC-MGT unit presents a higher efficiency (about 40%) compared to IC engine, ORC cycle or EFGT cycle. The self consumption of the system is insignificant and the low pressure inside the tanks ensures small leakage and good safety.

Furthermore, the SOFC unit fueled by the syngas works well also with small quantities of tar [188] and the lifetime of the cells is about 69000 hours equal to 8 years at constant full power. Also the efficiency of the cells decreases slowly over time (0.2% every 1000 hours) [190].

Further studies about economical and ecological sustainability of this kind of systems should be done. More advanced control algorithms that reduce the electrical production during the maintenance of the DG can optimize the volume of the storage and the whole system costs.

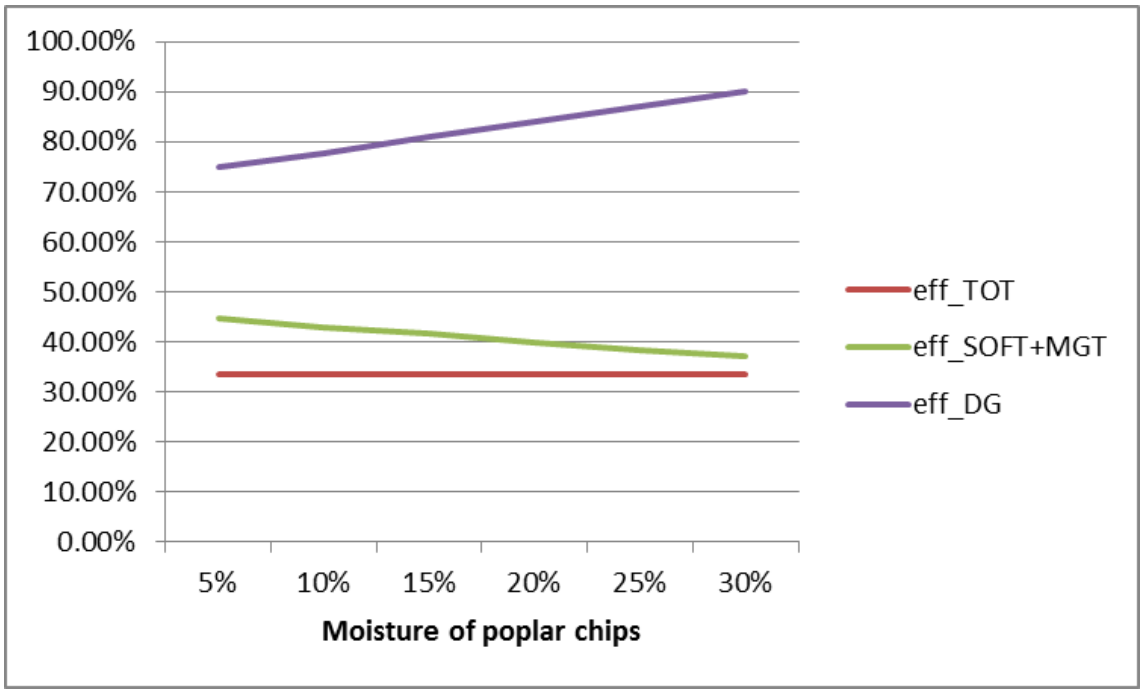


Figure 5.8: The efficiencies of the system varying the biomass moisture

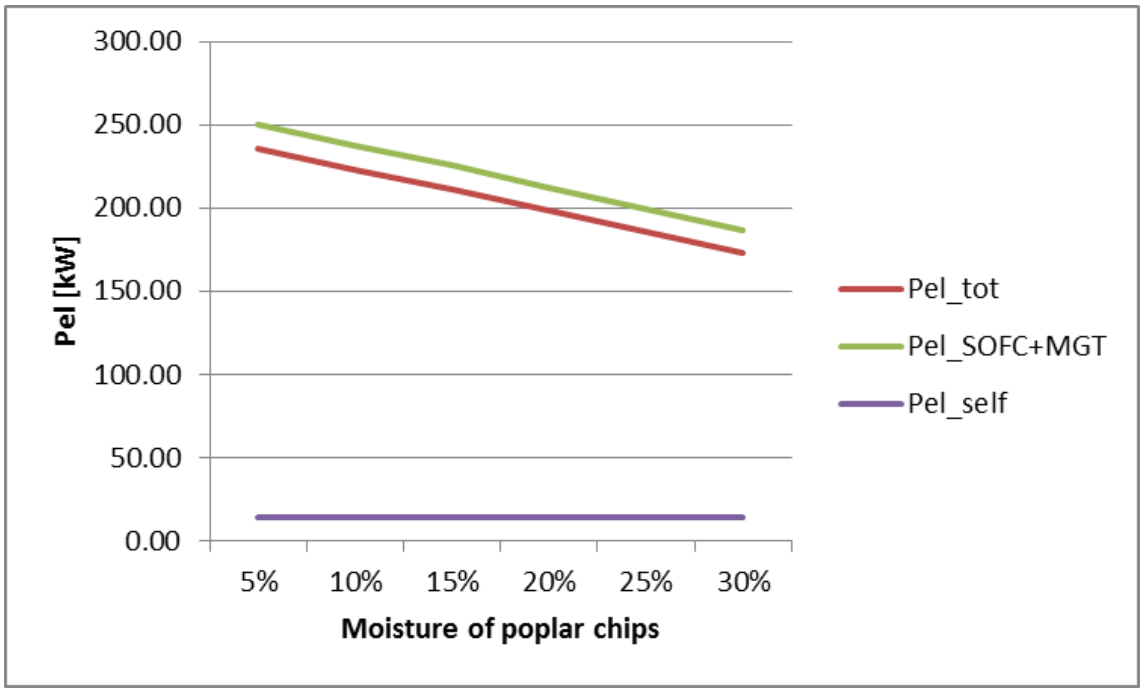


Figure 5.9: The net electrical power production varying the biomass moisture

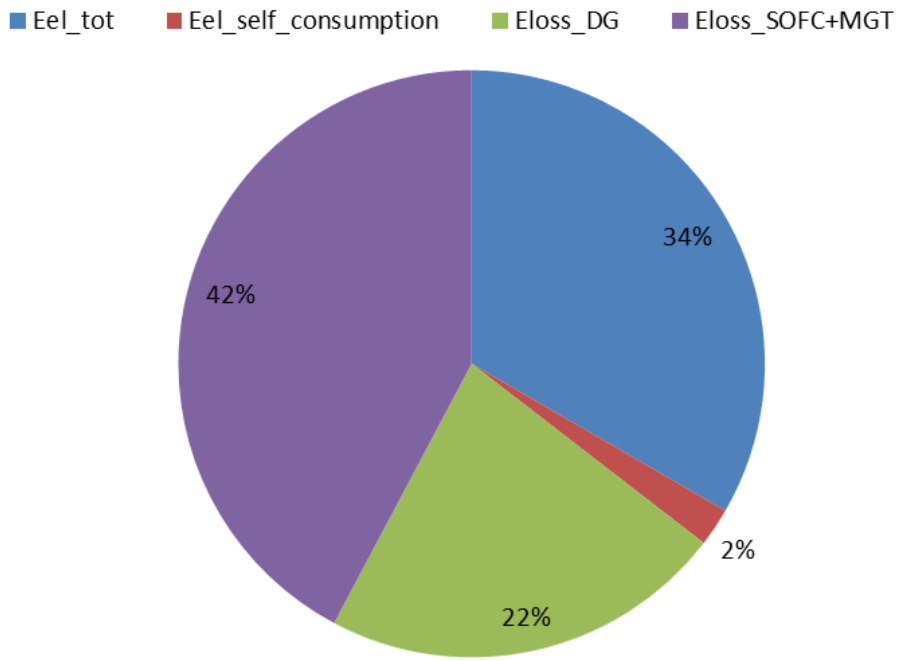


Figure 5.10: The overall energy balance of the system

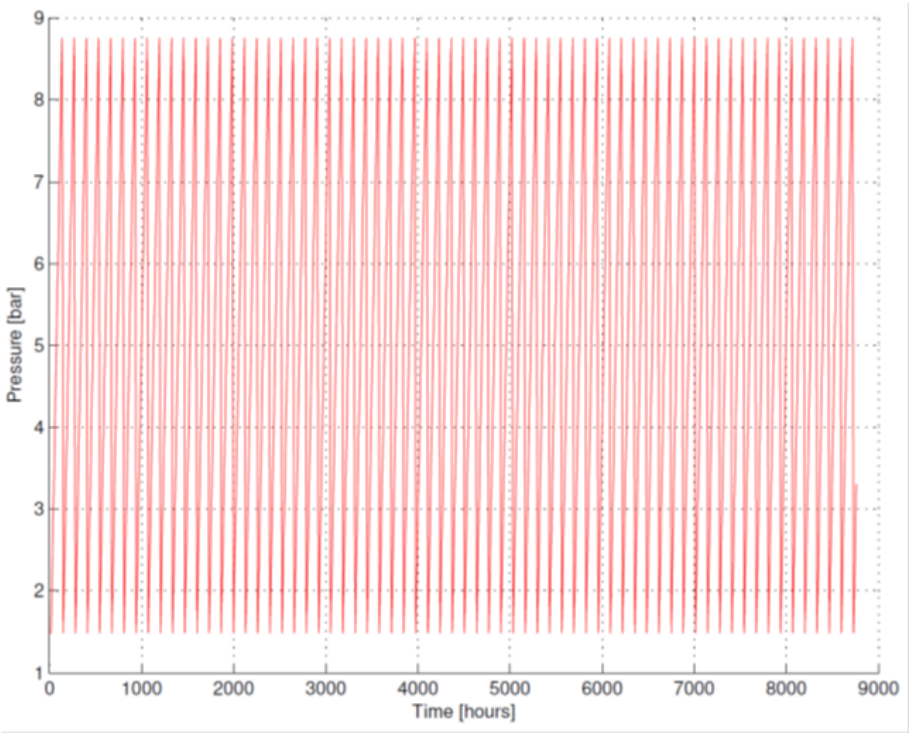


Figure 5.11: The pressure inside the tanks during the year of simulation

## 5.3 Modeling and simulation of a DG-SOFC-MGT system with $CO_2$ adsorption by zeolites and gasification with oxygen enriched air

The air gasification generates a low $HHV$ syngas composed also with no burner gases such as $N_2$ (about 50 %) and $CO_2$ (from 10 to 20%). A solution to eliminate the $N_2$ is to gasify with oxygen but it is expensive beacause the oxygen need to be produced in situ or need to be stored in tanks. The oxygen gasification is strongly exothermic and the temperature inside the reactor can reachs 1200-1300 K, for this reason the design of the reactor is complex and the materials adopted are more resistant to thermal stress than others reactors. Furthermore, the piping of oxygen is more dangerous than the piping of air and some safety measurements need to be adopted.

In this section, an advance solution with a polypropylene oxide (PPO) membrane is used to produce oxygen enriched air [191]. In such a way, an air with about 50% of oxygen is generates. This air creates a sort of mixed air-oxigen gasification with lower reactor thermal stresses compared to pure oxigen gasification. The syngas has a lower $N_2$ content than the syngas from the air gasification, furthermore the syngas flow rate decreases because the oxygen enriched air inlet flow is lower than the air flow for conventional gasification. This happens because the same amount of oxygen is used in both cases, but only 21% vol. of the inlet air is oxygen instead 50% vol. of the inlet oxygen enriched air is oxygen. Finally, the tar production of oxygen enriched air gasification is lower than the air gasification because the higher temperatures cracks more efficiently the primary tar.

The syngas has a variable $CO_2$ content depending on the gasification medium. This value ranges between 10 and 30% and it reduces significantly the higher heating value of the syngas. A possible solution to overcome this issue is to adopt a filter with selective synthetic zeolites before the storage tanks in order to separate carbon dioxide from the others gases of the syngas [192, 193]. The filter can be constantly regenerated using a structured zeolite adsorbent and rotary valve packaged into modules as depicted in Figure 5.16 [194].

In this section, modeling and simulation of the previuos DG-SOFC-MGT hybrid system is completed within the application of $CO_2$ adsorption by zeolites and oxygen enriched air as medium for gasification. The most efficient condition of poplar wood chip gasification at 10% of total moisture was investigated and compared with the results from the previous section. An annual simulation with gasifier maintenance was also considered.

### 5.3.1 System modeling and simulation

The new system case of study is depicted in Figure 5.12. It is essentially composed by the same components of the previuos system with the addition of the PPO membrane filter module on the inlet air and the zeolite (ZEO) filter module after the first syngas compressor. There is another syngas compressor before the tanks because the ZEO module works at 5 bars of pressure as explained below, instead in the tanks the pressure is often higher. Inside the PPO module there is another compressor, not depicted in the figure, that increases the pressure of the air before the PPO membrane filter to about 10 bars. The oxygen enriched air is sent to the gasifier at atmosferic pressure. A flow of nitrogen is purged from the PPO module and a flow of $CO_2$ is purged from the ZEO module.

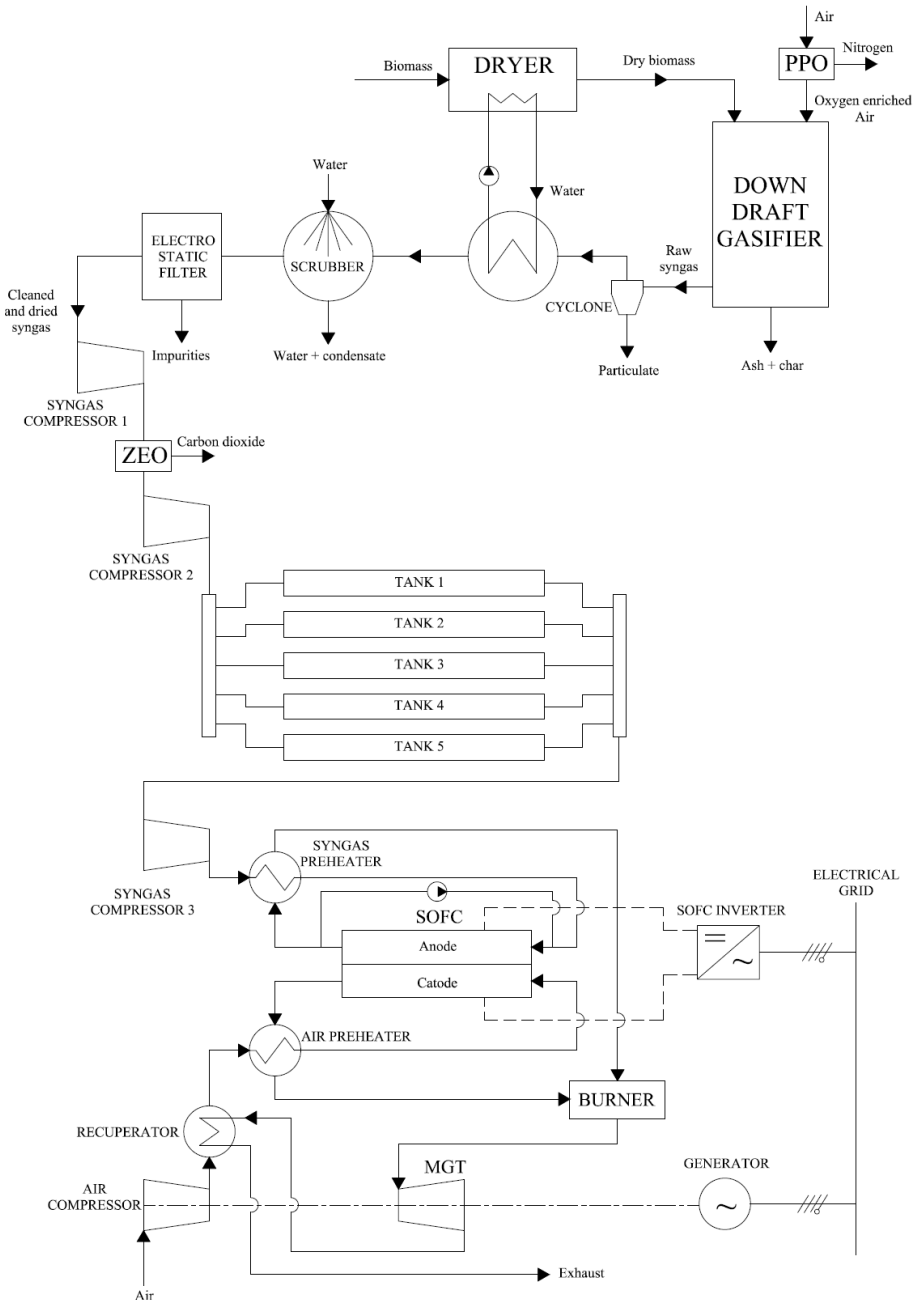


Figure 5.12: Basic layout of the DG-SOFC-MGT system with $CO_2$ adsorption by zeolites and gasification with oxygen enriched air

### PPO module modeling

The widely used polymeric membranes able to divide the air in nitrogen and oxygen are: Matrimid, Polyphenylenoxid (PPO) and Polydimethylsiloxan (PDMS) [191].

As show in Figure 5.13, in this membranes a flow of air $Q_{air}$ [mol/s] at high pressure $p_{feed}$ [atm] composed by a $x_{O2Feed}$ and $x_{N2Feed}$ molar fractions of oxygen and nitrogen, is divided in:

- A permeate molar flow $Q_P$ [mol/s] at atmosferic pressure $p_{permeate}$ [atm] composed by a $y_{O2}$ and $y_{N2}$ molar fractions of oxygen and nitrogen.
- A retentate molar flow $Q_R$ [mol/s] at high pressure $p_{feed}$ [atm] composed by a $x_{O2Retentate}$ and $x_{N2Retentate}$ molar fractions of oxygen and nitrogen.

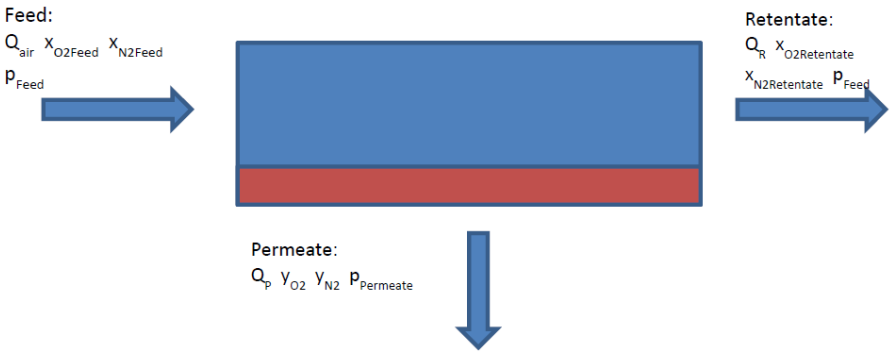


Figure 5.13: Oxygen enriched air membrane separator principle

Each membrane behaviour is identify through two parameters: selectivity and permeability to oxygen. The first factor rapresents the attitude of the membrane of attract the oxygen, the second quantify the attitude of the membrane to be crossed by the oxygen. High selectivity and permeability ensure a great filtering performance in terms of a high value of $y_{O2}$ and a low membrane area needed to filter a given amount of air. Table 5.17 resumes the parameters of Matrimid, PPO and PDSM membranes.

Table 5.17: Membranes parameters

| Material | Selectivity $\alpha$ [ad] | Oxigen Permeability $\gamma$ [mol m$^{-2}$ s$^{-1}$ bar$^{-1}$] |
|---|---|---|
| Matrimid | 6.7 | 62.0 x $10^{-5}$ |
| PPO | 4.7 | 37.2 x $10^{-4}$ |
| PDMS | 2.1 | 39.6 x $10^{-2}$ |

The choiche of the PPO membrane is a compromise in order to have an accetable value of selectivity and permeability. The mathematical model presented in References [191] has been implemented to simulate the behaviour of the membrane. The following assumptions are made in the model:

- Air is represented as a binary gas mixture with 21% Oxygen and 79% Nitrogen.

- Steady state conditions.
- Isothermal conditions.
- Isobaric conditions.
- Perfect gas law.
- Constant permeability.
- No flux coupling.
- Perfect mixing conditions on upstream and downstream sides.
- Concentration polarization at the membrane is neglected.
- Pressure loss in the porous support layer is neglected.
- The permeate can drain off freely.

The calculation of the permeate composition is made with the following formulas taken from Reference [191]:

$$y_{O2} = \frac{1}{2}\left[1+\phi\left(x_{O2Feed}+\frac{1}{\alpha-1}\right)\right] - \sqrt{\left[\frac{1}{2}\left[1+\phi\left(x_{O2Feed}+\frac{1}{\alpha-1}\right)\right]\right]^2 - \frac{\alpha\phi x_{O2Feed}}{\alpha-1}} \tag{5.3.1}$$

$$y_{N2} = 1 - y_{O2} \tag{5.3.2}$$

$$\phi = p_{feed}/p_{permeate} \tag{5.3.3}$$

where $\phi$ [ad] is the feed-permeate pressure ratio. Figure 5.14 reports the permeate composition over pressure ratio for the three membrane types. It can be seen that a specific maximum oxygen content can be achieved because the graphs are almost constant over a pressure ratio of 12. Therefore, a value of 10 was chosen for further calculations as suggested in Reference[191] and the $p_{retentate}$ was fixed at 1 atm.

The Matrimid membrane is able to produce the highest oxygen ratio of 58 % vol. in the permeate, however the PPO membrane present a good value of oxygen ratio (49 % vol.) and a acceptable value of permeability, so this membrane is adopted in the simulations.

The active area of membrane can be assessed from the molar flow of oxygen required for the gasification $Q_{PO2}$ [mol/s]:

$$A_{membrane} = \frac{Q_{PO2}}{\gamma * (x_{O2Feed} * p_{feed} + y_{O2} * p_{permeate})} \tag{5.3.4}$$

The molar flow of nitrogen $Q_{PN2}$ [mol/s] and the total permeate molar flow $Q_P$ [mol/s] is given by the following equations:

$$Q_{PN2} = \frac{\gamma}{\alpha} * [p_{feed} * (1 - x_{O2Feed}) + p_{permeate} * (1 - y_{O2})] \tag{5.3.5}$$

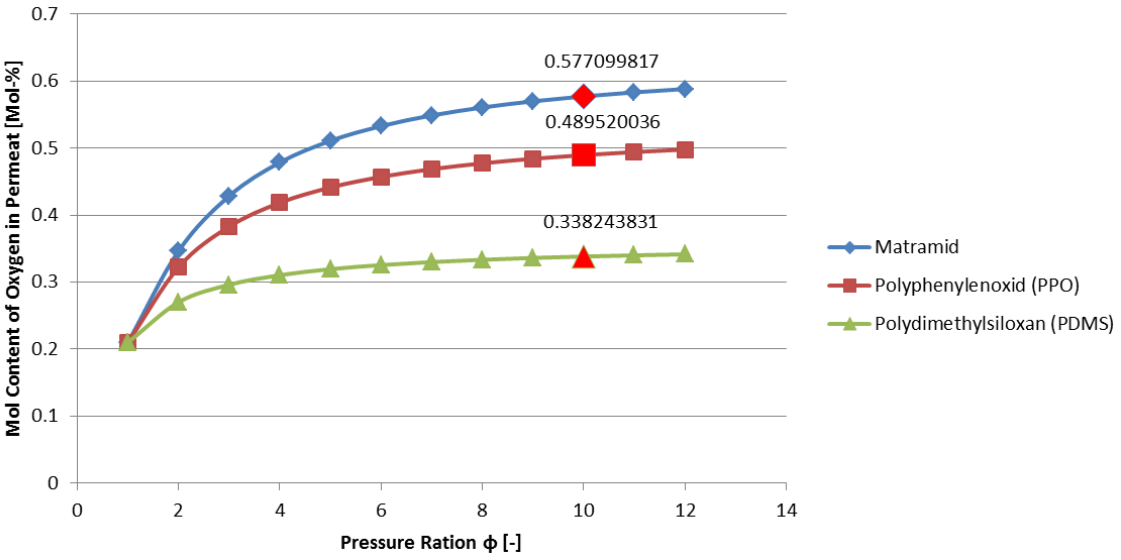


Figure 5.14: Separation characteristics of the membranes

$$Q_P = Q_{PN2} + Q_{PO2} \tag{5.3.6}$$

The molar flow of the inlet air $Q_{air}$, the retentate molar flow $Q_R$ and the retentate composition ($x_{O2Retentate}$ and $x_{N2Retentate}$) are calculated setting to zero the amount of oxygen in the retentate flow. In a such a way, a mass balance can be applied to estimate $Q_{air}$ and $Q_R$:

$$Q_{air} * x_{O2Feed} = Q_P * y_{O2} \rightarrow Q_{air} = \frac{Q_P * y_{O2}}{x_{O2Feed}} \tag{5.3.7}$$

$$Q_{air} = Q_P + Q_R \rightarrow Q_R = Q_{air} - Q_P \tag{5.3.8}$$

Finally, the eletrical power consumption for pressurize the inlet air is calculated as a polytropic compression by Equation 5.2.1 assuming $T_{in} = 20\ ^o$ C; $m = 1.2$ and $\eta_{comp} = 90\%$.

### Gasifier modeling

The thermodynamc equilibrium model with tar calculation was applied to simulate the gasification. However, the overall air gasification reaction must be adapted with the oxygen enriched air input:

$$\begin{aligned} CH_xO_yN_z + wH_2O + m\left(O_2 + \frac{y_{N2}}{y_{O2}}N\right) = n_{H_2}H_2 + n_{CO}CO \\ +n_{CO_2}CO_2 + n_{H_2O}H_2O + n_{CH_4}CH_4 + \left(z/2 + \frac{y_{N2}}{y_{O2}}m\right)N_2 + n_{tar}CH_pO_q \end{aligned} \tag{5.3.9}$$

The rest of the model do not need to be modified, however the initial temperature of the iterative cycle is settled higher as air gasification. This model allow us to calculate further

information: the tar yield and the gasification average temeperature. The parameters of the gasifier model is reported in the Table 5.18. The same biomass consumption is considered but the $ER$ is fixed to 0.335 because the oxygen enriched air reacts differently in the reactor. The properties of poplar wood chips are summarized in Table 5.19.

Table 5.18: Gasifier model parameters

| Description | Symbol | Value |
|---|---|---|
| Biomass consumption | $\dot{m}_{bio}$ | 187 kg/h |
| Gasifier cross area | $A_g$ | 0.668 $m^2$ |
| Initial calculation temperature | $T_{in}$ | 900 K |
| Pressure | p | 1 atm |
| Equivalence ratio | ER | 0.335 |
| Gasifier and filters self consumption | $P_{DG,self}$ | 12.5 kW |
| Cyclic operation hours | $h_{operation}$ | 120 h |
| Cyclic maintenance hours | $h_{maintenance}$ | 12 h |

Table 5.19: Poplar wood chips properties

| Description | Symbol | Value |
|---|---|---|
| Total moisture | $M$ | 10 % |
| Carbon content (as received) | $C_{ar}$ | 41.6 % |
| Hydrogen content (as received) | $H_{ar}$ | 6.0 % |
| Nitrogen content (as received) | $N_{ar}$ | 0.52 % |
| Oxygen content (as received) | $O_{ar}$ | 39.8 % |
| Ash content | $ASH$ | 2.75 % |
| Higher heating value (dry basis) | $HHV_{db}$ | 15.7 MJ/kg |

### ZEO module modeling

The zeolite filter is able to reduce the total syngas molar flow of about 20-30 % by the adsorption of $CO_2$. The Zeolite 5A is adopted because it has a great selectivity of carbon dioxide respect the other gases that constitute the syngas. The gas adsorption in porous solids has been described physically by the Langmuir equation [192, 193]:

$$q_i = \frac{q_{mi} * B_i * p_i}{1 + \sum_{j=1}^{n} B_j * p_j} \tag{5.3.10}$$

where $q_i$ [mmol/g] is the adsorbed amount of the component $i$; $q_{mi}$ [mmol/g] is the saturation adsorbed amount of the component $i$; $B_i$ [1/kPa] is the Langmuir constant of the component $i$; $p_i$ [kPa] is the partial pressure of the component $i$; $B_j$ [1/kPa] is the Langmuir constant of the component $j$; $p_j$ [kPa] is the partial pressure of the component $j$; $i$ and $j$ are the gas species of the syngas. Table 5.20 reports the Langmuir constants and the saturation adsorbed amounts for the Zeolite 5A, instead Figure 5.15 depicts the adsorption trend of the gases as function of pressure. It can be noted the high $CO_2$ selectivity of the zeolite respect others gases.

The mass of active adsorbent zeolite depends on the molar flow of the dry syngas and its $CO_2$ molar fraction. The ZEO filter module can be constantly regenerated using a

Table 5.20: Zeolite 5A parameters of adsorption

| Component | $B$ [1/kPa] | $q_m$ [mmol/g] |
|---|---|---|
| $CO_2$ | 0.019500 | 3.91900 |
| $H_2$ | 0.000361 | 0.54464 |
| $N_2$ | 0.000837 | 2.62543 |
| $CH_4$ | 0.002535 | 2.75403 |
| $CO$ | 0.004350 | 2.75800 |

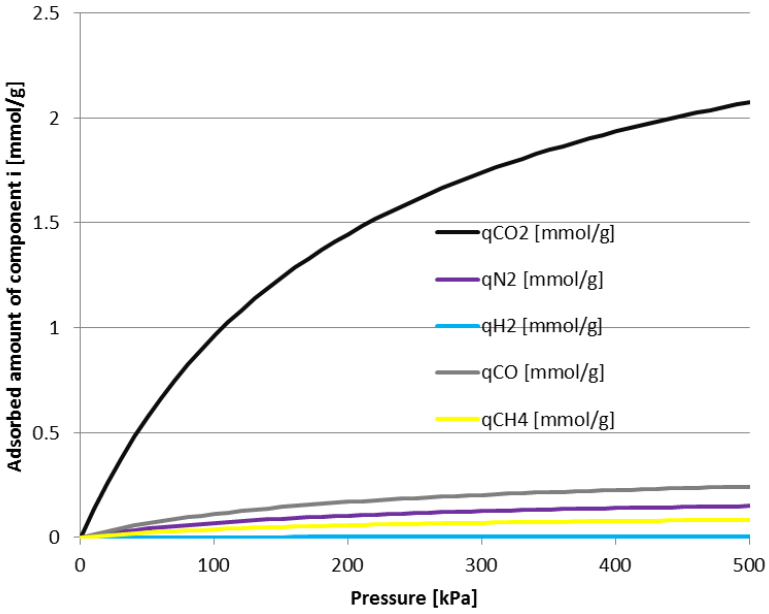


Figure 5.15: Zeolite 5A adsorption curves Vs. pressure

structured zeolite adsorbent and rotary valve packaged into modules as depicted in Figure 5.16 [194]. Assuming steady state conditions and low inertia of adsorption, the active mass of zeolite that need to be regenerated every cycle with duration of $t_{cycle}$ [s] can be calculated as follows:

$$m_{zeo} = t_{cycle} * \dot{n}_{DG} * \frac{1 + \sum_{j=1}^{n} B_j * p_j}{q_{m,CO_2} * B_{CO_2} * p_{ads} * x_{CO_2}} \tag{5.3.11}$$

where $p_{ads}$ [kPa] is the total pressure of the syngas inside the ZEO filter, in the simulation this parameters is set to 500 kPa as suggest in Reference [192, 193] instead the cycling time of regeneration is set to 60 seconds.

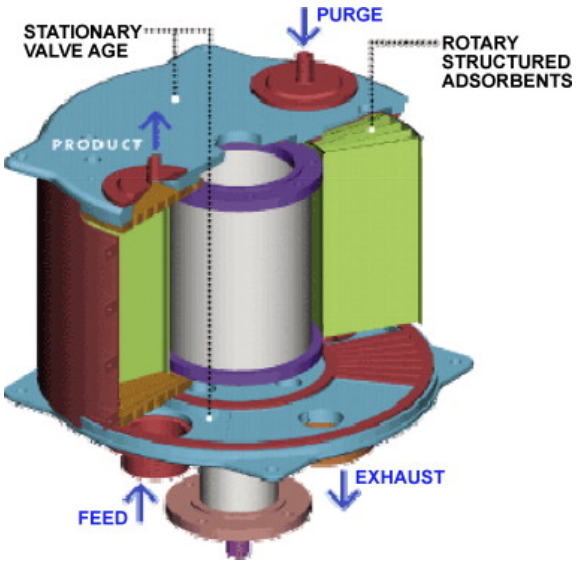


Figure 5.16: Rotary filter with structurated adsorbent [194]

### Compressor and storage system modeling

The models adopted in the previous section is applied for this simulation. Table 5.21 reports the parameters of the storage and compressor models. The total volume of storage and the initial syngas amount in the tanks are reduced of about 50% respect the hybrid system without PPO and ZEO modules. This incredible achievement has been reach because the molar flow of dry syngas decreases of about the 20-30 % and the syngas filtration in the ZEO module reduces it of about another 20-30% as shown in the results.

### SOFC-MGT modeling

The SOFC-MGT models is the same of the previuos section. Few modification of the parameters of the SOFC, reported in Table5.22, was done in order to simulate the SOFC operation with a medium $HHV$ syngas obtained from oxygen enriched air gasification and zeolites filtration.

Table 5.21: Storage and compressor model parameters

| Description | Symbol | Value |
|---|---|---|
| Politropic exponent of the syngas | $m$ | 1.33 |
| Syngas compressor efficiency | $\eta_{comp}$ | 92 % |
| Tanks temperature | $T_s$ | 298.15 K |
| Initial syngas amount in the tanks | $n_{in}$ | $1.5 * 10^4$ mol |
| Number of tanks | $N$ | 5 |
| Total tanks volume | $V$ | 250 $m^3$ |

Table 5.22: SOFC model parameters in the DG-SOFC-MGT hybrid system with zeolite $CO_2$ adsorption and oxygen enriched air

| Description | Symbol | Value |
|---|---|---|
| Fuel utilization factor | $U_f$ | 0.85 |
| Recirculation factor | $r$ | 0.2 |
| Operating temeprature | $T_{sofc}$ | 1073.15 K |
| Anode pressure loss | $\Delta p_a$ | 500 Pa |
| Cathode pressure loss | $\Delta p_c$ | 1000 Pa |
| Anode pressure loss | $\Delta p_a$ | 500 Pa |
| Current density | $i$ | 300 mA/$cm^2$ |
| Active cell area | $A_cell$ | 81 $cm^2$ |
| Cells for each stack | $n_{cell,stack}$ | 75 cells |
| Number of stacks | $n_{stack}$ | 145 stacks |
| Cathode air excess | $vent$ | 1.15 |
| Pressure ratio | $PR$ | 2.5 |
| Steam to carbon coefficient | $STC$ | 1.4 |
| Electrochemical parameters taken from [85] | | |

### 5.3.2 Simulation results

The SOFC-MGT unit has a constant energy production during the year of simulation in order to preserve the stability of the cells and the gaskets that are very sensible to the thermal stresses [190]. Starting from that, the syngas molar flow consumed by the SOFC-MGT unit has been set by Equation 5.2.9 which considers the cycling working of the DG.

Figure 5.17 depicts the overall model implemented in Matlab Simulink$^TM$ software environment. Table 5.23 shows the results of the simulations of the PPO module. The oxygen enriched air flow is lower as air flow in the system without membrane (about 2.38 mol/s), this fact reduces the inlet air passages and, consequently, the dimensione and the costs of the gasifier.

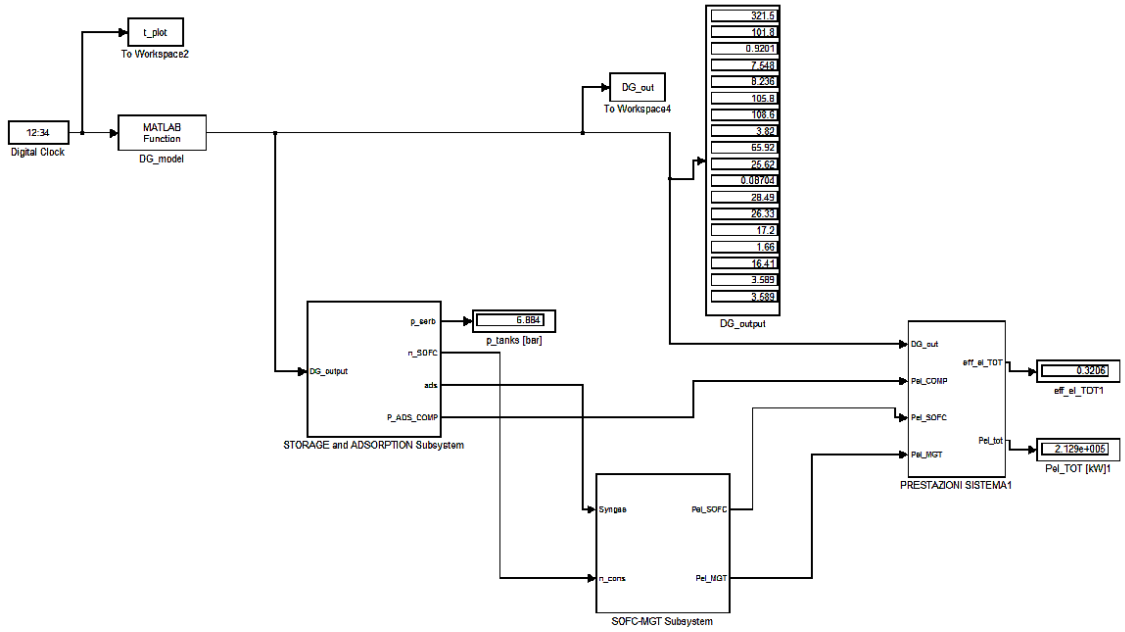


Figure 5.17: DG-SOFC-MGT system with the $CO_2$ adsorption by zeolites and gasification with oxygen enriched air in Matlab Simulink$^TM$

Table 5.23: PPO module simulation results

| Description | Symbol | Value |
|---|---|---|
| Air inlet flow | $Q_{air}$ | 2.97 mol/s |
| Permeate molar flow | $Q_P$ | 1.27 mol/s |
| Retentate molar flow | $Q_R$ | 1.69 mol/s |
| Molar fraction of $O_2$ in permeate | $y_{O2}$ | 48.9 % |
| Molar fraction of $N_2$ in permeate | $y_{N2}$ | 51.1 % |
| Electric power consumption | $P_{el,PPO}$ | 15.3 kW |

Downdraft gasifier model results are summarized in Table 5.24. The gasification with oxygen enriched air assures higher gasifier performance as air gasification, the tar production is very low and the syngas has a good calorific value. Furthermore, the syngas

outlet flow is lower than air gasification and the temperature increasing is lower than pure oxygen gasification, whereby the conventional materials adopted in air gasifier can be used (i.e. stailess steel and refractory brick [6, 21]).

Table 5.24: Gasifier module simulation results (dry basis)

| Description | Symbol | Value |
|---|---|---|
| $H_2$ syngas fraction | $x_{H_2}$ | 31.6 % |
| $CO$ syngas fraction | $x_{CO}$ | 29.2 % |
| $CH_4$ syngas fraction | $x_{CH_4}$ | 1.84 % |
| $CO_2$ syngas fraction | $x_{CO_2}$ | 19.1 % |
| $N_2$ syngas fraction | $x_{N_2}$ | 18.2 % |
| Syngas molar flow | $\dot{n}_{syngas}$ | 3.59 mol/s % |
| Syngas higher heating value | $HHV_{syngas,db}$ | 8.38 MJ/Nm$^3$ |
| Specific volumetric tar production | $m_{tar,Nm^3}$ | 0.30 g/Nm$^3$ |
| Gasifier cold gas efficiency | $\eta_{cold}$ | 92.0 % |
| Average temperature of gasification | $T$ | 931 K |

Instead, Table 5.25 resumes the simulation results for ZEO module and the storage subsystem. The filtered syngas has a good heating value similar to oxygen gasification syngas, the pressure of the storage is in line with the previous range and the zolite mass is accettable [194]. However, the $CO_2$ adsorbed by ZEO module can be stored in order to create a carbon sequestration technology.

Table 5.25: ZEO module and storage simulation results (db)

| Description | Symbol | Value |
|---|---|---|
| $H_2$ syngas fraction after adsoption | $x_{H_2}$ | 41.5 % |
| $CO$ syngas fraction after adsoption | $x_{CO}$ | 32.5 % |
| $CH_4$ syngas fraction after adsoption | $x_{CH_4}$ | 2.21 % |
| $CO_2$ syngas fraction after adsoption | $x_{CO_2}$ | 0 % |
| $N_2$ syngas fraction after adsoption | $x_{N_2}$ | 23.3 % |
| Syngas molar flow after adsoption | $\dot{n}_{syngas}$ | 2.73 mol/s % |
| Syngas higher heating value after adsoption | $HHV_{syngas,db}$ | 10.2 MJ/Nm$^3$ |
| Active zeolite mass for every regeration cycle | $m_{zeo}$ | 20.2 kg |
| Tanks pressure range | $p_{serb}$ | 1.49-12.1 bar |

The results concerning the SOFC-MGT module are reported in Table 5.26. The great power-production and electrical efficiency is reached as result of high $H_2$ and $CO$ amounts in the inlet syngas. Furthermore, the syngas consumption decreases of about 27 % respect the previuos case without ZEO and PPO modules.

Finally, the model results of the overall system are reported in Table 5.27. The self consumption of the system is greater than previous simulation because there are a compressor in PPO module and another compressor before ZEO modules in order to increase the pressure of the syngas to 5 bars. However, the electrical power production and the overall electrical efficiency are similar to the previous case with the advantage to have a storage with a volume of 250 m$^3$ and a lower specific tar production of 0.3 g/Nm$^3$ compared to 2 g/Nm$^3$ of the system without PPO filter module.

Table 5.26: SOFC-MGT simulation results

| Description | Symbol | Value |
|---|---|---|
| Syngas molar flow to SOFC-MGT unit | $\dot{n}_{SOFC}$ | 2.478 mol/s |
| SOFC power production | $P_{SOFC}$ | 249.3 kW |
| MGT power production | $P_{MGT}$ | 10.42 kW |
| Total SOFC-MGT power production | $P_{MGT}$ | 259.7 kW |
| SOFC eletrical efficiency | $\eta_{SOFC}$ | 55.4 % |
| MGT eletrical efficiency | $\eta_{MGT}$ | 25.4 % |
| Total SOFC-MGT electrical efficiency | $\eta_{SOFC}$ | 45.8 % |

Figure 5.18 depicts the total energy balance of the system. Most of the energy (about 53%) is lost in the SOFC+MGT unit, while the self consumption of the system is about the 7%. In addition, the total electrical energy production during the year of simulation is about 1890 MWh obtained by a power of about 216 kW constantly transferred to the electrical grid. Finally, Figure 5.19 reports the pressure inside the storage during the simulation.

Table 5.27: Overall system simulation results

| Description | Symbol | Value |
|---|---|---|
| Average self consumption | $P_{self}$ | 43.9 $kW_{el}$ |
| Average total power production | $P_{tot}$ | 215.8 $kW_{el}$ |
| Average total electrical efficiency | $\eta_{tot}$ | 32.27 % |

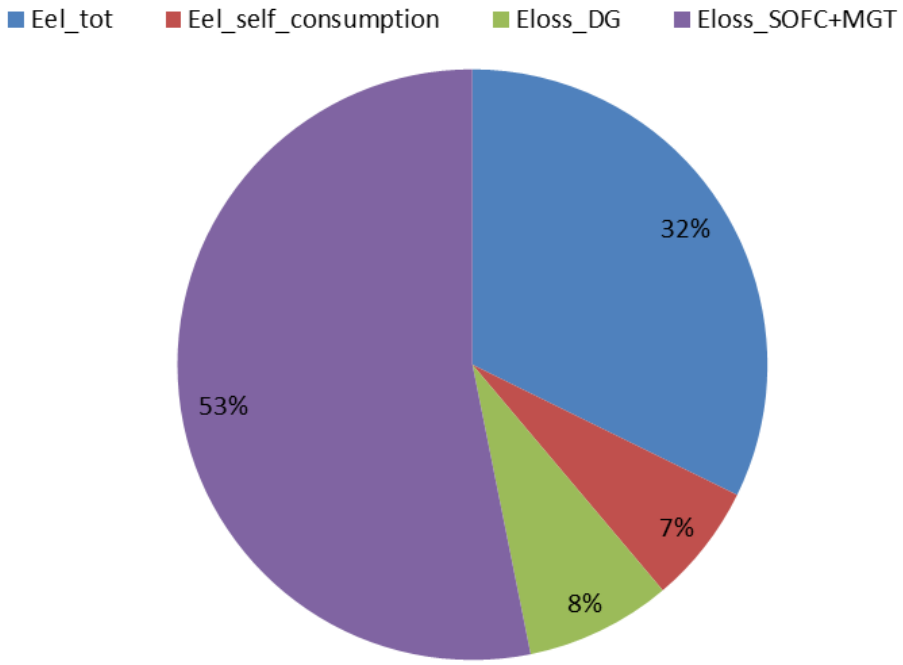


Figure 5.18: Energy balance of the system with ZEO and PPO modules

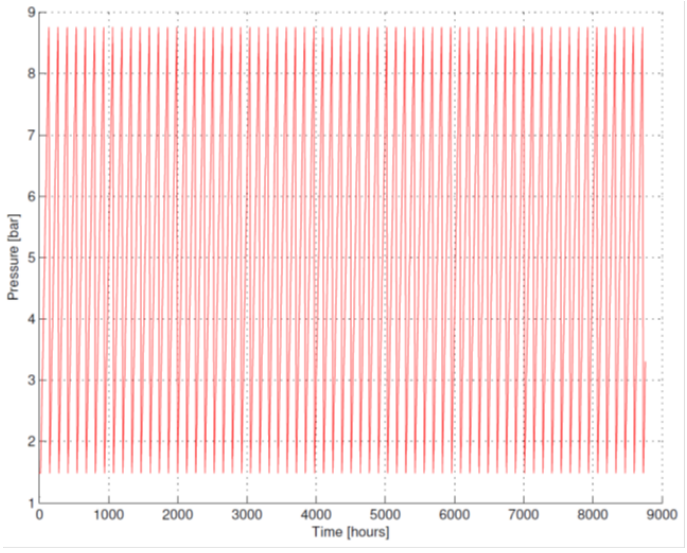


Figure 5.19: Pressure inside the tanks during the annual simulation of the system with ZEO and PPO modules

# Chapter 6

# Economical analysis of small downdraft gasifier for electrical power production

The economical sustainability of bioenergy is a big issue for every technologies at commercial state. The cost of raw feedstocks and the cost of plant maintenance play and important role for the economical balance. Often, the biomass transportation and pre-treatment are not taken into account, futhermore the disposal of byproducts is not considered.

The benefits from the bioenergy trade are bigger than others renewable energy sources such as wind or photovoltaics. The production of bioenergy can be easily planned and the working hours of a biomass power plant are over 7000 every years in most of the cases [5, 6, 21]. The specific investment cost is often greater compared to photovoltaics plants because the biomass plants are more complex and the safety measurements are more expensive.

However, the annual energy production of a biomass power plant is 6-7 times than a photovoltaics power plant with the same peak power in Italy. For example, a 100 $kW_p$ photovoltaic plants generates from 100 to 140 MWh every year [195]. A 100 $kW_p$ biomass power plant that works 7000 hours/year generates about 700 MWh.

In such a way, the NPV analysis is vital to understand the break even point and the economics advantage of these plants [196]. In this chapter, a briefly description of the economical analysis of two small power plants installed in Italy is exposed.

## 6.1 Biomass costs

Potential feedstocks are divided into four main categories as shown in Figure 1.4. This division is based on spatial availability and logistics which have an impact on the feedstock cost and on the economically feasible scale of conversion plants. Table 6.1 resumes typical feedstock costs and relative biomass plant capacities.

Indicative cost ranges for each of these categories, along with the scales of power generation that are most likely to be compatible with the availability of the fuels. In applications with small downdraft gasifiers, wood chips biomass is the more suitable. This biomass is an internationally traded feedstock with a $HHV_{db}$ of about 20 MJ/kg [6]. Assuming the value of 6-9 €/GJ from Table 6.1, the cost of 1000 kg of total dry wood

Table 6.1: Typical feedstock costs and plant capacities [1]

| | Wastes | Processing residues | Localy collected feedstocks | Internationally traded feedstocks |
|---|---|---|---|---|
| Feedstock cost [€/GJ] | negatite to 0 | 0-3 | 3-6 | 6-9 |
| Plant size [$MW_{el}$] | 0.5-50 | 0.5-50 | 10-50 | >50 |

chips is between 120 and 180 €.

## 6.2 Plant maintenance and by-products disposal

The maintenance of gasifier power plants is vital to ensure the design performance and to prevent hazardous events and expensive failures. Channeling phenomena and ash with low melting point create slugging agglomerates which can interrupt the syngas flow. The formation of these agglomerates often called klinker is characteristical of bad biomass feedstocks and/or bad gasification conditions. Unfortunately, a strong maintenance operation is needed to remove the klinkers. The gas filter medium need to be changed every several hours of working, furthermore the regular maintenance of the engine (oil, sparks, filters etc.) is fundamental.

It is difficult to quantify exactly the cost of the maintenance. Normally, full service contracts are made to cover the ordinary maintenance. In Italy the cost of these service is about 0.03 €/$kWh_{el}$ for small and medium scale power plant. Not ordinary maintenance, such as the replacement of the engine or the reactor, can be estimated for every single case.

Tar disposal is very expensive because it contains high levels of poly nuclear aromatic hydrocarbons (PAH) [47]. For this reason, tar is classified as hazardous waste, especially if it is formed at high temperatures [5]. Several technologies are available for treatment of this contaminant before its final disposal. The disposal costs is higher compared to municipal solid waste, it is about 0.5 €/kg. The char disposal can be done using the char as fertilizer if the PAH level is lower than the limit of 6 mg/$kg_{char}$ [197]. If PAH level ranges from 6 to 1000 mg/$kg_{char}$ the char is considered as regular waste, if the PAH level is higher 1000 mg/$kg_{char}$ (few case) it is an hazardous waste [197]. Normally, the cost for char disposal in case of regular waste is about 0.05 €/kg.

## 6.3 Italian subsidies for RES-E plants

The Ministerial Decree of July 6, 2012 [198] establishes the procedures for supporting electricity generation by RES-E plants (other than photovoltaic ones) with a capacity of at least 1 kW. The Decree provides that the indicative cumulative cost of all types of incentives awarded to RES-E plants (other than photovoltaic ones) shall not exceed an overall value of 5.8 billion of €per year. The new support scheme also introduces yearly supportable-capacity quotas, in each year from 2013 to 2015, divided by type of source and plant and in accordance with the applicable procedures for access to the incentives. The decree provides for two separate support schemes, based on plant capacity, renewable source used and type of plant: all-inclusive feed-in tariff (To) and incentive (l) for plants with a capacity of above 1 MW.

For small and medium gasification power system below 300 $kW_{el}$, the access of subsidies is direct with the all-inclusive feed-in tariff scheme where the value of the found is given by the sum of a base feed-in tariff (whose value is defined for each source, type of plant and capacity class) with premiums (e.g. high-efficiency CHP, emission reductions, etc.). The tariffs will decrease by 2% in each of the subsequent years until 2015. The tariffs is constant for 15 years after the project approval. In case of wood biomass power plants with electrical power below 200 $kW_{el}$, the base tariff of today is 229 €/MWh, furthermore a premium of 40 €/MWh is given for cogeneration with high efficiency (CAR) and other 30 €/MWh is given for plants with low emissions [198].

## 6.4 Small gasifier NPV analysis

### 6.4.1 Commercial state small gasifiers

Today, most bioenergy plants are based on conventional steam turbines. A further set of generation technologies is becoming available, including gasification and use of the resulting gases in an engine or a fuel cell to produce power.

Such systems potentially offer better generation efficiency and lower capital costs, but as the systems are so far not deployed on a commercial scale it is difficult to find reliable cost and operating data.

However, the demonstration of such systems may well open up opportunities for reduced costs and improved efficiencies, particularly at lower scales, and these technologies are expected to play an increasing role in the longer term. Now, few producers all around the world sell small or medium size gasifier [89, 87, 199, 200, 201]. In this thesis, two producer are considered: All Power Labs$^{TM}$ and Spanner$^{TM}$.

#### All Power Labs$^{TM}$

All Power Labs (APL) [87] builds a very small scale gasifier power plant called "Power Pallet" (PP) of nominal electrical power of 10 or 20 $kW_{el}$. The plant is compact and cheap but able to eletrify rural areas or to send the energy into the grid. The system, depicted in the Figure 6.1, uses by a single throat imbert type downdraft gasifier. An hermetic hopper full of biomass feedstock is connected to the reactor by a drying bucket where the hot syngas coming out from the cyclone heats and dries the biomass. An auger pushs the dried feedstock into the pyrocoil: a double vessel cylinder where the exhaust from the engine pyrolyses the biomass. After the gasification inside the rector, the char is disposed from the bottom of the gasifier and the syngas passes through the cyclone, the drying bucket and the bio-filter full of charcoal or wood chips. The syngas can be burned in a torch in transient phases or used in an IC engine to move a generator to produce electricity.

Wood biomasses with a total moisture of 30% can be used in the APL gasifier thanks to its internal heat recovery (TOTTI system [87]), however the autonomy of 6 hours and no CHP opportunities are two great disavantage of this system. The bio-filter is a great solution for small scale generator because avoids the expensive tar disposal [5], in fact the filter medium can be gasified directly in the PP. For these reasons, the system is very cheap (about 35000 €equivalent to 1750 €/ $kW_{el}$) but effective.

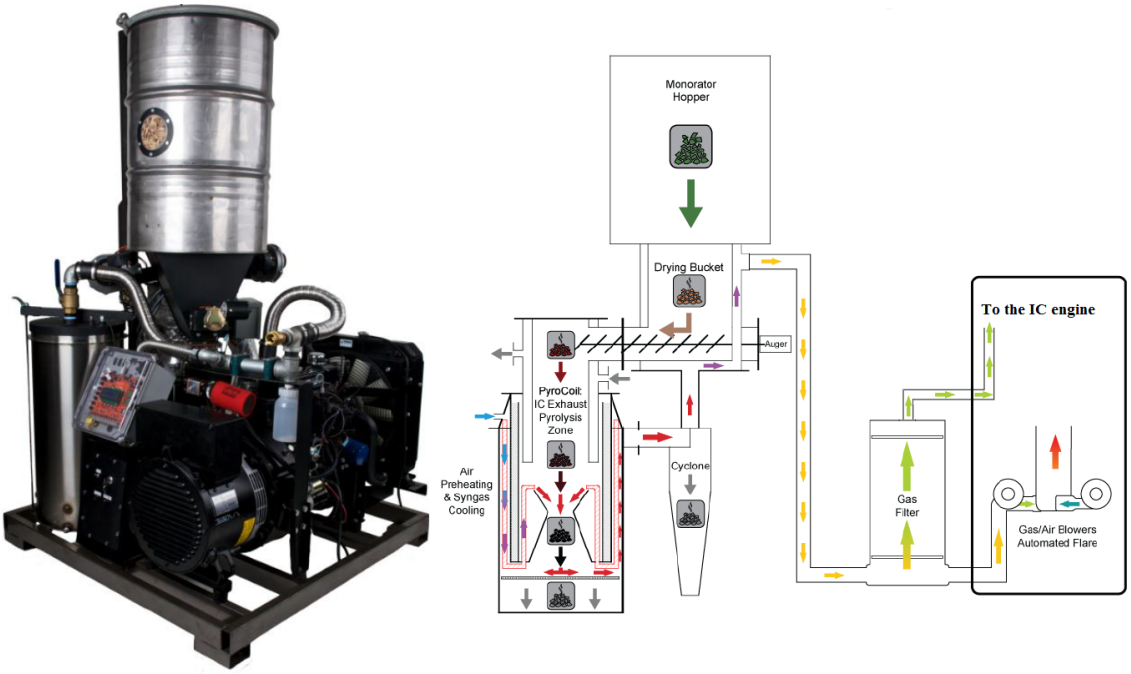


Figure 6.1: APL Power Pallet$^{TM}$

### Spanner Re$^2$ GmbH$^{TM}$

Spanner gasifier [199] is a more sophisticated system which uses a downdraft gasifier with a pneumatic control system. The gas filter is made of a textile material, in this case tar disposal is present because after a running time, influenced by the biomass and the plant operation, the filter need to be washed or changed. The gasifier depicted in Figure 6.2 works with wood chips of quality G40 or G50 [5] with a total moisture lower than 15%. The producer garantees about 7000 hours of working every years. There are two plant size (30 and 45 $kW_{el}$) and there is the possibilities to do CHP. However, the cost of the system of 45 $kW_{el}$ is about 200000 €equivalent to 4445 €/ $kW_{el}$.

## 6.5 Economical analysis of two small power plant

In this section, the economical analysis of two small power plants below 300 $kW_{el}$ installed in Italy is presented in order to describe the mathematical approach to evaluate the economical sustainability of gasifier systems. The first plant is the Spanner Re$^2$ with 45 $kW_{el}$ of nominal power, the second is a cluster of two APL Power Pallet of 20 $kW_{el}$ each. In both cases, the following costs and benefits are taken into account:

- **The cost of biomass fuel:** A poplar wood chips feedstock with total moisture of 30% is considered. The minimum cost of this biomass in dry condition is 0.12 €/kg [1]. However, the cost is reduced to 0.084 €/kg in order to consider the presence of the moisture inside the biomass.
- **The total cost of the investment:** This cost includes fuel storage bins, fuel feeding devices, utility connection and installation cost. For the Spanner Re$^2$, a total

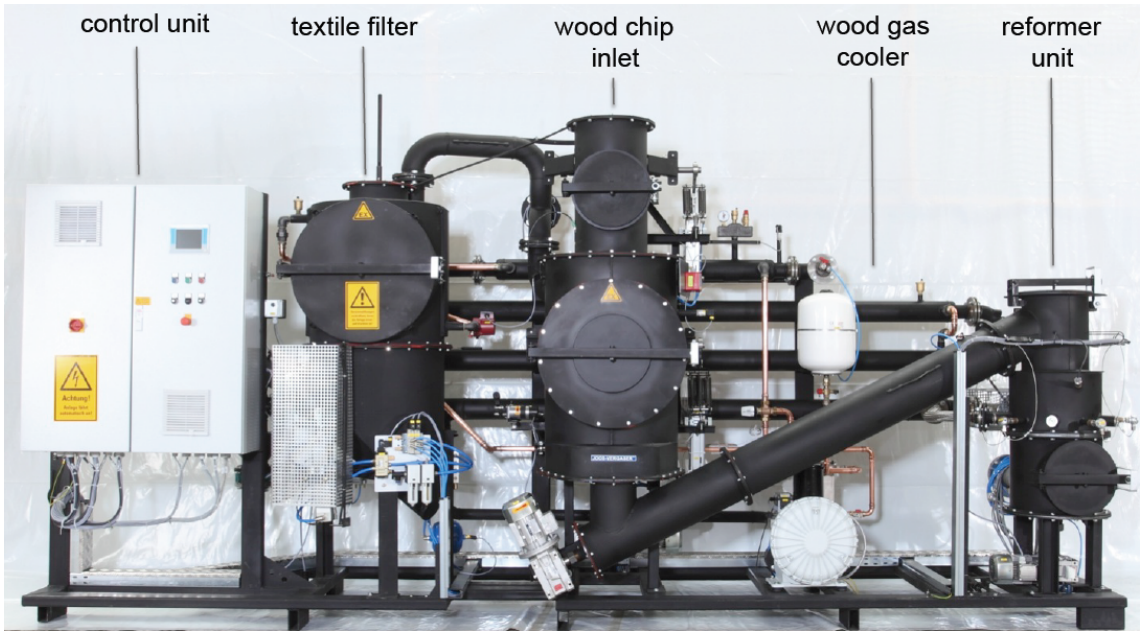


Figure 6.2: Spanner $Re^2$ $GmbH^{TM}$

investment of 230000 €is considered, instead for the two APL Power Pallet a cost of 100000 €is taken into account.

- **The cost of ordinary maintenance:** A full service contract with a fixed cost of 0.03 €/$kWh_{el}$ is adopted in each case.
- **The cost of not ordinary maintenance:** A cost equal to the 5 % of the total initial investment cost is considered every 5 years of operation. These money will be used to change the engine, reactor, filters and pipe parts.
- **The cost of insurance policy:** A contract with a fixed cost of 10 €/$kW_{el}$ every year is assumed for the insurance.
- **The cost of the operating labor:** A fixed cost of 20 €/hour for the operating labor is considered. In this analysis, one hour a day is assumed for ordinary operating procedures.
- **The cost of the tar and char disposal:** A production of char and tar equal to the 5% and 2% of the biomass consumed is adopted. A cost of 0.05 €/$kg_{char}$ and 0.5 €/$kg_{tar}$ for char and tar disposal is considered. Spanner $Re^2$ plant needs to dispose the char and tar, instead APL plant need to dispose only the char.
- **The benefits:** A basic tariffs of 224.4 €/MWh for the 2014 is applied in each case. Further premiums are not considered here. After the 20 years of benefits, the sale of energy produced to the market will be possible. Foe example, a simplified purchase and resale arrangements (RID) convention [202, 203] will be done. For this convention, the selling price for bioenergy from small gasification system is 92.3 €/kWh for the year 2014. In this analysis, a duration of 20 years is considered.

The soft wood biomass consumption suggested by the producer is 1.2 $kg_{wood}$/kWh equal to 48 kg/h for the APL cluster and 1 $kg_{wood}$/kWh equal to 45 kg/h for the Spanner Re$^2$. A value of 7000 hours of working every year is set for the Spanner Re$^2$ system and the APL system. Taking into account these information, an NPV analysis is exposed for each solution. The following formula was used to calculate the net present value (NPV) at the N-th year as the sum of the discounted cash inflow in the years from 0 to N [196]:

$$NPV = \sum_{n=0}^{N} \frac{(I_{To,n} - C_{tot,n})}{(1+i)^n} - I_0 \tag{6.5.1}$$

where $N$ is the number of years of interest, this value is set to 20; $I_{To,n}$ [€] is the annual incoming calculated from the all-inclusive feed-in tariff (To) scheme; $C_{tot,n}$ [€] is the annual total operation cost; $I_0$ [€] is the initial total investment; $i$ is the discount rate [196], its value is considered equal to 1% typical of alternative investments in government bonds (adjusted for the inflation) or 5% typical of mortgage in Italy [23]. Figure 6.3 depicts the NPV trend of the Spanner technology. The payback time is about 10 years with i=1% and about 13 years with i=5%.

Instead, Figure 6.4 depicts the NPV trend of the APL technology. The payback time is about 6 years with i=1% and about 7 years with i=5%. In each cases, the not ordinary maintenance at the fifth, tenth and fifteenth year influences significantly the profit and the NPV curves changes drastically the slope in these years. The numerical results of the analysis for i=1% are reported in Table 6.2.

It can be noted that the APL solution the higher internal rate of return (IRR) [196] of 15.75%. This happens because the initial investment cost of the APL is half compared to the Spanner and the annual incoming and cost are comparable. Further advantage of the APL Power Pallet is no disposal of tar and lower not ordinary maintenance as Spanner Re$^2$. The presence of two indipendet gasifier in the APL cluster permits to have a continuos operation and energy generation because the maintenance of one gasifier can be done independently of the other.

Table 6.2: Spanner Vs. APL Power Pallet economical comparison with i=1%

| | Spanner | APL |
|---|---|---|
| Annual incoming from $To$ | 70686 €/year | 62832 €/year |
| Annual total cost | 44762.5 €/year | 45164 €/year |
| Biomass cost | 26460 €/year | 28224 €/year |
| O.m. cost | 9450 €/year | 8400 €/year |
| N.o.m. cost | 11500 €/year | 5000 €/year |
| Insurance cost | 450 €/year | 400 €/year |
| Operating labor cost | 7300 €/year | 7300 €/year |
| Char disposal cost | 788 €/year | 840 €/year |
| Tar disposal cost | 315 €/year | 0 €/year |
| Annual net profit | 25923.5 €/year | 17668 €/year |
| Final NPV value | 206546 € | 199175 €/year |
| IRR of the investment | 8.45 % | 15.75 % |

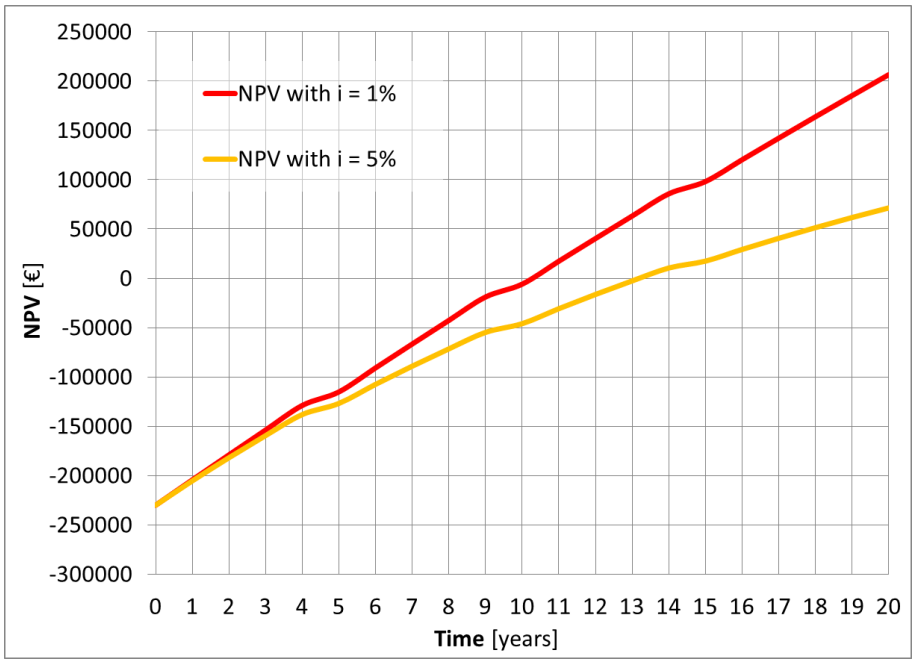


Figure 6.3: Spanner Re$^2$ NPV analysis

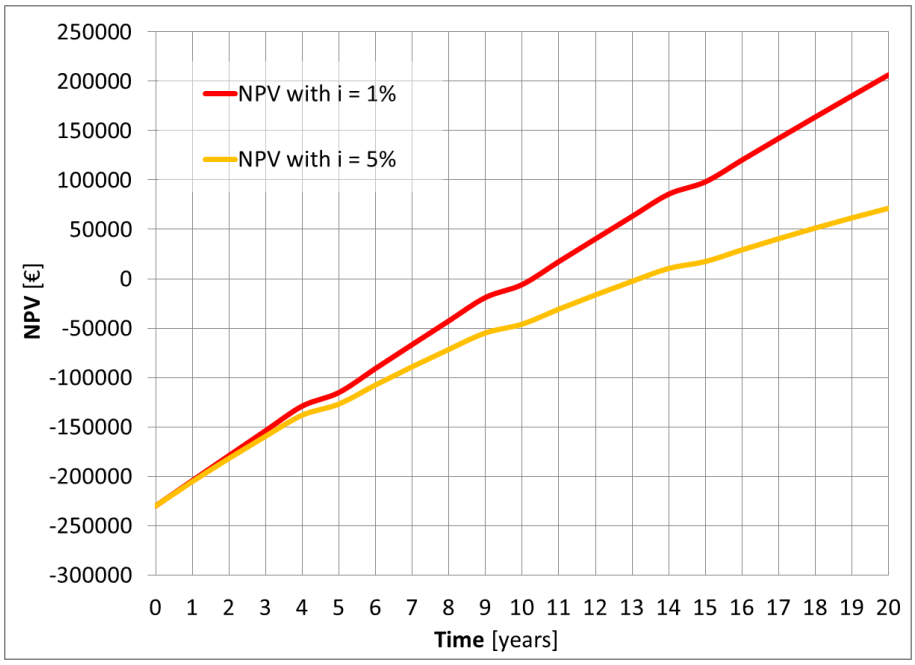


Figure 6.4: APL cluster NPV analysis

# Chapter 7

# An innovative integrated biodiesel production system from biomass gasification

In the last decades, with the increasing demand and price of crop derived fuels, a total utilization of byproducts of crop rotations for energy production is becoming a solution for the higher profitability of farming. Moreover, the "European Union guidelines for energy sustainability" encourages the partial integration of fossil fuels with biofuels. Aim of this chapter is the present an innovative method for on-field biodiesel production from a vegetable oil conversion. The method proposed here is innovative because there is a gasification process where the protein cake from seed press is utilized as fuel. The syngas obtained from the gasifier is used to produce electrical power or to convert it into methanol. The methanol is used to convert the vegetable oil into biodiesel. An IC engine is also implemented into the system in order to convert the syngas excess which is not used for the methanol production, into electrical energy. During a three year cycle the process was investigated as such: in year one the soy, in year two the rapeseed and in year three the sunflower. Between the energetic and economic modelling of the system, its performance proved to be highly effective. This system was simulated using ASPEN PLUS$^{TM}$and MATLAB$^{TM}$program codes and that it takes 15 hectares of land to implement 7 $kW_{el}$ power plant. This is the minimum surface area required to auto-sustain the system. The calculation was done considering the productivity of the land together with the characteristics shown by the protein cakes.

## 7.1 Biofuels production

The production and utilization of biofuels are a central topic for renewable energy for three reasons [204, 205, 206]:

- The promise to reduce the effect of climate change.
- Cost savings.
- This technology can be distribuited easily in many different location instead of being supplied by one central location.

In addition, electric or "fuel cell" vehicle such as cars and buses, require major changes to implement, whereas, biofules can be integrated with fossil fuels or substitute then easily, needing only minor modifications [207, 208, 209, 210, 211].

Biofuels also have a key role in industrial and agricultural businees providing new sources of income, particularly when related to waste oil management [212, 213, 214, 215].

On the other hand, biofuels and especially biodiesel obtained from dedicated cultures and rotations guarantee high efficiency and reliability of the processes [216, 217]. The passages that come in succession from the seeds cultivation to the biodiesel sell on the market can be subdivided into two different macro areas: on one hand there are the farmers who cultivate the energy crops and sell the seeds on the market, on the other hand there are the seeds pressing and oil conversion plants which buy the seeds or the vegetable oil and the methanol from the market and then produce and sell biodiesel [218, 219].

This chapther is aimed at introducing a different way to produce biodiesel through a synergy of different technologies with two major purposes: maximization of the earnings of the farmers and increasing of the sustainability of the system through centralization of all the passages in a single place.

The study is based on a crop rotation composed of oleaginous crops only. The choice of the rotation had been entrusted to literature where Zegada-Lizarazu and Monti have proposed in 2010 and 2011 two possible rotations adequate to Mediterranean zones: rapeseed, flax, sunflower and rapeseed, soy, sunflower [220, 221]. For this work the second rotation mentioned was taken into account.

The simulations of the system were based on data obtained from literature about average oil production from these cultures in the Emilia Romagna region of Italy. In this region, rapeseed crops can easily produce between 4.0 and 4.5 ton/ha of seeds with 9% of moisture, with peak production to 5.7 ton/ha [222]. About 46-47% of rapeseed seeds can be converted into PVO by mechanical processes [222]. Sunflower crops can produce more than 2.8 ton/ha of seeds [223]. About 45% of sunflower seeds can be converted into PVO by mechanical processes [224]. The oleaginous soy crop yields 3.7 ton/ha of beans, with a peak production up to of 4.5 ton/ha [225, 226]. About 20% of soy beans can be converted into oil by mechanical processes [226].

The system layout proposed here is represented in Figure 7.1. The approach of single culture cultivation is the following: every year a different crop is cultivated on the whole surface and the seeds are converted into PVO by a mechanical process. The protein cake obtained as a byproduct of the oil extraction is gasified in a downdraft stratified reactor connected to an electrical generator of 10 kW of peak power. A small part of the syngas is converted into methanol in a chemical reactor. The methanol is then used in the transesterification reaction of the PVO to produce biodiesel.

The gasifier model is based on the following parameters: ultimate analysis of the protein cake, dimensions and physical properties of the cake pellets and geometrical parameters of the gasifier. The geometrical and physical properties of the protein cake are obtained through a series of experimental analysis, the results of these analysis are reported in Table 7.2.

The biodiesel production process is divided into two stages: first the syngas is converted into methanol, then PVO and methanol are mixed in a second reactor with a catalyzing agent for biodiesel production. The methanol production conversion reactions are simulated with an equilibrium-based approach, the biodiesel production is modeled by a stoichiometric approach with a known conversion rate typical of the catalytic reactions. The whole model

allows to calculate the mass of biodiesel oil and glycerin obtained every year and the electrical energy produced by the generator connected to the gasifier. An economical analysis is made to evaluate the return of the investment.

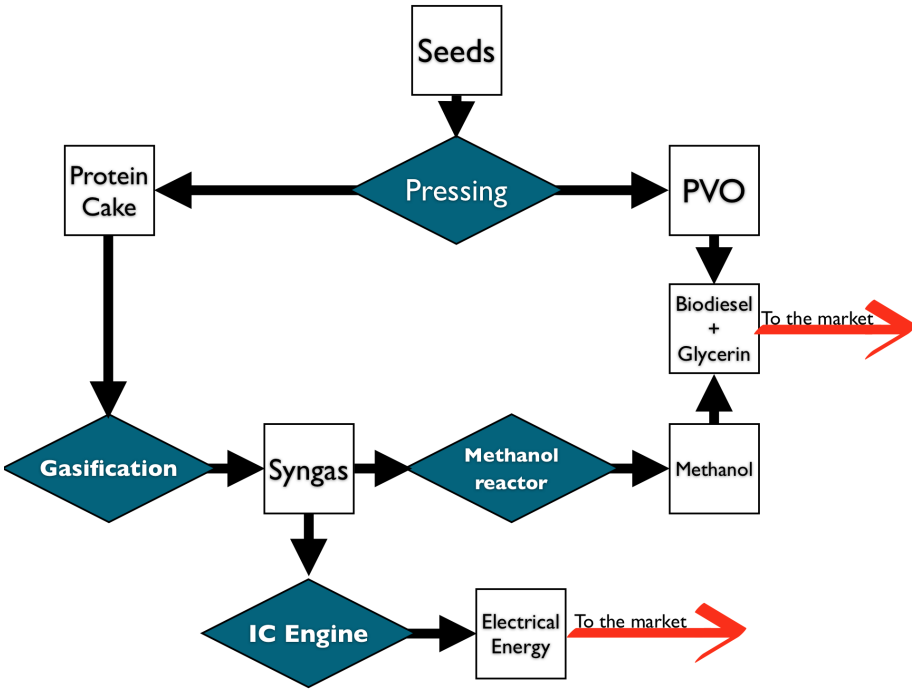


Figure 7.1: Basic layout of the system

## 7.2 Modeling approach

The input data used in the gasifier model can be obtained from literature review, but for a more specific comprehension of the gasification of the protein cake, different analysis have been carried out on a sample of sunflower cake pellet.

The gasifier model requires the fuel bulk density and the void fraction, these two values have been obtained with a gas pycnometer with helium as working gas. The average value obtained with this measurement was 1790 kg/m$^3$. The void fraction was obtained from the apparent density of the sample measured by hydrostatic weighting. The average apparent density is 930 kg/m$^3$. The geometrical properties of the cake pellet were obtained with a series of 50 measurements with a caliber. The average diameter is 8.5x10$^{-3}$ m and the average length is 8.8x10$^{-3}$ m. The average particle volume is 4.9x10$^{-7}$m.

Further analysis were made on the sample for the evaluation of the moisture content, ash content. Four ultimate analysis was done and the results are reported in Table 7.1. The geometrical and physical proprieties of the sunflower pellets has been used for description of all the pellet considered in this section.

### 7.2.1 Gasifier mathematical model

The kinetic model explained in Chapter4 was applied to calculate gasifier behaviour with different protein cake pellets. Table 7.2 rapresents the chemical, physical and geometrical

Table 7.1: Sunflower cake pellets: experimental results

| | | | | |
|---|---|---|---|---|
| Ash content | 3.82 % | | | |
| Moisture content | 10.81% | | | |
| Ultimate analysis: | | | | |
| Test number | N [%] | C [%] | H [%] | S [%] |
| I | 0.87 | 47.18 | 6.31 | 0 |
| II | 0.81 | 46.63 | 6.5 | 0 |
| III | 0.87 | 46.41 | 6.45 | 0 |
| IV | 0.97 | 46.91 | 6.44 | 0 |
| Average | 0.88 | 46.78 | 6.42 | 0 |

properties of the following protein cakes used as model input in this work: rape, sunflower and soy. Table 7.3 shows the geometrical and physical parameters of the gasifier and generator. Furthermore, Table 7.5 resumes the syngas compositions, $HHV_{syngas}$ and the gasifier "cold gas" efficiency $\eta_{cold}$ for rapeseed, sunflower and soy protein cakes.

Table 7.2: Protein cakes parameters

| Parameter | Rapeseed protein cake | Sunflower protein cake | Soy protein cake |
|---|---|---|---|
| Equivalent pellet diameter $d_p$ | 0.01 m | 0.01 m | 0.01 m |
| Density $F_d$ | 1.79 $kg/m^3$ | 1.79 $kg/m^3$ | 1.79 $kg/m^3$ |
| Void fraction $F_v$ | 0.48 | 0.48 | 0.48 |
| Moisture | 10.8% | 10.8% | 10.8% |
| C (wt%) | 43.2% | 46.78% | 55.89% |
| H (wt%) | 6% | 6.425% | 6.57% |
| O (wt%) | 44.27% | 45.91% | 28.25% |
| N (wt%) | 5.6% | 0.88% | 9.29% |
| S (wt%) | 0.93% | 0 % | 0% |
| Ash (wt%) | 7.20% | 3.82% | 5.36% |
| $HHV_{bio,dry}$ | 15.37 MJ/kg | 16.76 MJ/kg | 21.34 MJ/kg |

Table 7.3: Parameters of the downdraft stratified gasifier and generator

| Parameter | Value |
|---|---|
| Gasifier diameter $D_g$ | 0.28 m |
| Gasifier area $A_g$ | 0.0616 $m^2$ |
| Fixed bed height H | 0.4 m |
| Flaming pyrolysis temperature $T_s$ | 1173 K |
| Char reduction temperature T | 1073 K |
| Equivalence ratio ER [6] | 0.35 |
| Pressure in the gasifier p | 1 bar |
| Generator electrical efficiency $\eta_{gen}$ [21] | 25% |

### 7.2.2 Biodiesel production model

The biodiesel production model was developed in ASPEN$^{TM}$ Plus software. The model uses two different kinds of input: the PVO flow rate input is based on the data coming from a literature review on seeds and oil production of rapeseed, soy and sunflower in Emilia Romagna region. The model uses the results of the kinetic model applied to simulate the

gasification of the three protein cakes adopted. The process is reported in Figure7.2 and it is subdivided into two steps:

- Syngas to methanol conversion.
- Biodiesel production from the reaction of PVO with the produced methanol.

The amount of oil produced every year from one hectare of crop rotation is known. The amount of methanol (therefore syngas) for total conversion of PVO in biodiesel is initially unknown. For this reason, the algorithm of the process needs to be followed from the bottom up:

- **Biodiesel production:** The biodiesel production model is used for back-calculating the required methanol amount for the reaction of the known amount of PVO produced. The methanol production is modeled in ASPEN plus starting from the composition of the syngas obtained as output in the gasifier model. The output of the ASPEN simulation of biodiesel production combined with methanol production is the amount of syngas necessary for the reaction of the known amount of PVO produced by one hectare of culture. This is done by the function 'Design Specification' available in ASPEN Plus. The gasifier model gives the syngas volume produced by the gasification of known amount of protein cake. The difference between the syngas produced from cake gasification and the syngas required for methanol production represents the gas excess that can be sent to the IC engine for a further electrical power production. The biodiesel production model from PVO and methanol is based on the reaction of Transesterification of Triolein [219]:

$$\text{TRIOLEIN} + 3CH_3OH \rightarrow^{KOH} 3 \text{ METHYL OLEATE} + \text{GLYCEROL} \quad (7.2.1)$$

  In this part of the model the inputs are: the mass of PVO produced by one hectare of soil during the rotations, the typology of reactor and its operating conditions as reported in Table 7.4. A "RSOITC" reactor configuration based on stoichiometric approach with a defined conversion was used for simulating the biodiesel production process. Due to the presence of highly polar components, an universal quasi-chemical thermodynamic activity (UNIQUAC) model was used. The outputs are the amount of biodiesel and glycerine and the amount of methanol required for 95% of PVO conversion. Figure 7.1 schematizes the process as reported in ASPEN$^{TM}$ plus. The results, reported in Table 7.6, are used for the second part of the model.

- **Syngas to methanol conversion:** The methanol formation is based on the following reactions[227]:

$$CO + 2H_2 \rightarrow CH_3OH \quad (7.2.2)$$

$$CO_2 + 3H_2 \rightarrow CH_3OH + H_2O \quad (7.2.3)$$

$$CO_2 + H_2O \rightarrow CO_2 + H_2 \quad (7.2.4)$$

The conversion from syngas to methanol has been described analytically and modeled with ASPEN$^{TM}$ plus. The reactor configuration used for this part of the simulation was "REQUIL" which uses an equilibrium approach. The syngas obtained from biomass gasification is not composed of carbon monoxide and hydrogen only as it contains also different gases like carbon dioxide, nitrogen and methane. The CO and $CO_2$ are in stoichiometric excess compared to hydrogen, therefore the molar flow rate of methanol produced in the reactor is limited by the conversion of $H_2$. For the operating conditions of the reactor, given in Table 7.4, the hydrogen conversion is about 15%. The syngas composition depends on the solid fuel used, the thermal stratigraphy and the equivalence ratio of the gasifier. An average syngas composition has been used in this part of the model. The inputs are the methanol amount required by the first part of the model, the syngas composition from the gasifier model, the temperature and pressure of the methanol reactor, these parametersa are reported in Table 7.4. The whole system has been resolved using the "Design Specification" function of Aspen Plus in order to obtain the flow rate of syngas necessary for producing the methanol required for PVO conversion. The results are summarized in the Table 7.6 and are the amount of syngas required for the process and the amount and the composition of the syngas purged as result of the presence of inert $N_2$.

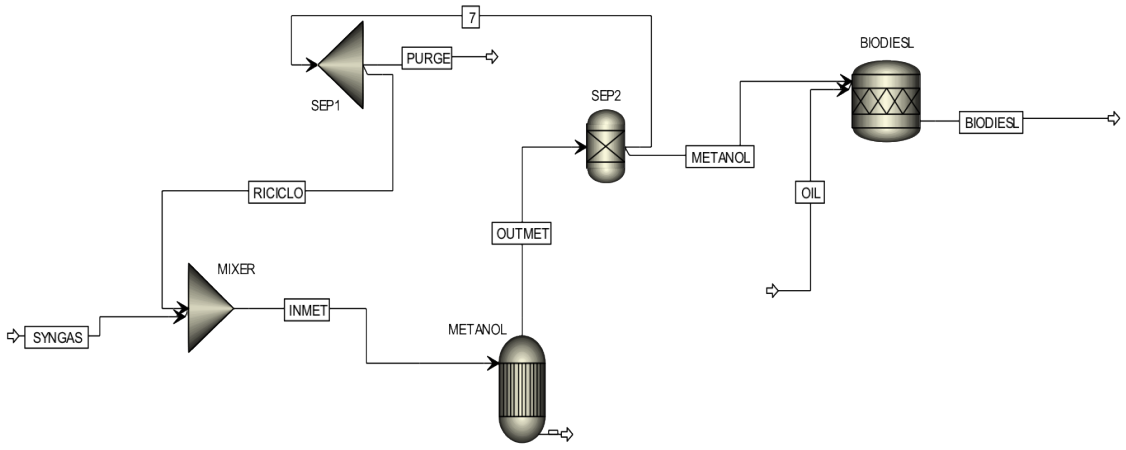


Figure 7.2: Biodiesel production model in $ASPEN^{TM}$ plus software

Table 7.4: Parameters of the biodiesel production model

| Parameter | Value |
|---|---|
| Methanol reactor pressure | 76 bar |
| Methanol reactor temperature | 523.15 K |
| Recycle ratio | 8 |
| Biodiesel reactor pressure | 1 bar |
| Biodiesel reactor temperature | 343.15 K |

## 7.3 Results and discussion

### 7.3.1 Chemical balance

Table 7.6 shows the productivity of one hectare in terms of syngas, oil, biodiesel and glycerin. Table 7.7 resumes the energy production of one hectare of different crops. The three cultures chosen for this work produce more syngas than required by the biodiesel conversion, this makes the system self-sustainable from a chemical point of view. The soy has the lowest performance in terms of oil production as shown in Figure 7.3, but it has more protein cake that produce a big amount of syngas. This result outline one of the major advantage of this approach: the oil productivity of the seeds is not the only parameter necessary to estimate the economical value of the culture. Crops such as the soy can recover its low oil production with an high syngas yield and therefore energy production.

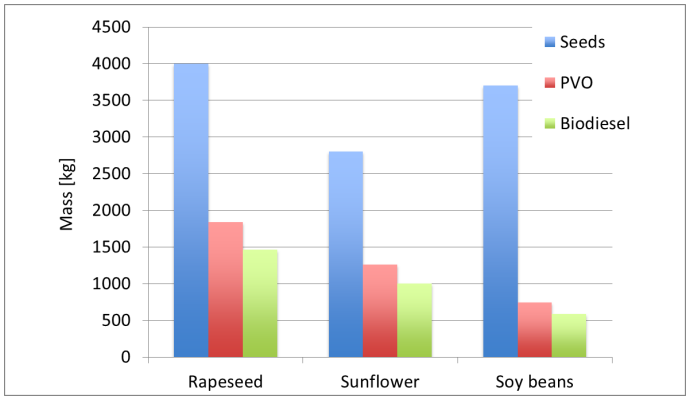


Figure 7.3: Productivity differences

Table 7.5: Results of the gasification model

| Variable | Rape seed | Sunflower seed | Soybean |
|---|---|---|---|
| $H_2$ [%vol] | 9.40 % | 9.73 % | 10.61 % |
| $CO$ [%vol] | 13.17 % | 14.33 % | 15.78 % |
| $CH_4$ [%vol] | 6.52 % | 6.31 % | 5.37 % |
| $CO_2$ [%vol] | 15.55 % | 15.51 % | 10.90 % |
| $N_2$ [%vol] | 54.82 % | 54.12 % | 57.35 % |
| Syngas production per hectare | 4863 kg | 3799 kg | 8761 kg |
| $HHV_{syngas}$ | 5.08 $MJ/Nm^3$ | 5.12 $MJ/Nm^3$ | 5.06 $MJ/Nm^3$ |
| $\eta_{cold}$ | 63.98 % | 65.44 % | 63.55% |

As the system is self-sustainable, it is possible to design the plant on the basis of the engine peak power value. This value determines the total surface that needs to be tilled because it is related to the syngas excess previously discussed. One of the major advantages of the approach proposed is the energy recovery during the process: even if the methanol reactor has a low conversion rate, the unreacted gas chemical energy is not wasted because the purge line is connected with the engine. The results obtained show that every hectare of culture allows the engine to run from 254 to 469 hours depending on the kind of culture

Table 7.6: Results of the biodiesel production model for 1 hectare of soil

| Variable | Rapeseed | Sunflower | Soy |
|---|---|---|---|
| Seeds | 4000 kg | 2800 kg | 3700 kg |
| PVO | 1840 kg | 1260 kg | 740 kg |
| Biodiesel | 1465 kg | 997 kg | 583 kg |
| Glycerin | 488 kg | 332 kg | 194 kg |
| Methanol required | 204 kg | 138 kg | 77 kg |
| Syngas required | 4160 kg | 2718 kg | 1173 kg |
| Syngas purged | 3956 kg | 2580 kg | 1093 kg |
| $H_2$ purged | 4.36 % | 4.45 % | 4.6% |
| CO purged | 11.28 % | 11.47 % | 14.24 % |
| $CH_4$ purged | 6.85 % | 6.78 % | 5.69 % |
| $CO_2$ purged | 19.97 % | 19.45 % | 14.01% |
| $N_2$ purged | 57.41 % | 57.76 % | 61.30 % |
| $HHV_{purged}$ | 4.350 MJ/N$m^3$ | 4.355 MJ/N$m^3$ | 4.345 MJ/N$m^3$ |

(see Table 7.7).

Table 7.7: The IC engine output for 1 hectare

| Output | Rapeseed | Sunflower | Soy |
|---|---|---|---|
| Gasified protein cake kg/ha | 2160 | 1540 | 2960 |
| Operating hours at 7 kWel | 254 | 201 | 469 |
| Energy produced kWh/ha | 1778 | 1406 | 3281 |

The engine has been designed to run at 7 kW of average power, allowing small fluctuations in the gas production rate or in the gas composition without exceeding the maximum power production [6, 22]. The waste heat coming from the methanol reactor and the engine can be used for several application. Furthermore, if the heat produced by the processes is used entirely, the system can be considered "CHP with high efficiency" and this solution guarantees a higher subsidy [198].

Basically, regardless of the fuel used, IC engines produce two kind of low-grade heat: one with higher temperature that is recovered from the exhausts and a low temperature heat that can be extracted from the engine radiator. Further to CHP applications, both these kind of heat can be used for cake drying as well as heat supply in part of the plant that will require it (i.e. for heating up the biodiesel reactor to increase the glycerin flowability).

The data discussed here allows the calculation of the number of hectares necessary to guarantee the running of the plant for a fixed number hours a day every year. Because the higher the surface tilled, the less the specific cost of cultivation, the system considers only one crop a year. If the protein cake is properly dried, there is no reason to consume all the cake in one year. Under these conditions it is possible to balance the whole system after 3 years of running, when the rotation is ended.

Figure 7.4 shows two significant results: 1) three lines with low slope which give the number of hours of engine runs as a function of the surface tilled for every crop and 2) a line with higher slope obtained as sum of the previuos line.

The cumulative line represents the total number of hours which the engine have to run in the three year period fixing a surface value. Horizontal dashed lines are placed at 8760

and 13140. These two values are obtained as 8 or 12 hours a day multiplied by 1095 days which represent 3 years. Therefore, the values of surface where the cumulative line crosses the dashed ones represent the surfaces required to ensure the plant run for 8 or 12 hours a day for three years.

The cumulative line crosses the first horizontal line for a surface between 9 and 10 hectares. Instead, the minimum surface required in case of 12 hours of plant run a day is 15 hectares. From the logistic point of view, because the three cultures do not produce the same amount of solid feedstock, the system is balanced over a three year period instead of year by year. For example, the soy seeds collected on the first year can be stored allowing the plant operations for 12 hours a day for 19 months, sunflower seeds allow the plant operations for more than 8 months, and rapeseed seeds more than 9. Only at the end of the third year all the biomasses are consumed and all the oil is converted into biodiesel.

### 7.3.2 Economical analysis

The analysis was based on a few conservative assumptions:

- The cost for the oil extraction is evaluated starting from the work of Singh and Bargale[228]. They developed a small capacity double stage compression screw press for oil expression with an average specific consumption of 0.05 kWh/kg of seeds[228]. This electrical energy is absorbed from the grid and not self-consumed from the power output of the engine. The considered cost for electricity at the current grid price for industrial uses is 0.1565 €/kWh$_{el}$ [229]).
- The annual costs for cultivating the rapeseed, sunflower and soy per hectare of soil are 680 €, 850 €, 1245 €. These costs were obtained as sum of seed, fertilization and farming costs[225].
- This analysis does not take into account the electrical energy surplus obtainable through gasification of the stalks and other vegetable byproducts of seeds crop. This surplus can be used for increasing the engine power output or, together with the protein cake, to increase the gasifier performance.
- The income for sale of the glycerin is 0.145 €/kg [230]).
- The electrical energy required for the biodiesel conversion has been taken from the following work [231] where for the conversion of one kilogram of oil are necessary 0.15 kWh of electrical energy.

With regard to the sale of biodiesel and electrical energy, two different options are considered, both referred to 8 and 12 hours of plant running a day:

A The selling of the biodiesel at the sale price of 0.982 €/L which is the current value on the Italian industrial market [232] and the tariff for the energy generated of 0.269 €/kWh$_{el}$ in accordance with the current RES-E subsidies program [198] (base tariff plus premium for CAR).

B The self consumption of the biodiesel which is considered at the net industrial price of fuel for agricultural uses (about 0.790 €/L in 2012 [232]) and the self consumption of the electrical energy generated.

The option B consists in self-consumption of all the electrical energy and biodiesel produced. It was found to generates a positive cash flow of about 4163 €/year. On the other hand, the Option A (electrical power and biodiesel sell) generates a more positive cash flow of about 11636 €/year with 12 hours of plant running a day. A conventional net present value analysis is showed in Figure 7.5. It is based on an investment of about 50000 € ($I_0$) for the whole system. Considering the option A, the capital cost is amortized within about 4.5 years with 1% of discount rate typical of alternative investments in government bonds (adjusted for inflation). Whereas 5 years are needed if the discount rate is that of typical mortgage, al least 5% in Italy.

The choice of the more suitable gasifier for this application is determined by the characteristics of the protein cakes processed. For this non-conventional fuel an open core or an Imbert gasifier are good choices due to the capability of these reactors to process different kind of biomasses, but only an experimental analysis on a reactor with this specific fuel can guarantee the sustainability of the process [22, 233]. The market offers different reactors for the power output size required in this work [88, 87, 89]. For cost estimations the ALL Power Labs device has been used as an example. The cost of the whole system has been estimated on the following assumptions:

- A 10 kW gasifier equipped with internal combustion engine can be found on the market for about 22000 € comprehensive of shipping extra costs [87].
- The costs of the methanol and biodiesel production reactors and the seed-press have been approximated to be 28000 € [234, 235].

The following formula was used to calculate the net present value (NPV) at the N-th year as the sum of the discounted cash inflow in the years from 0 to N:

$$NPV = \sum_{n=0}^{N} \frac{(I_{bd+ee} - I_{seeds,cultivation} - I_{el\ consumption})}{(1+i)^n} - I_0 \tag{7.3.1}$$

where $i$ is the discont rate; $I_{bd+ee}$ [€] is the annual incoming from subsidies and biodiesel selling in the option A and from the self consumption of biodiesel and electricity in the option B; $I_{seeds,cultivation}$ [€] is the annual cost for the cultivation of the crop and $I_{el\ consumption}$ [€] is the annual cost for the electricity self consumed by the process.

It is interesting to note that 65% of all income of the option A come from biodiesel, thus about 35% comes from electricity. Increasing the production of syngas and electrical energy through utilization of stalks and other byproducts of seeds crops can thus improve significantly the cash flow.

## 7.4 Summary

The system proposed and discussed was able to convert into biodiesel, glycerin and electricity the seeds coming from a three years, 15 hectares crop rotation. From a chemical point of view, the system investigated was advantageous due to the possibility to convert both the solid and liquid matter obtained from seeds pressing. Furthermore, the economical analysis showed the high profit obtained through this solution.

For a complete comprehension of the complex phenomena and interactions that occur in this system, an experimental analysis in a lab-scale reactor is vital. There are many points

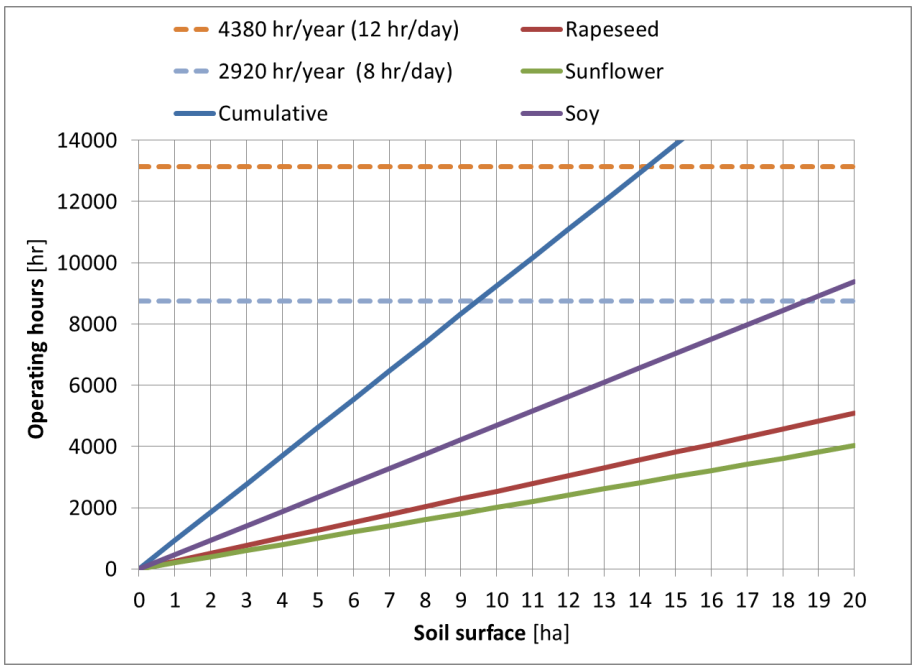


Figure 7.4: Hours of plant running per hectare of tilled surface

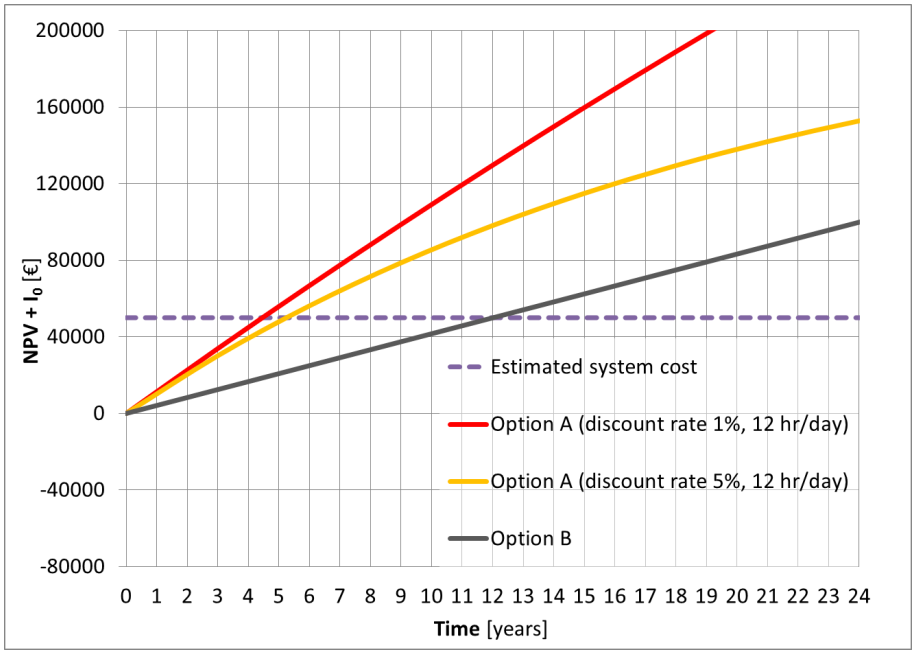


Figure 7.5: The NPV analysis of the system

that need to be investigated in future work, such as capability to avoid ashes slagging in the gasifier or the effect of syngas composition fluctuations on methanol conversion rates. Once the system model is validated, different rotations can be simulated in order to maximize the profit.

# Concluding Remarks

The purpose of this thesis is to model and optimize power plants for electical energy production using wood chips as feedstock. The goal has been reached both for conventional biomass system and for advanced plants equipped with high-tech apparatus. A further implementation of the gasification of an agricoltural byproducts in order to produce biodiesel was illustrated.

In Chapter 1 a brief introduction on world bioenergy scenario and prospects was reported. The advantages of using biomass as energy fuels and the widely used conversion technologies from biomass to energy were discussed. Furthermore, a comparison with these technologies found that the gasification of wood and the utilization of the clean syngas in an IC engine is the more efficient method to convert wood biomass into electrical energy. For this reason, all the thesis was focused on gasification.

The thermochemical and physical properties of wood biomass were summarized in Chapter 2. Ultimate and proximate analysis was reported because theirs results are used in modeling of biomass system. In Chapter 3 was reported a short compendium of gasification. Here processes, chemical reaction, gasifier classification and fixed bed gasifier were described.

The modeling of fixed bed gasifier was the topic of Chapter 4. Different modeling approaches were exposed and an application of a kinetic modeling was applied to justify the channeling phenomenon in fixed bed downdraft stratified reactors. Chapter 5 was focused on the modeling and on the simulation of wood gasification power plants. A conventional medium scale gasifier-IC engine power plant was modeled and the result was compared with experimental data. Subsequently, the annual simulation of an advanced DG-SOFC-MGT power system was made in order to assess the long term performance and the maintenance effects of the gasifier on the eletrical power production. Furthermore, this system was optimized with the addition of a PPO membrane module to increment the oxygen in the gasifier agent and with the addition of a ZEO module in order to eliminare the $CO_2$ in the dry syngas. Using these apparatus, the tar production and the storage volume decrease considerably.

An economical NPV analysis of two small gasifier power plants was done in Chapter 6. In this chapter prons and cons of gasifier was quantified economically. The cost of biomass, maintenance and byproducts disposal are some issues that make the investment advantageous only with high subsidies from the state.

An innovative integrated biodiesel production system from biomass gasification was described in Chapter 7. This system uses a three year crop rotation to produce seed. From the mechanical pressing of the seed, oil and protein cake are obtained. The gasification of the protein cake generates syngas, a fraction of this gas can be converted in methanol and the rest can be used to produce electricity through an IC engine and an alternator.

The methanol mixed with oil generates a mixture of about 95% of biodiesel and 5% of glycerine. The farmer is now able to sell biodiesel to the market instead of seeds with several advantages. All the cycle was simulated and the results revealed that the surface necessary for sustainability of the system is about 15 hectares for a pilot plant equipped with a small 7 $kW_{el}$ engine.

The gasification is a old technology heavily exploited in the first half of the twentieth century where the char was used as feedstock. Now, the wood or byproducts gasification for energy production is a field of interest by investors as result of high subsidies and economical valorization of some feedstocks normally dispose. However, the gasification is complex and sensible to biomass quality fluctuations, furthermore plant maintenance is vital to ensure higher level of security and efficiency.

Several issue of biomass gasification such as "channeling" phenomenom, loading frequency, tar overproduction, maintenance and plant monitoring are also reported. Some solution to overcome this problem are presented and the validity of these solution is discussed. In addition, this thesis collects mathematical approaches, experimental data and innovative researches that can be useful tools to design and simulate gasifier power plant systems.

The surplus value of this thesis from the scientific point of view, is the innovative kinetic model presented in Chapter 4 able to simulate the gasifier operation when occours "channeling". Also the application of zeolites to separate $CO_2$ from the syngas and the application of a PPO membrane to increase the oxygen of the air as gasification agent are two novel application in this scientific field. Finally, the biodiesel production using methanol obtained from the protein cake gasification is a new application of gasification in the chemical industry.

# List of Figures

# List of Tables

# Bibliography


[1] IEA. Technology roadmap - bioenergy for heat and power. Technical report, IEA, 2012.

[2] N. Kautto and P. Peck. Regional biomass planning: Helping to realise national renewable energy goals? *Renewable Energy*, 46(0):23 – 30, 2012.

[3] IEA. Policies and measures database. Technical report, International Energy Agency, 2012.

[4] IEA. Technology roadmap: Biofuels for transport. Technical report, IEA, 2011.

[5] Prabir Basu. *Biomass Gasification and Pyrolysis: Practical Design and Theory*. Academic Press, Elsevier, 2010.

[6] Thomas B. Reed and Agua Das. *Handbook of Biomass Downdraft Gasifier Engine Systems*. The biomass energy foundation press, 1988.

[7] J. Lehmann. Bio-energy in the black. *Frontiers in Ecology and the Environment*, 5, 2007.

[8] J. Lehmann, J. Gaunt, and M. Rondon. *Mitigation and Adaptation Strategies for Global Change*, 11:403–427, 2006.

[9] J. Lehmann and S. Joseph. *Biochar for Environmental Management: Science and Technology*. Earthscan Publ., 2009.

[10] J. Lehmann. A handful of carbon. *Nature*, 447:143–144, 2007.

[11] Sebnem Yilmaz and Hasan Selim. A review on the methods for biomass to energy conversion systems design. *Renewable and Sustainable Energy Reviews*, 25(0):420 – 430, 2013.

[12] H V Sridhar, G Sridhar, S Dasappa, N K S Rajan, and P J Paul. Experience of using various biomass briquettes in ibg (iisc bioresidue gasifier). Technical report, Advanced Bio-residue Energy Technologies Society Combustion Gasification and Propulsion Laboratory Department of Aerospace Engineering, Indian Institute of Science, Bangalore, India, -.

[13] T.C. Acharjee, C.J. Coronella, and V.R. Vasquez. Effect of thermal pretreatment on equilibrium moisture content of lignocellulosic biomass. *Bioresource Technology*, 102:4849–4854, 2011.

[14] M.J.C. van der Stelt, H. Gerhauser, J.H.A. Kiel, and K.J. Ptasinski. Biomass upgrading by torrefaction for the production of biofuels: a review. *Biomass and Bioenergy*, 35:3748–3762, 2011.

[15] ENEA. Energia dalle biomasse, tecnologie e prospettive. Technical report, Ente per le Nuove tecnologie, l'Energia e l'Ambiente - Regione Siciliana, assessorato industria, 2008.

[16] John E. White, W. James Catallo, and Benjamin L. Legendre. Biomass pyrolysis kinetics: A comparative critical review with relevant agricultural residue case studies. *Journal of Analytical and Applied Pyrolysis*, 91(1):1–33, 2011.

[17] Ozlem Onay and O.Mete Kockar. Slow, fast and flash pyrolysis of rapeseed. *Renewable Energy*, 28(15):2417–2433, 2003.

[18] G. Grinzi, L. Guidetti, G. Allesina, A. Libbra, P. Martini, and A. Muscio. Increase of net power generation of biogas plants by reduction of heat loss. In *20th European Biomass Conference and Exhibition*, 2012.

[19] Waldir Antonio Bizzo, Paulo CÃČÂľsar LenÃČÂğo, Danilo JosÃČÂľ Carvalho, and JoÃČÂčo Paulo Soto Veiga. The generation of residual biomass during the production of bio-ethanol from sugarcane, its characterization and its use in energy production. *Renewable and Sustainable Energy Reviews*, 29(0):589 – 603, 2014.

[20] Guido Galeno. *Modellizzazione di un micro cogeneratore basato sulla tecnologia mcfc accoppiata ad un gassificatore di biomassa.* PhD thesis, University of Cassino, Italy, 2006-2007.

[21] FAO Forestry Department Mechanical Wood Products Branch. *Woodgas as engine fuel*, volume ISBN 92-5-102436-7. F.A.O., 1986.

[22] H.A.M. Knoef. *Handbook of Biomass Gasification.* BTG, 2005.

[23] G.Allesina, A. Muscio, S. Tebianian, S. Pedrazzi, and P. Tartarini. Biodiesel production through synergy of on-field pvo extraction and protein cake gasification. *3th International Conference of Microgeneration and Related Technologies; Naples, IT*, 2013.

[24] David Martin Alonso, Jesse Q. Bond, and James A. Dumesic. Catalytic conversion of biomass to biofuels. *Green Chem.*, 12:1493–1513, 2010.

[25] A. Demirbas. Mechanisms of liquefaction and pyrolysis reactions of biomass. *Energy Conversion and Management*, 41(6):633 – 646, 2000.

[26] Ayhan Demirbas. Competitive liquid biofuels from biomass. *Applied Energy*, 88(1):17–28, 2011.

[27] F. Behrendt, Y. Neubauer, M. Oevermann, B. Wilmes, and N. Zobel. Direct liquifaction and biomass. *Chemical Engineering Technology*, 31 (5):667–77, 2008.

[28] A. Duvia and M. Gaia. Cogenerazione a biomassa mediante turbogeneratori orc turboden: tecnologia, efficienza, esperienze pratiche ed economia. *Congress: Cogenerazione a biomassa mediante Turbogeneratori ORC Turboden: tecnologia, efficienza, esperienze pratiche ed economia.*, 2004.

[29] F. Martelli, G. Riccio, S. Maltagliati, and D. Chiaramonti. Technical study and environmental impact of an external fired gas turbine power plant fed by solid fuel. *1st world Conference of Biomass, Sevilla*, 2000.

[30] V. Naso. *La macchina di Stirling.* CEA, 1991.

[31] S. Compaore. *MOTORI A COMBUSTIONE INTERNA E TURBINE A GAS DI PICCOLA TAGLIA PER GAS DI SINTESI.* PhD thesis, University of Padova, bachelor thesis, 2011-2012.

[32] G. Allesina, S. Pedrazzi M.Puglia, and P. Tartarini. Upgrading or substituting the gasification process for electrical energy production: an energy-based comparison. In *XXX UIT Conference, Bologna 2012*, 2012.

[33] USDA. Wood handbook - wood as an engineering material. Technical report, Forest Products Laboratory - United States Department of Agriculture Forest Service, 2010.

[34] P.C.A. Bergman. Combined torrefaction and pelletisation. Technical report, Energy Research Center of The Netherlands ECN, 2005.

[35] D.L. Klass. *Biomass for Renewable Energy, Fuels, and Chemicals.* Academic Press, 1998.

[36] N.S.S. Rajapaksha, K.R. Butt, E.I. Vanguelova, and A.J. Moffat. Earthworm selection of short rotation forestry leaf litter assessed through preference testing and direct observation. *Soil Biology and Biochemistry*, 67(0):12 – 19, 2013.

[37] J.M. Jones, M. Nawaz, L.I. Darvell, A.B. Ross, M. Pourkashanin, and A. Williams. Towards biomass classification for energy applications. In A.V. Bridwater and A.V. Boocock, editors, *Science in Thermal and Chemical Biomass Conversion*, volume 1, pages 331–39. CPL Press, 2006.

[38] B.M. Jenkins. Physical properties of biomass. In O. Kitani and C.W. Hall, editors, *Biomass Handbook.* Gordon & Breach Science Publishers, Amsterdam, 1989.

[39] Vytenis Babrauskas. Ignition of wood: A review of the state of the art. In *Interflam.* Interscience Communications Ltd., London, 2001.

[40] ASTM. Astm d240 - 09 standard test method for heat of combustion of liquid hydrocarbon fuels by bomb calorimeter. Technical report, ASTM International, 2007.

[41] ECN. Database for biomass and waste, 2013.

[42] V. Mettanant, P. Basu, and J. Butler. Agglomeration of biomass fed fluidized bed gasifier and combustor. *Canadian Journal of Chemical*, 87 (Oct):656–684, 2009.

[43] Giulio Allesina, Simone Pedrazzi, and Paolo Tartarini. Modeling and investigation of the channeling phenomenon in downdraft stratified gasifers. *Bioresource Technology*, 146(0):704 – 712, 2013.

[44] M. Paganelli and D. Sighinolfi. New double optic heating microscope for multi-standard analysis. *CFI. Ceramic forum international*, 86(5):E18–E21, 2009.

[45] S.A. Channiwala and P.P. Parikh. A unified correlation for estimating hhv of solid, liquid and gaseous fuels. *Fuel*, 81(8):1051–1063, May 2002.

[46] Y. A. Cengel. *Introduction to thermodynamics and heat transfer*. McGraw-Hill, 1997.

[47] Lopamudra Devi, Krzysztof J Ptasinski, and Frans J.J.G Janssen. A review of the primary measures for tar elimination in biomass gasification processes. *Biomass and Bioenergy*, 24(2):125–140, 2003.

[48] T.A. Milne, R.J. Evans, and N. Abatzoglou. *Biomass gasifier" tars": their nature, formation, and conversion*. National Renewable Energy Laboratory Golden, CO, 1998.

[49] H.A.M. Knoef. *Handbook of Biomass Gasification, Second Edition*. BTG, 2012.

[50] Christopher Higman and Maarten van der Burgt. *Gasification*. GPP, 2008.

[51] C.C.P. Pian and K. Yoshikawa. Development of a high-temperature air-blown gasification system. *Bioresource Technology*, 79(3):231–241, 2001.

[52] J. Chen, X. Lu, H. Liu, and J. Liu. The effect of solid concentration on the secondary air-jetting penetration in a bubbling fluidized bed. *Power Technology*, 185(2):164–169, 2008.

[53] Scott Hurley, Chunbao (Charles) Xua, Fernando Preto, Yuanyuan Shao, Hanning Li, Jinsheng Wang, and Guy Tourigny. Catalytic gasification of woody biomass in an air-blown fluidized-bed reactor using canadian limonite iron ore as the bed material. *Fuel*, 91(1):170–176, 2012.

[54] Steve Lysenko, Samy Sadaka, and Robert C. Brown. Comparison of mass and energy balances for air blown and thermally ballasted fluidized bed gasifiers. *Biomass and Bioenergy*, 45:95–108, 2012.

[55] V. Belgiorno, G. De Feo, C. Della Rocca, and R.M.A. Energy from gasification of solid wastes. *Waste Management*, 23:1–15, 2003.

[56] Lath E. and P. Herbert. Make co from coke, co2, and o2. *Hydrocarbon Processing*, 64(8):55–58, 1986.

[57] P. Lv, Z. Yuan, L. Ma, C. Wu, T. Chen, and J. Zhu. Hydrogen-rich gas production from biomass air and oxygen/steam gasification in a downdraft gasifier. *Renewable Energy*, 32(13):2173–2185, 2007.

[58] B.O. Oboirien, A.D. Engelbrecht, B.C. North, V.M. du Cann, and R. Falcon. Textural properties of chars as determined by petrographic analysis: Comparison between air-blown, oxygen-blown and oxygen-enriched gasification. *Fuel*, 101:16–22, 2012.

[59] Gong Cheng, Pi wen He, Bo Xiao, Zhi quan Hu, Shi ming Liu, Le guan Zhang, and Lei Cai. Gasification of biomass micron fuel with oxygen-enriched air: Thermogravimetric analysis and gasification in a cyclone furnace. *Energy*, 43(1):329–333, 2012.

[60] G. Schuster, G. Löffler, K. Weigl, and H. Hofbauer. Biomass steam gasification – an extensive parametric modeling study. *Bioresource Technology*, 77(1):71–79, 2001.

[61] H. Hofbauer and R. Rauch. Hydrogen-rich gas from biomass steam gasification. Technical report, Institute of Chemical Engineering Fuel and Environmental Technology, 1998.

[62] Toshiaki Hanaoka, Seiichi Inoue, Seiji Uno, Tomoko Ogi, and Tomoaki Minowa. Effect of woody biomass components on air-steam gasification. *Biomass and Bioenergy*, 28(1):69–76, 2005.

[63] Yoshinori Tanaka, Tsuyoshi Yamaguchi, Kenji Yamasaki, Akifumi Ueno, and Yoshihide Kotera. Catalyst for steam gasification of wood to methanol synthesis gas. *Ind. Eng. Chem. Res.*, 23(2):225–229, 1984.

[64] E.G. Baker and M.D. Brown. Catalytic steam gasification of bagasse for the production of methanol. In *energy from biomass and wastes meeting*, 1983.

[65] M. Kautz and U. Hansen. The externally-fired gas-turbine (efgt-cycle) for decentralized use of biomass. *Applied Energy*, 84(7-8):795–805, 2007.

[66] B. G. Miller. *Coal Energy Systems*. Elsevier academic press, 2005.

[67] P. Upham and S. Shackley. Local public opinion of a proposed 21.5 mw(e) biomass gasifier in devon: Questionnaire survey results. *Biomass and Bioenergy*, 31(6):433–441, 2007.

[68] Isabella Aigner, Christoph Pfeifer, and Hermann Hofbauer. Co-gasification of coal and wood in a dual fluidized bed gasifier. *Fuel*, 90(7):2404–2412, 2011.

[69] J. S. Brar, K. Singh, J. Wang, and S. Kumar. Cogasification of coal and biomass: A review. *International Journal of Forestry Research*, 2012.

[70] K. Sjöström, G. Chen, Q. Yu, C. Brage, and C. Rosén. Promoted reactivity of char in co-gasification of biomass and coal: synergies in the thermochemical process. *Fuel*, 78(10):1189–1194, 1999.

[71] Daniele Fiaschi and Riccardo Carta. Co2 abatement by co-firing of natural gas and biomass-derived gas in a gas turbine. *Energy*, 32(4):549–567, 2007.

[72] Nexterra corporation. Nexterra systems corp. project. Technical report, BC Bioenergy Network, 2011.

[73] LTD HENAN JIEBANG ELECTRIC TECHNOLOGY CO. 2mw power plant proposal. Technical report, Great POwer, 2011.

[74] C. Z. Wu, H. Huang, S. P. Zheng, and X. L. Yin. An economic analysis of biomass gasification and power generation in china. *Bioresource Technology*, 83(1):65–70, 2002.

[75] Bram van der Drift. Status of biomass gasification. Technical report, ECN, 2008.

[76] I. Obernberger and G. Thek. Combustion and gasification of solid biomass for heat and power production in europe-state-of-the-art and relevant future developments. *8th European conference on industrial furnaces and boilrs*, 2008.

[77] Septimus van der Linden, Mark Wiley, Gary Williams, and Roel Swart. Syngas fuel hybrid 45 mw gtcc/orc power plant using modular 500 tpd coal/biomass modular pyrolytic gasification. *ASME Conference Proceedings*, 2010.

[78] C.M. van der Meijden, W. Sierhuis, and A. van der Drift. Waste wood fueled gasification demonstration project. *European Biomass conference and exhibition*, 2011.

[79] Giulio Donolo, Giulio De Simon, and Maurizio Fermeglia. Steady state simulation of energy production from biomass by molten carbonate fuel cells. *Journal of Power Sources*, 158(2):1282 – 1289, 2006. <ce:title>Special issue including selected papers from the 6th International Conference on Lead-Acid Batteries (LABAT 2005, Varna, Bulgaria) and the 11th Asian Battery Conference (11 ABC, Ho Chi Minh City, Vietnam) together with regular papers</ce:title>.

[80] Stefano Cordiner, Massimo Feola, Vincenzo Mulone, and Fabio Romanelli. Analysis of a {SOFC} energy generation system fuelled with biomass reformate. *Applied Thermal Engineering*, 27(4):738 – 747, 2007. <ce:title>Energy: Production, Distribution and Conservation</ce:title>.

[81] C. Ozgur Colpan, Ibrahim Dincer, and Feridun Hamdullahpur. Thermodynamic modeling of direct internal reforming solid oxide fuel cells operating with syngas. *International Journal of Hydrogen Energy*, 32(7):787 – 795, 2007. <ce:title>Fuel Cells</ce:title>.

[82] Rami Salah El-Emam, Ibrahim Dincer, and Greg F. Naterer. Energy and exergy analyses of an integrated {SOFC} and coal gasification system. *International Journal of Hydrogen Energy*, 37(2):1689 – 1697, 2012. <ce:title>10th International Conference on Clean Energy 2010</ce:title>.

[83] Yurany Camacho Ardila, Jaiver Efren Jaimes Figueroa, Betânia Hoss Lunelli, Rubens Maciel Filho, and Maria Regina Wolf Maciel. Syngas production from sugar cane bagasse in a circulating fluidized bed gasifier using aspen plus$^{TM}$: Modelling and simulation. *Computer aided chemical engineering*, (2012):1093–1097, 30.

[84] L. Fryda, K.D. Panopoulos, and E. Kakaras. Integrated {CHP} with autothermal biomass gasification and sofc-mgt. *Energy Conversion and Management*, 49(2):281 – 290, 2008.

[85] C. Bang-Moller and M. Rokni. Thermodynamic performance study of biomass gasification, solid oxide fuel cell and micro gas turbine hybrid systems. *Energy Conversion and Management*, 51(11):2330 – 2339, 2010.

[86] Made Sucipta, Shinji Kimijima, and Kenjiro Suzuki. Performance analysis of the sofc-mgt hybrid system with gasified biomass fuel. *Journal of Power Sources*, 174(1):124 – 135, 2007. <ce:title>Hybrid Electric Vehicles</ce:title>.

[87] All-Power-Labs. Gasifier experimental kit, 2013.

[88] *Victory Gasifier, http://gasifier.wpengine.com/*, feb 2013.

[89] Stak-Gasifier. http://www.stakproperties.com. *Stak*, feb 2013.

[90] Leilei Dong, Hao Liu, and Saffa Riffat. Development of small-scale and micro-scale biomass-fuelled chp systems – a literature review. *Applied Thermal Engineering*, 29(11-12):2119–2126, 2009.

[91] Ronney Arismel Mancebo Boloy, Jose Luz Silveira, Celso Eduardo Tuna, Christian R. Coronado, and Julio Santana Antunes. Ecological impacts from syngas burning in internal combustion engine: Technical and economic aspects. *Renewable and Sustainable Energy Reviews*, 15(9):5194–5201, 2011.

[92] Marianne Salomón, Tuula Savola, Andrew Martin, Carl-Johan Fogelholm, and Torsten Fransson. Small-scale biomass chp plants in sweden and finland. *Renewable and Sustainable Energy Reviews*, 15(9):4451–4465, 2011.

[93] T.B. Reed and M.L. Markson. A predictive model for stratified downdraft stratified. *Progress in Biomass Conversion*, 4:219–254, 1983.

[94] J. Herguido, J. Corella, and J. González-Saiz. Steam gasification of lignocellulosic residues in a fluidized bed at small pilot scale. effect of the type of feedstock. *Ind. Eng. Chem. Res.*, 31(5):1274–1282, 1992.

[95] Debyani Ghosha, Ambuj D Sagara, and V.V.N. Kishore. Scaling up biomass gasifier use: an application-specific approach. *Energy Policy*, 34(13):1566–1582, 2006.

[96] Robert P. Ma, Richard M. Felder, and James K. Ferrell. Modeling a pilot-scale fluidized bed coal gasification reactor. *Fuel Processing Technology*, 19(3):265–290, 1988.

[97] T. B. Reed, R. Walt, S. Ellis, A. Das, and S. Deutch. Superficial velocity - the key to downdraft gasification. *4th Biomass Conference of the Americas; Oakland, CA*, 1999.

[98] F. Marini. *Monitoraggio e valutazione delle prestazioni di un impianto di cogenerazione a cippato di legno con gassificatore e motore Stirling.* CISA, http://www.centrocisa.it/ImpiantiRealizzati/stirlingCasteldaiano.php, 2012.

[99] D. Khummongkol and W. Arunlaksadamrong. Performance of an updraft mangrove-wood gasifier. *Energy*, 15(9):781–784, 1990.

[100] E. Kurkela, P. Ståhlberg, P. Simell, and J. Leppälahti. Updraft gasification of peat and biomass. *Biomass*, 19(1-2):37–46, 1989.

[101] J.G. Brammer and A.V. Bridgwater. The influence of feedstock drying on the performance and economics of a biomass gasifier–engine chp system. *Biomass and Bioenergy*, 22(4):271–281, 2002.

[102] Arjan F. Kirkels and Geert P.J. Verbong. Biomass gasification: Still promising? a 30-year global overview. *Renewable and Sustainable Energy Reviews*, 15(1):471–481, 2011.

[103] F.P. Nagel, S. Ghosh, C. Pitta, T.J. Schildhauer, and S. Biollaz. Biomass integrated gasification fuel cell systems–concept development and experimental results. *Biomass and Bioenergy*, 35(1):354–362, 2011.

[104] J.G. Brammer and A.V. Bridgwater. The influence of feedstock drying on the performance and economics of a biomass gasifier–engine chp system. *Biomass and Bioenergy*, 22(4):271–281, 2002.

[105] B.S. Pathak, S.R. Patel, A.G. Bhave, P.R. Bhoi, A.M. Sharma, and N.P. Shah. Performance evaluation of an agricultural residue-based modular throat-type down-draft gasifier for thermal application. *Biomass and Bioenergy*, 32(1):72–77, 2008.

[106] P. N. Sheth and B. V. Babu. Production of hydrogen energy through biomass (waste wood) gasification. *International journal of hydrogen energy*, 35(19):10803–10810, 2010.

[107] M. Ouadi, J.G. Brammer, M. Kay, and A. Hornung. Fixed bed downdraft gasification of paper industry wastes. *Applied Energy*, 103:692–699, 2013.

[108] T.H. Jayah, Lu Aye, R.J. Fuller, and D.F. Stewart. Computer simulation of a downdraft wood gasifier for tea drying. *Biomass and Bioenergy*, 25(4):459–469, 2003.

[109] Inna Rudakova. Use of biomass gasification for transport. Master's thesis, LAPPEENRANTA UNIVERSITY OF TECHNOLOGY, 2009.

[110] Prokash C. Roy, Amitava Datta, and Niladri Chakraborty. Assessment of cow dung as a supplementary fuel in a downdraft biomass gasifier. *Renewable Energy*, 35(2):379–386, 2010.

[111] A. Saravanakumara, T.M. Haridasanb, and Thomas B. Reed. Flaming pyrolysis model of the fixed bed cross draft long-stick wood gasifier. *Fuel Processing Technology*, 91(6):669–675, 2010.

[112] Er. Bhakta B. Ale, Nawaraj Bhattarai, Jitendra Gautam, Pradeep Chapagain, and Pushpa K.C. Institutional gasifier stove: A sustainable prospect for institutional cooking. *Journal of the institute of engineering*, 7(1):1–8, 2009.

[113] J. Hasan, D. R. Keshwani, S. F. Carter, and T. H. Treasure. Thermochemical conversion of biomass to power and fuels. *Biomass to Renewable Energy Processes*, pages 437–489, 2010.

[114] Z.A Zainal, Ali Rifau, G.A Quadir, and K.N Seetharamu. Experimental investigation of a downdraft biomass gasifier. *Biomass and Bioenergy*, 23(4):283–289, 2002.

[115] Yan Cao, Yang Wang, John T. Riley, and Wei-Ping Pan. A novel biomass air gasification process for producing tar-free higher heating value fuel gas. *Fuel Processing Technology*, 87(4):343–353, 2006.

[116] X.T. Li, J.R. Grace, C.J. Lim, A.P. Watkinson, H.P. Chen, and J.R. Kim. Biomass gasification in a circulating fluidized bed. *Biomass and Bioenergy*, 26(2):171–193, 2004.

[117] O.L. Kowalke. *A study of gas calorimeters*. University of Wisconsin–Madison, 1909.

[118] Y.I. Aleksandrov, V.P. Varganov, and S. Sarge. Design and study of gas calorimeter for absolute measurements of the combustion heat of natural gas. *Russian Journal of Applied Chemistry*, 74:1534–1538, 2001.

[119] J. Rouquerol and W. Zielenkiewicz. Suggested practice for classification of calorimeters. *Thermochimica Acta*, 109:121–137, 1986.

[120] E Calvet and H Prat. Different types of calorimeters. *Recent Progress in Microcalorimetry*, pages 3–11, 1963.

[121] K.N. Sheeba, J. Sarat Chandra Babu, and S. Jaisankar. Air gasification characteristics of coir pith in a circulating fluidized bed gasifier. *Energy for sustainable development*, 13(3):166–173, 2009.

[122] David Brown, Martin Gassner, Tetsuo Fuchino, and François Maréchal. Thermo-economic analysis for the optimal conceptual design of biomass gasification energy conversion systems. *Applied Thermal Engineering*, 29(11-12):2137–2152, 2009.

[123] Francisco V. Tinaut, Andrés Melgar, Juan F. Pérez, and Alfonso Horrillo. Effect of biomass particle size and air superficial velocity on the gasification process in a downdraft fixed bed gasifier. an experimental and modelling study. *Fuel Processing Technology*, 89(11):1076–1089, 2008.

[124] Juan Daniel Martínez, Electo Eduardo Silva Lora, Rubenildo Viera Andrade, and René Lesme Jaén. Experimental study on biomass gasification in a double air stage downdraft reactor. *Biomass and Bioenergy*, 35(8):3465–3480, 2011.

[125] L.C. Laurence and D. Ashenafi. Syngas treatment unit for small scale gasification-application to ic engine gas quality requirement. *Journal of Applied Fluid Mechanics*, 5(1):95–103, 2012.

[126] P. Hasler and Th. Nussbaumer. Gas cleaning for ic engine applications from fixed bed biomass gasification. *Biomass and Bioenergy*, 16(6):385–395, 1999.

[127] Z. Abu El-Rub, E. A. Bramer, and G. Brem. Review of catalysts for tar elimination in biomass gasification processes. *Ind. Eng. Chem. Res.*, 43:6911–6919, 2004.

[128] SERI. *Generator Gas: The Swedish Experience from 1939-1945, Di Ingenjörsvetenskapsakademien (Sweden)*. Solar Energy Research Institute, United States. Dept. of Energy,, Golden, Colorado, 1979.

[129] Kevin Jay Timmer. *Carbon conversion during bubbling fluidized bed gasification of biomasses*. PhD thesis, Iowa State University, 2008.

[130] Yi-Shun Chen, Shu-San Hsiau, Hsuan-Yi Lee, and Yau-Pin Chyou. Filtration of dust particulates using a new filter system with louvers and sublouvers. *Fuel*, 99:118.128, 2012.

[131] Thana Phuphuakrat, Tomoaki Namioka, and Kunio Yoshikawa. Absorptive removal of biomass tar using water and oily materials. *Bioresource Technology*, 102(2):543–549, 2011.

[132] R.S. Singh, S.S. Agnihotri, and S.N. Upadhyay. Removal of toluene vapour using agro-waste as biofilter media. *Bioresource Technology*, 97(18):2296–2301, 2006.

[133] R. Rameshkumar and K. Mayilsamy. A novel compact bio-filter system for a down-draft gasifier: An experimental study. *AASRI PROCEDIA*, 3:700–706, 2012.

[134] S. Anis and Z.A Zainal. Tar reduction in biomass producer gas via mechanical, catalytic and thermal methods: A review. *Renewable and Sustainable Energy Reviews*, 15(5):2355–2377, 2011.

[135] S. Jarungthammachote and A. Dutta. Thermodynamic equilibrium model and second law analysis of a downdraft waste gasifier. *Energy*, 32(9):1660 – 1669, 2007.

[136] C. Mandl, I. Obernberger, and F. Biedermann. Modelling of an updraft fixed-bed gasifier operated with softwood pellets. *Fuel*, 89(12):3795–3806, 2010.

[137] Niladri Sekhar Barman, Sudip Ghosh, and Sudipta De. Gasification of biomass in a fixed bed downdraft gasifier – a realistic model including tar. *Bioresource Technology*, 107:505–511, 2012.

[138] C. Di Blasi. Dynamic behaviour of stratified downdraft gasifiers. *Chem. Eng. Sci.*, 55(15):2931–2944, 2000.

[139] A. Gómez-Barea and B. Leckner. Modeling of biomass gasification in fluidized bed. *Progress in energy combustion science*, 36(4):444–509, 2010.

[140] Susanna Nilsson, Alberto Gómez-Barea, Diego Fuentes-Cano, and Pedro Ollero. Gasification of biomass and waste in a staged fluidized bed gasifier: Modeling and comparison with one-stage units. *Fuel*, 97:730–740, 2012.

[141] Qi Miao, Jesse Zhu, Shahzad Barghi, Chuangzhi Wu, Xiuli Yin, and Zhaoqiu Zhou. Modeling biomass gasification in circulating fluidized beds. *Renewable Energy*, 50:655–661, 2013.

[142] Wayne Doherty, Anthony Reynolds, and David Kennedy. The effect of air preheating in a biomass cfb gasifier using aspen plus simulation. *Biomass and Bioenergy*, 33(9):1158–1167, 2009.

[143] Naveed Ramzan, Asma Ashraf, Shahid Naveed, and Abdullah Malik. Simulation of hybrid biomass gasification using aspen plus: A comparative performance analysis for food, municipal solid and poultry waste. *Biomass and Bioenergy*, 35(9):3962–3969, 2011.

[144] A. K. Sharma. Equilibrium and kinetic modeling of char reduction reactions in a downdraft biomass gasifier: A comparison. *Sol. Energy*, 82(10):918–928, October 2008.

[145] Prokash C. Roy, Amitava Datta, and Niladri Chakraborty. Modelling of a downdraft biomass gasifier with finite rate kinetics in the reduction zone. *International journal of energy research*, 33(9):833–851, 2009.

[146] H. Molintas and A.K. Gupta. Kinetic study for the reduction of residual char particles using oxygen and air. *Applied Energy*, 88(1):306–315, 2011.

[147] B.V. Babu and Pratik N. Sheth. Modeling and simulation of reduction zone of downdraft biomass gasifier: Effect of char reactivity factor. *Energy Conversion and Management*, 47:2602–2611, 2006.

[148] K. Jaojaruek and S. Kumar. Numerical simulation of the pyrolysis zone in a downdraft gasification process. *Bioresource Technology*, 100(23):6052–6058, 2009.

[149] Nicolas Piatkowski and Aldo Steinfeld. Reaction kinetics of the combined pyrolysis and steam-gasification of carbonaceous waste materials. *Fuel*, 89(5):1133–1140, 2010.

[150] N. Gao and A. Li. Modeling and simulation of combined pyrolysis and reduction zone for a downdraft biomass gasifier. *Energy Conversion and Management*, 49(12):3483–3490, 2008.

[151] A. Kr. Sharma. Modeling fluid and heat transport in the reactive, porous bed of downdraft (biomass) gasifier. *International Journal of Heat and Fluid Flow*, 28(6):1518–1530, 2007.

[152] S. Murgia, M. Vascellari, and G. Cau. Comprehensive cfd model of an air-blown coal-fired updraft gasifier. *Fuel*, 101:129–138, 2012.

[153] Alireza Abbasi, Paul E. Ege, and Hugo I. de Lasa. Cpfd simulation of a fast fluidized bed steam coal gasifier feeding section. *Chemical Engineering Journal*, 174(1):341–350, 2011.

[154] I. Petersen and J. Werther. Three-dimensional modeling of a circulating fluidized bed gasifier for sewage sludge. *Chemical Engineering Science*, 60(16):4469–4484, 2005.

[155] Z.A. Zainal, R. Ali, C.H. Lean, and K.N. Seetharamu. Prediction of performance of a downdraft gasifier using equilibrium modeling for different biomass materials. *Energy Conversion and Management*, 42(12):1499 – 1515, 2001.

[156] G. Allesina, C. Cattini, S. Pedrazzi, and P. Tartarini. Sperimentazione di metodi non invasivi per il monitoraggio di un impianto di gassificazione a biomasse legnose. *La Termotecnica*, March 2012.

[157] Giulio Allesina. *Experimental and analytical investigation of downdraft stratified gasifiers*. PhD thesis, HIGH MECHANICS AND AUTOMOTIVE DESIGN & TECHNOLOGY, University of Modena and Reggio Emilia, Dep. of Engineering 'Enzo Ferrari', 2012.

[158] Takashi Yamazaki, Hirokazu Kozu, Sadamu Yamagata, Naoto Murao, Sachio Ohta, Satoru Shiya, and Tatsuo Ohba. Effect of superficial velocity on tar from downdraft gasification of biomass. *Energy & Fuels*, 19:1186–1191, 2005.

[159] A. Bottino, A. Comite, G. Capannelli, R. Di Felice, and P. Pinacci. Steam reforming of methane in equilibrium membrane reactors for integration in power cycles. *Catalysis Today*, 118(1ÃćâĆňâĂIJ2):214 – 222, 2006. <ce:title>Catalysis in Membrane Reactors</ce:title> <xocs:full-name>Proceedings of the 7th International Conference on Catalysis in Membrane Reactors</xocs:full-name>.

[160] K.J. Ptasinski, M.J. Prins, and A. Pierik. Exergetic evaluation of biomass gasification. *Energy*, 32:568–74, 2007.

[161] T.B. Reed, B. Levie, M.L. Markson, and M.S. Graboski. A mathematical model for stratified downdraft gasifier. *Symposium on Mathematical Modeling of Biomass Pirolysis Phenomena*, 1983.

[162] T.B. Reed and B. Levie. A simplified model of the stratified downdraft gasifier. *International Bio-Energy Directory and Handbook*, pages pag. 379–389, 1984.

[163] Carlos R. Altafini, Paulo R. Wander, and Ronaldo M. Barreto. Prediction of the working parameters of a wood waste gasifier through an equilibrium model. *Energy Conversion and Management*, 44:2763–2777, 2003.

[164] Y. Wang and C. Kinoshita. Kinetic model of biomass gasification. *Sol. Energy*, 51(1):19–25, 1993.

[165] Jin-Shi Chen and Wesley W. Gunkel. Modeling and simulation of co-current moving bed gasification reactors -part i. a non-isothermal particle model. *Biomass*, 14:51–72, 1987.

[166] Jin-Shi Chen and Wesley W. Gunkel. Modeling and simulation of co-current moving bed gasification reactors – part ii. a detailed gasifier model. *Biomass*, 14:75–98, 1987.

[167] C. Di Blasi and C. Branca. Modeling a stratified downdraft wood gasifier with primary and secondary air entry. *Fuel*, 104:847–860, 2013.

[168] S. Pedrazzi, G. Allesina, and P. Tartarini. Aige conference: A kinetic model for a stratified downdraft gasifier experimental assessment and modeling of energy conversion effectiveness in a gasification power plant. *International Journal of Heat and Technology*, 30(1):41–44, 2012.

[169] E.R. Huff. Effect of size, shape, density, moisture and furnace wall temperature on burning time of wood pieces. *Fundamentals of thermo-chemical biomass conversion: An international conference, Estes Park, CO*, 1982.

[170] K. J. Laidler. *Chemical kinetics*. Harper sRow Publishers, New York, 1987.

[171] R. C. Everson, H. V. J. P. Neomagus, H. Kasaini, and D. Njapha. Reaction kinetics of pulverized coal-chars derived from inertinite-rich coal discards: Gasification with carbon dioxide and steam. *Fuel*, 85:1076–82., 2006.

[172] S. Dasappa, H. V. Sridhar, G. Sridhar, and P. J. Paul. Science and technology aspects of bio-residue gasification. *Biomass Conversion and Biorefinery*, 1(3):121–131, September 2011.

[173] L. Waldheim and T. Nilsson. Heating value of gases from biomass gasification. Technical report, IEA Bioenergy Agreement, Task 20 - Thermal Gasification of Biomass, 2001.

[174] D. Beedie, P.J. Bowen, T. O'Dohery, and N. Syred. Cyclic variations and control of a batch biomass gasifier-combustor. *Combust. Sci. Technol.*, 1(113):529–556, 1996.

[175] Mark J. Prins, Krzysztof J. Ptasinski, and Frans J.J.G. Janssen. Torrefaction of wood: Part 1. weight loss kinetics. *J. Anal. Appl. Pyrolysis*, 77(1):28–34, 2006.

[176] M.P. Arnavat, J. C. Bruno, and A. Coronas. Review and analysis of biomass gasification models. *Renewable and Sustainable Energy Reviews*, 14:2841–2851, 2010.

[177] A. Kr. Sharma. Modeling and simulation of global reduction reactions for downdraft (biomass) gasifier. *Energy Conversion and Management*, 52:1386–1396, 2011.

[178] A. Sarvi and R. Zevenhoven. Large-scale diesel engine emission control parameters. *Energy*, 35(2):1139–1145, 2010.

[179] Bernardo Hellrigl. Il potere calorifico del legno. *Congress: Le biomasse agricole e forestali nello scenario energetico nazionale, Progetto Fuoco*, 2004.

[180] C. Souleymane. Motori a combustione interna e turbine a gas di piccola taglia per gas di sintesi. Master's thesis, UniversitÃă degli Studi di Padova, Italy., 2012.

[181] Wayne Doherty, Anthony Reynolds, and David Kennedy. Computer simulation of a biomass gasification-solid oxide fuel cell power system using aspen plus. *Energy*, 35(12):4545 – 4555, 2010. <ce:title>The 3rd International Conference on Sustainable Energy and Environmental Protection, {SEEP} 2009</ce:title>.

[182] E. Achenbach. Three-dimensional and time-dependent simulation of a planar solid oxide fuel cell stack. *Journal of Power Sources*, 49:333–348, 1994.

[183] F. Calise, M. Dentice dÃćâĆňâĎćAccadia, A. Palombo, and L. Vanoli. Simulation and exergy analysis of a hybrid solid oxide fuel cell (sofc)ÃćâĆňâĂIJgas turbine system. *Energy*, 31(15):3278 – 3299, 2006. {ECOS} 2004 - 17th International Conference on Efficiency, Costs, Optimization, Simulation, and Environmental Impact of Energy on Process Systems 17th International Conference on Efficiency, Costs, Optimization, Simulation, and Environmental Impact of Energy on Process Systems.

[184] Pegah Ghanbari Bavarsad. Energy and exergy analysis of internal reforming solid oxide fuel cellÃćâĆňâĂIJgas turbine hybrid system. *International Journal of Hydrogen Energy*, 32(17):4591 – 4599, 2007. Fuel Cells.

[185] Penyarat Chinda and Pascal Brault. The hybrid solid oxide fuel cell (sofc) and gas turbine (gt) systems steady state modeling. *International Journal of Hydrogen Energy*, 37(11):9237 – 9248, 2012.

[186] S.H. Chan, H.K. Ho, and Y. Tian. Modelling of simple hybrid solid oxide fuel cell and gas turbine power plant. *Journal of Power Sources*, 109(1):111 – 120, 2002.

[187] Tae Won Song, Jeong Lak Sohn, Jae Hwan Kim, Tong Seop Kim, Sung Tack Ro, and Kenjiro Suzuki. Performance analysis of a tubular solid oxide fuel cell/micro gas turbine hybrid power system based on a quasi-two dimensional model. *Journal of Power Sources*, 142(1ÃćâĆňâĂIJ2):30 – 42, 2005.

[188] Ph. Hofmann, K.D. Panopoulos, P.V. Aravind, M. Siedlecki, A. Schweiger, J. Karl, J.P. Ouweltjes, and E. Kakaras. Operation of solid oxide fuel cell on biomass product gas with tar levels >10 g nmÃćËĘâĂŹ3. *International Journal of Hydrogen Energy*, 34(22):9203 – 9212, 2009.

[189] S. Pedrazzi, G. Zini, and P. Tartarini. Complete modeling and software implementation of a virtual solar hydrogen hybrid system. *Energy Conversion and Management*, 51(1):122 – 129, 2010.

[190] DOE. *Fuel Cell Handbook (Seventh Edition)*. 2004.

[191] T. Melin and R. Rautenbach. *Membranverfahren, Grundlagen der Modul- und Anlagenauslegung*. 2007.

[192] Saeed Pakseresht, Mohammad Kazemeini, and Mohammad M. Akbarnejad. Equilibrium isotherms for co, co2, {CH4} and {C2H4} on the 5a molecular sieve by a simple volumetric apparatus. *Separation and Purification Technology*, 28(1):53 – 60, 2002.

[193] Gi-Moon Nam, Byung-Man Jeong, Seok-Hyun Kang, Byung-Kwon Lee, and Dae-Ki Choi. Equilibrium isotherms of ch4, c2h6, c2h4, n2, and h2 on zeolite 5a using a static volumetric method. *Journal of Chemical & Engineering Data*, 50(1):72–76, 2005.

[194] Marco Tagliabue, David Farrusseng, Susana Valencia, Sonia Aguado, Ugo Ravon, Caterina Rizzo, Avelino Corma, and Claude Mirodatos. Natural gas treating by selective adsorption: Material science and chemical engineering interplay. *Chemical Engineering Journal*, 155(3):553 – 566, 2009.

[195] JRC. Pvgis atalnte ssolar europeo, 02 2014.

[196] A.R. Brealey, S.C. Myers, F. Allen, and S. Sandri. *Capital budgeting 4/ed*. Mc, 2011.

[197] D.l. 30/12/2008.

[198] D.m. 16/07/2012, 2012.

[199] Spanner ReÂš GmbH. Spanner gasifier, 02 2014.

[200] ANKUR-SCIENTIFIC. Biomass gasifiifer systems, 02 2014.

[201] ESPE. Micro cogenerazione espe ad alto rendimento, 02 2014.

[202] AEEG. AutoritÃă italiana per l'energia elettrica ed il gas, 02 2014.

[203] GSE. Gestore dei servizi energetici, 02 2014.

[204] L. Tao and A. Aden. The economics of current and future biofuels. *Vitro Cellular & Developmental Biology - Plant*, 45(3):199–217, 2009.

[205] D.A. Walker. Biofuels, facts, fantasy, and feasibility. *Journal of Applied Phycology*, 21(5):509–517, 2009.

[206] D. Russo, M. Dassisti, V. Lawlor, and A.G. Olabi. State of the art of biofuels from pure plant oil. *Renewable and Sustainable Energy Reviews*, 16(6):4056 – 4070, 2012.

[207] C.E. Sandy Thomas. Transportation options in a carbon-constrained world: Hybrids, plug-in hybrids, biofuels, fuel cell electric vehicles, and battery electric vehicles. *International Journal of Hydrogen Energy*, 34(23):9279 – 9296, 2009.

[208] Orkun Ozener, Levent Yuksek, Alp Tekin Ergenc, and Muammer Ozkan. Effects of soybean biodiesel on a di diesel engine performance, emission and combustion characteristics. *Fuel*, 115(0):875 – 883, 2014.

[209] Jinlin Xue. Combustion characteristics, engine performances and emissions of waste edible oil biodiesel in diesel engine. *Renewable and Sustainable Energy Reviews*, 23(0):350 – 365, 2013.

[210] Paolo Sementa, Bianca Maria Vaglieco, and Francesco Catapano. Thermodynamic and optical characterizations of a high performance gdi engine operating in homogeneous and stratified charge mixture conditions fueled with gasoline and bio-ethanol. *Fuel*, 96(0):204 – 219, 2012.

[211] *Hydrogen Infrastructure*. Navigant-Research, 2011.

[212] Johanna H. Ulmanen, Geert P.J. Verbong, and Rob P.J.M. Raven. Biofuel developments in sweden and the netherlands: Protection and socio-technical change in a long-term perspective. *Renewable and Sustainable Energy Reviews*, 13(6ÃćâĆňâĂIJ7):1406 – 1417, 2009.

[213] Amin Talebian-Kiakalaieh, Nor Aishah Saidina Amin, and Hossein Mazaheri. A review on novel processes of biodiesel production from waste cooking oil. *Applied Energy*, 104(0):683 – 710, 2013.

[214] Ednildo Andrade Torres, Gilberto S. Cerqueira, Tiago. M. Ferrer, Cristina M. Quintella, Massimo Raboni, Vincenzo Torretta, and Giordano Urbini. Recovery of different waste vegetable oils for biodiesel production: A pilot experience in bahia state, brazil. *Waste Management*, 33(12):2670 – 2674, 2013.

[215] Zahira Yaakob, Masita Mohammad, Mohammad Alherbawi, Zahangir Alam, and Kamaruzaman Sopian. Overview of the production of biodiesel from waste cooking oil. *Renewable and Sustainable Energy Reviews*, 18(0):184 – 193, 2013.

[216] GÃijnnur KoÃğar and NilgÃijn CivaÅ§. An overview of biofuels from energy crops: Current status and future prospects. *Renewable and Sustainable Energy Reviews*, 28(0):900 – 916, 2013.

[217] A.E. Atabani, A.S. Silitonga, Irfan Anjum Badruddin, T.M.I. Mahlia, H.H. Masjuki, and S. Mekhilef. A comprehensive review on biodiesel as an alternative energy resource and its characteristics. *Renewable and Sustainable Energy Reviews*, 16(4):2070 – 2093, 2012.

[218] M. Balat. Prospects for worldwide biodiesel market development. *Energy Sources*, 4(1):48–58, 2009.

[219] J. Van Gerpen, B. Shanks, R. Pruszko, D. Clements, and G. Knothe. Biodiesel production technology. Technical report, NREL, Colorado, 2004.

[220] Walter Zegada-Lizarazu and Andrea Monti. Energy crops in rotation. a review. *Biomass and Bioenergy*, 35(12-25), 2011.

[221] Walter Zegada-Lizarazu and Andrea Monti. Non-food energy crops rotation possibilities. Technical report, Department of Agroenvironmental Science and Technology, University of Bologna (IT), 2010.

[222] A. Innocenti, M. Poli, and L. Dal Re. Coltivazione della colza: Esperienze nel ravennate. *Rivista Agricoltura*, (11):77–79, 2008.

[223] ISTAT. Consultazione dati: Navigazione tra i dati: Coltivazioni: Seminativi: Coltivazioni industriali: Tav. c14/2012 – superficie (ettari) e produzione (quintali): arachide colza girasole. Technical report, http://agri.istat.it, feb 2013.

[224] Atlante delle coltivazioni erbacee – piante industriali: Girasole – helianthus annuus l. Technical report, Istruzione Agraria online, feb 2013.

[225] Maisadour. Seed cultivation costs. Technical report, http://www.maisadour-semences.fr/it/, March 2013.

[226] B.B. Uzun, A.E. Putun, and E. Putun. Fast pyrolysis of soybean cake: Product yields and compositions. *Bioresource Technology*, 97:569–576, 2006.

[227] G. A. Foulds N. Dave. Comparative assessment of catalytic partial oxidation and steam reforming for the production of methanol from natural gas. *Industrial and Engineering Chemistry Research*, 34:1037–1043, 1995.

[228] Jaswant Singh and P.C. Bargale. Development of a small capacity double stage compression screw press for oil expression. *Journal of food engineering*, 43(2):75–82, 2000.

[229] Europe's Energy Porta. Electricity – industry (italy), 2013.

[230] A. Bordin. *Biocombustibili e biocarburanti. Soluzioni, tecnologie, agevolazioni Data di Pubblicazione: 2008*. Ipsoa, 2008.

[231] Janulis. Reduction of energy consumption in biodiesel fuel life cycle. *Renewable Energy*, 29:861–871, 2004.

[232] Databook 2012 p. 103, 2013.

[233] Giulio Allesina, Simone Pedrazzi, and Caterina Cattini. Experimental assessment and modeling of energy conversion effectiveness in a gasification power plant. *International Journal of Heat and Technology*, 29:151–156, 2011.

[234] Seeds press cost. model clb-500-em, http://www.croplandbiodiesel.com, feb 2013.

[235] CRPA. Presse a vite continua per la spremitura a freddo di semi e la produzione di olio vegetale. Technical report, Cecchetti energia srl, La Mecanique Moderne, 2010.

# Ringraziamenti

Ringrazio il professor Paolo Tartarini per avermi dato l'occasione di intraprendere questo straordinario percorso di dottorato. Vorrei poi ringraziare il mio grande compagno Giulio con il quale ho intrapreso strade in salita e discesa ma sempre con grandi risultati. Ringrazio infine tutta la mia famiglia che mi ha supportato durante tutto il mio percorso di studi.